

Acoustic and Statistical Methods for Sucker Rod Pump States Description

Dipl. Ing. Elena Chevelcha

23 July 2014

Chair of Petroleum Production and Geothermal Energy
Department Mineral Resources and Petroleum Engineering
University of Leoben

A-8700 LEOBEN, Franz Josef Straße 18
Phone: +43/(0)3842-402-3020
Fax: +43/(0)3842-402-8202

Declaration of authorship

„I declare in lieu of oath that this thesis is entirely my own work except where otherwise indicated. The presence of quoted or paraphrased material has been clearly signaled and all sources have been referred. The thesis has not been submitted for a degree at any other institution and has not been published yet.”

Acknowledgement

I take this opportunity to express my deep gratitude and regards to my adviser Univ.-Prof. Dipl.-Ing. Dr. mont. Herbert Hofstätter for given opportunity and constant encouragement throughout the thesis.

I also take this opportunity to express a deep sense of gratitude to Dipl.-Ing. Dr. mont. Rudolf Fruhwirth for his profound support, valuable information and guidance, which helped me complete this task.

My appreciation also goes to Univ.-Prof. Mag. et Dr. rer. nat. Erika Hausenblas for the willing to help in different matters.

I am obliged to staff members of RAG for the research material provided by them in their respective fields. I am grateful for their cooperation during the period of my assignment.

I am thankful to my colleagues from the Chair of Petroleum Production and Geothermal Energy (Montanauniversität Leoben) for the support and warm atmosphere.

Lastly, I thank almighty, my parents, Gabriel and friends for their wholehearted support without which this research would not be possible.

Резюме

Общая идея исследовательской работы основывается на предположении, что любая скважина, оснащенная глубинным штанговым насосом (SRP) испускает характерный звуковой спектр, который может быть оценен. Каждое изменение в системе (износ, начало сбоев и т.д.) должно быть отражено изменением соответствующего звука, создавая, таким образом, корреляцию. Целью научного исследования является изучение звука, произведенного скважиной, и определение взаимосвязи между издаваемым звуком и эксплуатационным состоянием SRP. Корреляция будет исследована на основе динамограмм (DC) и фактических эксплуатационных мероприятий.

Звук представляет собой функцию динамического поведения жидкостей, газа, скважинного и наземного оборудования. Звук, созданный этой системой записывается в режиме он-лайн с помощью специального устройства, установленного на устье скважины. Звуковые данные затем загружаются на сервер и доступны для дальнейшей обработки. Акустический анализ основан на методах обработки сигналов в сочетании со статистическими инструментами. Они используются для того, чтобы получить характеристики звука, которые впоследствии коррелированы с динамограммами и характеристиками динамограмм.

Результат исследований поддерживает применение звука в качестве метода для наблюдения за SRP. Высокие коэффициенты корреляции подтверждают наличие взаимосвязи между SRP звуком и DC. В исследовании звук используется для моделирования характеристик динамограмм для наблюдения за SRP. Это расширяет применение акустики как инструмента, используемого для мониторинга и прогнозирования состояния SRP.

Zusammenfassung

Die Hypothese dieser Forschungsarbeit basiert auf der Annahme, dass eine Ölbohrung mit Gestängepumpe (SRP) ein charakteristisches Schallenwellenspektrum emittiert, welches analysiert werden kann. Jede Veränderung des Systems (Verschleiß, Versagensbeginn, etc.) wird in einer entsprechenden Änderung der Schallwellen reflektiert, und eine Korrelation kann erstellt werden. Das Ziel der Forschungsarbeit ist die Untersuchung des Schalls, welcher von der Bohrung produziert wird, und der Zusammenhang zwischen dem emittierten Schallwellen und dem Produktionszustand der SRP zu untersuchen. Die Korrelation wird untersucht basierend auf Dynamometerkarten (DC) und realen Vorkommnissen während der Produktion.

Geräuschwellen sind eine Funktion des dynamischen Verhaltens der Fluide, Gase, Untertage- und Obertage-Anlagen. Die Geräuschwellen des Systems werden im Online Modus mit Hilfe spezieller Geräte am Bohrlochskopf aufgenommen. Die Daten der Schallwellen werden übertragen, auf einen Server geladen und stehen dann bereit zur Verarbeitung. Die akustische Analyse basiert auf Methoden der Signalverarbeitung in Kombination mit statistischen Werkzeugen. Diese werden benutzt, um Eigenschaften des Schalls festzustellen, welche mit Dynamometerkarten und deren Eigenschaften korreliert werden können.

Das Resultat der Forschungsarbeit zeigt, dass die Analyse von Schallwellen für die Überwachung von SRPs angewendet werden kann. Hohe Korrelationskoeffizienten bestätigen einen Zusammenhang zwischen SRP Schallwellen und DCs. In der Forschungsarbeit werden die Schallwellen genutzt, um Merkmale von DCs für die Überwachung von SRPs zu modellieren. Dies erweitert den Anwendungsbereich der Akustik im Bereich der Überwachung und als SRP Vorhersage Instrument.

Abstract

The general idea of the research is based on the assumption that an oil well with an installed sucker rod pump (SRP) emits a characteristic sound spectrum that can be assessed. Every change to the system (wear, beginning of failures, etc.) should be reflected in a corresponding change of the sound, creating thus a correlation. The scope of the research is to study noise, produced by a well and to study relationship between the emitted sound and the production state of the SRP. Correlation will be researched on the basis of dynamometer cards (DC) and actual production events.

Noise represents a function of dynamic behavior of fluids, gas, downhole and surface equipment. Noise created by this system is recorded in on-line mode with the help of a special device installed on the wellhead. The sound data then are transmitted, uploaded to a server and available to process. The acoustic analysis is based on the signal processing techniques combined with statistical tools. They are utilized in order to obtain sound features that are correlated with the dynamometer cards and DC features.

The result of the research supports the application of the sound as a method for SRP supervising. High correlation coefficients corroborate the relationship between the SRP-emitted sound and DCs. In the research, the sound is used to model the DC features for the SRP monitoring. This widens the application of acoustics as a monitoring and SRP state prediction tool.

Content

1	Introduction	13
1.1	Objectives of the Thesis	14
1.2	Outline of the Thesis	15
2	Sucker Rod Pump	16
2.1	Surface Equipment	16
2.2	Rod String	18
2.3	Pump Components	24
2.3.1	<i>Barrels</i>	25
2.3.2	<i>Plungers</i>	25
2.3.3	<i>Valves</i>	25
2.3.4	<i>Additional Components</i>	25
2.4	How Sucker Rod Pump Works	25
2.5	SRP Kinematics	27
2.6	Sucker Rod Pump Advantages and Disadvantages	30
2.7	Sucker Rod Pump Failures	30
2.7.1	<i>Common Rod Problems and their Solutions</i>	31
2.7.2	<i>Sand Problems</i>	32
2.7.3	<i>Free Gas</i>	32
2.7.4	<i>Paraffin Precipitation</i>	34
2.7.5	<i>Knocking Travelling Valve</i>	34
2.7.6	<i>Pumped-Off Well</i>	35
2.8	Production Data	36
2.9	Audio Collector File	36
3	Dynamometer Cards	42
3.1	General Information	42
3.2	Dynamometer Cards Acquisition	43
3.3	Harmonic Motion of the Rods	44
3.4	Dynamometer Card Preparation and Quality Control	46
3.5	Dynamometer Card Features	48
4	Sound Data	50
4.1	Sound Data Acquisition	50
4.2	Sound Data Preparation	54
4.2.1	<i>Bias Offset Removal</i>	56
4.2.2	<i>Fourier Transform</i>	56
4.2.3	<i>Sampling Theorem and Decimation</i>	60
4.2.4	<i>Power Spectrum Density</i>	64

4.2.5	<i>Hilbert Transform</i>	65
4.3	Sound Features.....	66
4.3.1	<i>Features Definition</i>	66
4.3.2	<i>Real Trace</i>	68
4.3.3	<i>Quadrature Trace</i>	68
4.3.4	<i>Signal Envelope</i>	68
4.3.5	<i>Z-Score</i>	68
4.3.6	<i>Instantaneous Frequency</i>	68
4.3.7	<i>Spectral Centroid</i>	69
4.3.8	<i>Temporal Centroid</i>	69
4.3.9	<i>Spectral Bandwidth</i>	70
4.3.10	<i>Roll-off Frequency</i>	70
4.3.11	<i>BT Product</i>	70
4.3.12	<i>Amplitude in the Frequency Domain</i>	70
4.3.13	<i>Signal Entropy</i>	71
4.3.14	<i>Spectral Skewness</i>	71
4.3.15	<i>Spectral Kurtosis</i>	71
4.3.16	<i>Spectral Flatness</i>	71
4.3.17	<i>Mel Frequency Cepstral Coefficients (MFCC)</i>	72
4.4	Statistical Analysis	73
4.4.1	<i>Minimum</i>	73
4.4.2	<i>Maximum</i>	73
4.4.3	<i>Mean</i>	73
4.4.4	<i>Median</i>	74
4.4.5	<i>Mode</i>	74
4.4.6	<i>Range</i>	74
4.4.7	<i>Interquartile Range</i>	74
4.4.8	<i>Percentile</i>	75
4.4.9	<i>Variance</i>	75
4.4.10	<i>Average Deviation</i>	75
4.4.11	<i>Standard Deviation</i>	75
4.4.12	<i>Root mean Square</i>	75
4.4.13	<i>Skewness</i>	75
4.4.14	<i>Kurtosis</i>	76
4.4.15	<i>Mean Absolute Deviation</i>	77
4.4.16	<i>Trimmed Mean</i>	77
4.4.17	<i>Modified Statistical Methods</i>	77
4.5	Features and their Notation	78
4.6	Sound Data Quality Control.....	78
4.6.1	<i>Data Acquisition Quality Control</i>	79
4.6.2	<i>Labels for Quality Control</i>	80
4.6.3	<i>Usable and Not Usable Files</i>	84

4.6.4	<i>Sound of Standard State</i>	84
4.7	Neural Network for Data Quality Control	85
5	Dynamometer Card and Sound Data Correlation and Results	93
5.1	Correlation of Sound Features and DC values.....	93
5.2	Second Type of Correlation	98
6	Recommendations	109
7	References	113
Appendix A	General Completion Information	117
Appendix B	Well BH – 003 History	118
Appendix C	Well BH – 009 History	119
Appendix D	Well V – 041 History	120
Appendix E	Dynamometer Cards Full Table	121
Appendix F	Final List of the Sound Features	124

List of Figures

Figure 1: Research system	14
Figure 2: Subsurface sucker rod pump installation, after Rischmüller, 1989 [17]	17
Figure 3: Natural period at SPM=3.5	21
Figure 4: Natural period at SPM=1.3	22
Figure 5: Natural period at SPM=4.5	22
Figure 6: Natural frequency at SPM=1.3	23
Figure 7: Natural frequency at SPM=3.5	23
Figure 8: Forced frequency F1 as a function of SPM	24
Figure 9: Sucker rod pump, after Tan, 2008 [71]	24
Figure 10: SRP components and pumping cycle, after Lea, 2003 [22]	26
Figure 11: Sucker rod pump types, after Gray, 1963 [16]	28
Figure 12: Polished rod motion of conventional units, after Nind, 1981 [41]	29
Figure 13: Polished rod motion of conventional units, after Tackas, 2003 [59]	29
Figure 14: Free gas example, after Kudu Industries Inc.	33
Figure 15: Surface and downhole card of a pump with the free gas, after Sage Technologies, Inc. ..	33
Figure 16: DC of normal operating pump with SPM 3.5	35
Figure 17: DC of the pumped-off well with SPM 4.5	35
Figure 18: History of well BH-003	38
Figure 19: History of well BH-009	39
Figure 20: History of well V-041	40
Figure 21: Ideal dynamometer card	43
Figure 22: Example of analog dynamometer card from the well BH-003	43
Figure 23: Geometry of the Lufkin Conventional pumping unit, after Lufkin [72]	45
Figure 24: BH-003 polished rod vs crank angle motion	45
Figure 25: V-041 polished rod vs crank angle motion	46
Figure 26: Example of digitized DC	46
Figure 27: Example of digitized and corrected DC	47
Figure 28: Load vs position flared-out example	47
Figure 29: Overlaid harmonic movement of the polished rod and flared-out DC card	48
Figure 30: Upstroke notation	49
Figure 31: Downstroke notation	49
Figure 32: Murag surface installation	51
Figure 33: Number of sound files per well	55
Figure 34: Example of a sound file before and after the bias removal	56
Figure 35: A rectangular impulse as a sum of harmonics	58
Figure 36: Decimation in the time domain, after Matlab R2014a Documentation	61
Figure 37: Effect of decimation in the frequency domain, after Matlab R2014a Documentation	61
Figure 38: Filter to prevent aliasing when reducing F_s , after Matlab R2014a Documentation	62
Figure 39: Rectangular window in the time and the frequency domain	63
Figure 40: Triangular window in the time and the frequency domain	63

Figure 41: Hanning window in the time and the frequency domain	63
Figure 42: A complex trace and its attributes, after Taner, 1979 [33]	65
Figure 43: Spectral centroid	69
Figure 44: Roll-off frequency	70
Figure 45: Boxplot example	74
Figure 46: Examples of distributions	76
Figure 47: Examples of distributions with different kurtosis	76
Figure 48: Spectrogram of a sound file with the working pump	80
Figure 49: Spectrogram of a sound file with pump switched off	81
Figure 50: Example of a signal with gaps	81
Figure 51: Spectrogram of a sound file with gaps	81
Figure 52: Example of a clipped file	82
Figure 53: Example of a clipped file enlarged	82
Figure 54: Spectrogram of a clipped sound file	82
Figure 55: Example of a not clipped file	82
Figure 56: Example of a file with audible and visible drops	83
Figure 57: Example of a sound with the file changing envelope	83
Figure 58: Spectrogram of a sound file with the changing envelope	83
Figure 59: Example of a sound file with the peaky envelope	83
Figure 60: Spectrogram of a sound file with the peaky envelope	84
Figure 61: NN structure, after cVision User's Manual, 2009 [8]	86
Figure 62: NN learning process	87
Figure 63: Example of NN output, well BH-009	88
Figure 64: Best representative features for usable files of well V-041	89
Figure 65: Example of 2D plot	89
Figure 66: DC and sound features correlation	93
Figure 67: Example of the determination coefficient and regression line	94
Figure 68: Example of correlation	95
Figure 69: The features with the highest r^2 over a day	95
Figure 70: Radar plot of the sound feature rLB:CC44 and the polished rod load	96
Figure 71: Final correlation plots	97
Figure 72: NN application for DC features modelling	99
Figure 73: BH-003 Production events. $F_{dn\ avsd}$ and $F_{up\ avsd}$	100
Figure 74: BH-003. Enlarged pipe treatment event $P_{up\ sd}$	101
Figure 75: BH-003. Enlarged pipe treatment event $E_{up\ sd}$	101
Figure 76: BH-009 Production events $E_{dn\ av}$	102
Figure 77: V-041 Production events $E_{dn\ av}$ and $E_{up\ av}$	103
Figure 78: V-041 Paraffin case $E_{up\ av}$	104
Figure 79: V-041 POF state $P_{up\ av}$	104
Figure 80: V-041 Production events $P_{up\ av}$ and $P_{dn\ av}$	105
Figure 81: V-041 well treatment $F_{dn\ avsd}$	106
Figure 82: V-041 Production events $F_{up\ avsd}$ and $F_{dn\ avsd}$	108

List of Tables

Table 1: Period calculation results for SPM=3.5	21
Table 2: DC amount per well, per year.....	44
Table 3: Geometry of the pumping units	45
Table 4: DC final amount per well, per year.....	48
Table 5: Number of sound files per well, per year	54
Table 6: Equations of window functions	64
Table 7: Frequency range division into linear bands.....	73
Table 8: Combination of statistical measures and their formulas	78
Table 9: Estimation of features efficiency for well V-041, label “Standard”.....	90
Table 10: Estimation of features efficiency for well BH-009, label “Usable”	91
Table 11: Final number of usable/not usable data after data QC.....	91
Table 12: Percentage of usable and not usable files after data QC	92
Table 13: Correlation results	96
Table 14: Determination coefficient percentage per well	97
Table 15: Estimation of the DC features as SRP states indicators.....	107

1 Introduction

Sucker rod pumping (SRP) system is the oldest and the most popular production method used in the oil industry due to its simple design and reliability. In view of its widespread application, it is essential to provide supporting and monitoring methods and techniques that estimate sucker rod pump system efficiency. This thesis suggests using acoustics as a tool for SRP analysis. This use of acoustics application for sucker rod pump analysis is extremely new to the market, although some American companies (e.g., “Hydraulic Rod Pumps, Int’l”) tried to implement the concept, but could not achieve sufficient results, therefore this approach was abandoned. Both non-destructive and remote applications make its application possible again.

Acoustics is the science of sound creation, transmission and propagation through solids and fluids. Sound is defined as a transition of pressure fluctuations through a medium, as the result of mechanical disturbances. The realm of sound application has broadened to include the use of ultrasonic and infrasonic in addition to the audible range; acoustics, among other applications are widely used in material science, medicine, communications, animal bioacoustics and speech analysis [51]. The general idea behind the research originates from the assumption that an oil well with a newly installed SRP system emits a characteristic sound spectrum that can be assessed. Every change to the system according to wear, its failing components or the production events, is assumed to be reflected in a corresponding change of its sound spectrum, thus creating a correlation. Dynamometer card (DC) measurements are the robust method of the SRP diagnosis and, together with production events, reflect the pump and well conditions. Acoustic recordings, dynamometer cards, and production events describe the SRP system in three different ways. Figure 1 shows how they are related:

- production events characterize the SRP system;
- the SRP can be also evaluated with the aid of the sound emitted by the pump. To represent sound, sound features are introduced;
- DC reflects the pump operating condition and is related to its operating state. DC is characterized with the DC features.
- a correlation between the components can limit the amount of information needed to estimate the well production conditions, yet stay efficient and sufficient.

This research is conducted in collaboration with an Austrian oil company, RAG. To record the sound, a special device – the Murag box – is used. This system is installed and operated on several wells in the RAG fields. The data from three wells are taken for the detailed research in this thesis. Through

the use of the Murag box it is possible to remotely monitor and control the wells' system behavior in real time, thus providing a guarantee of optimal production, less operating costs and extended equipment life.

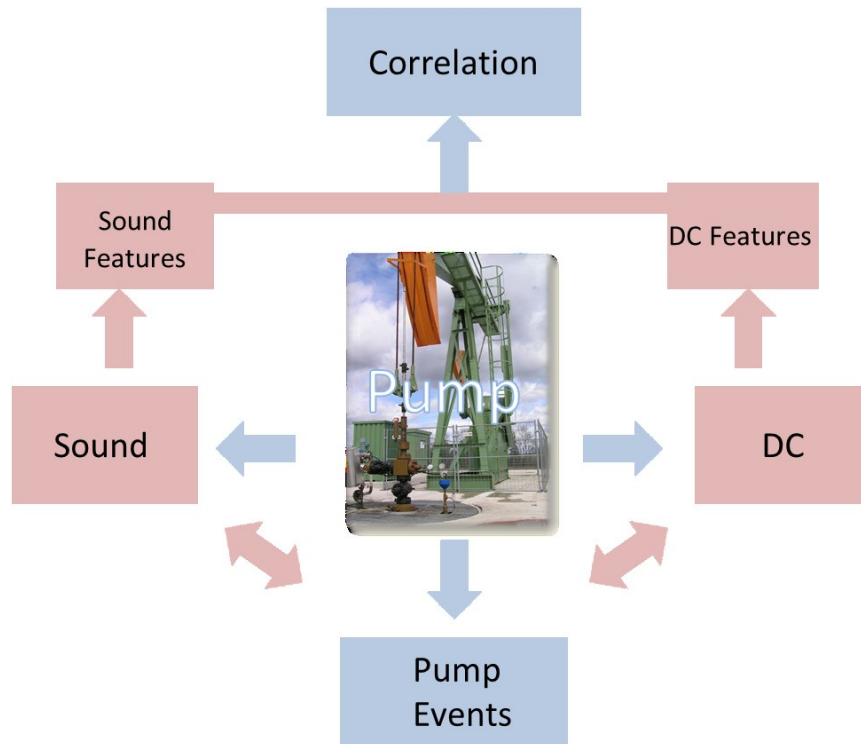


Figure 1: Research system

1.1 Objectives of the Thesis

The objective of this work is to check the use of sound for the SRP system analysis. Therefore, the correlation of the sound with the system's behavior will be researched based on dynamometer readings and actual system failure events. To perform this task, statistical processing, sound processing, speech and music recognition, and seismic analysis methods are considered. To symbolize the sound, sound features are introduced, the calculation of which is developed by the use of the robust algorithms borrowed from different fields of acoustics application.

DC features that are indicators of the pump state are introduced. DC features are correlated with the emitted sound in order to check their relationship and subsequently use this for DC features modelling.

The thesis aims to introduce employed techniques, which also involve the neural networks application for the sound data quality control, and DC features modelling and correlation. Correlation retrieval procedures are to be explained and applied.

1.2 Outline of the Thesis

The thesis is divided into six chapters. The first four chapters provide the theoretical base needed for the sound and production data treatment and features extraction. Since the thesis discusses the SRP, Chapter 2 gives a short introduction in this subject, describing the SRP components, kinematics, main failures that can happen in the system, and the pump advantages and disadvantages. It also presents production events registered for each well, which are used for data correlation.

Dynamometer cards acquisition, preparation, and features are discussed in Chapter 3. In addition, this chapter introduces the theory of harmonic motion of the sucker rods and equations used to describe it.

Chapter 4 concentrates on the sound handling. It includes descriptions of sound acquisition, sound preparation and methods for the sound features calculation. Emphasis is attached to the Fourier Transform, the sampling theorem, along with decimation and windowing. The problem of aliasing is also discussed; it is of significance when a continuous signal is collected by an analog-to-digital converter or when a digital signal is decimated. A full list of the signal processing and statistical methods for the sound features extraction, as well as their notation, are presented in the chapter. Sound data quality control and quality control insurance methods, which include application of the neural networks, are also presented in Chapter 4.

In Chapter 5, the final correlation procedure is introduced. The strength of the correlations is estimated with the correlation and determination coefficients. The positive results of the performed correlation are extended to the DC features sound modeling. The behavior of modelled DC features throughout the production history of each well is analyzed and conclusions on modelled data are presented.

Finally, in Chapter 6 the recommendations for further proceedings are given. The recommendations are issued based on the experience gathered during the research, and mainly distinguished by the modifications of the recording sensor and sound data sampling, searching new methods for features extraction and relationship searching methods, etc. The recommendations also propose the application of the sound be used to model entire DC.

2 Sucker Rod Pump

An Artificial Lift System (ALS) is any system that adds energy to the fluid column in a wellbore with the objective to initiate and improve production. ALS uses a range of operating principles, including rod pumping, gas lift, electrical submersible pumps, etc. The choice of ALS depends on many factors, such as expected production daily rate, gas – oil ratio (GOR), sand production, chemical composition of the produced fluid, HPHT reservoirs, etc. SRP is the oldest onshore artificial lift method in widespread use throughout the world. In fact, SRP is used in approximately 68 % of all well utilizing ALS. Around the world, implementation of artificial lifts is increasing due to several factors: mature oilfields decline in productivity, newer oil fields require the introduction of an ALS sooner, global increase in oil demand, improvements in oilfield management practice become more widely deployed and more rapidly adopted [4]. The SRP system generates the data used in this work for its state analysis: sound and dynamometer cards. This chapter presents SRP elements, explains the principles of how the pump works, the system's advantages and disadvantages, and tells about types of failures that can happen to the system. Production data collected throughout the research time, which are used as SRP state indicators, are introduced and explained. Production data is also used in further steps of the research as reference points for sound and DC correlations.

Simply stated, the SRP system is divided into three related components according to Coproven [7]: surface equipment, downhole equipment, and the rod string component (the element that interconnects the surface and downhole equipment). With the division mentioned above, it is possible to concentrate the study's attention on each component separately, and then determine its influence over the whole system seriatim. Figure 2 depicts a well equipped with the SRP. The surface equipment includes a prime mover, pumping unit, stuffing box, polished rod, the flowlines, and wellhead. Downhole equipment comprises of the downhole pump, casing, tubing, seating nipple, gas anchor (this piece is optional and depends on GOR), perforated nipple and mud anchor.

2.1 Surface Equipment

The surface equipment includes the pumping unit, gearbox and counterweights, prime mover, polished rod and stuffing box. The prime mover is usually an electrical motor, but in remote areas can be a gas engine. The prime mover's function is to provide the SRP system with the energy it needs. The prime mover's design depends on several factors, such as dynamic fluid level (DFL), pump setting depth and pumping speed (stroke per minute, SPM), and plays a significant role in the system efficiency. The DFL is an important concept of the SRP as it influences the fluid load on the pump plunger.

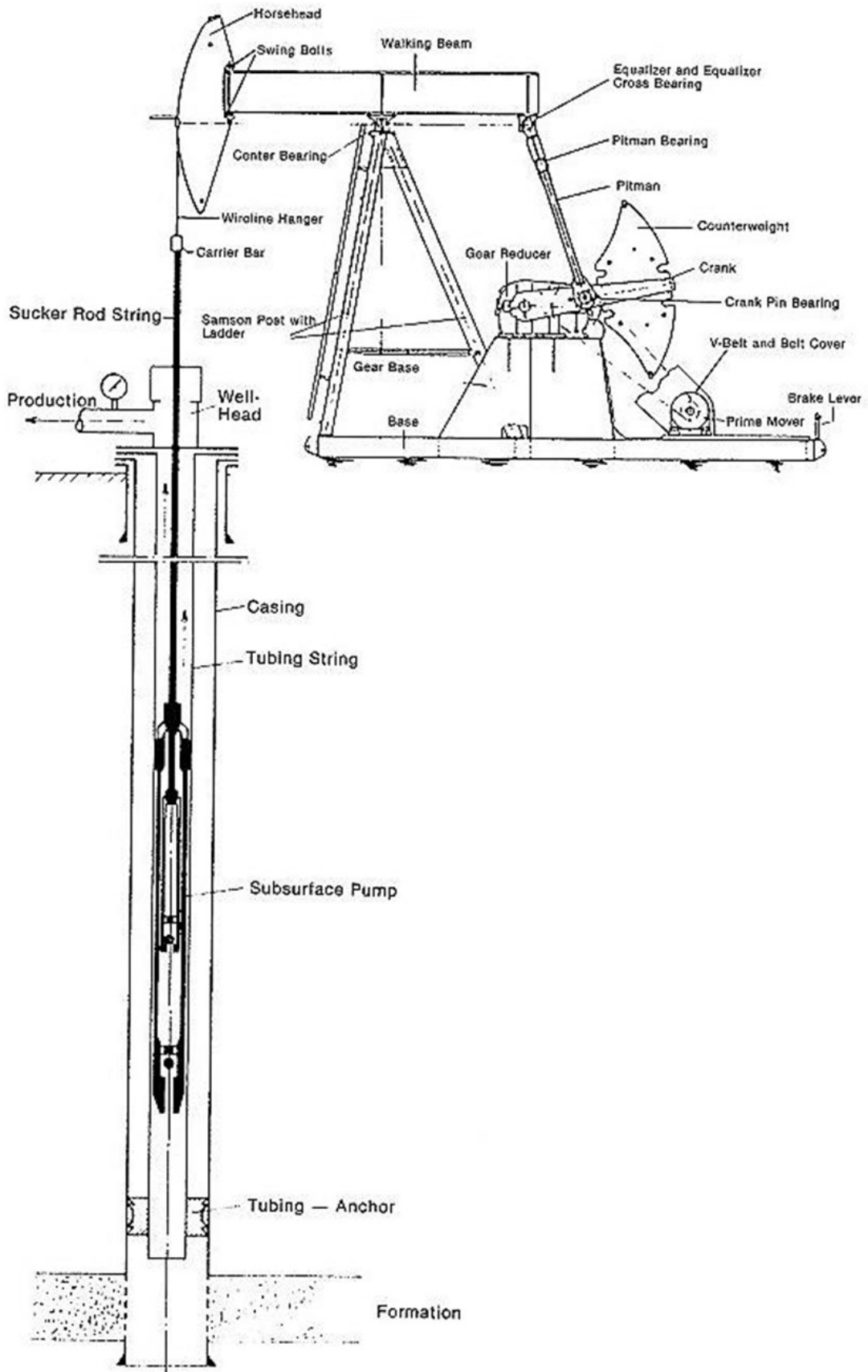


Figure 2: Subsurface sucker rod pump installation, after Rischmüller, 1989 [17]

The main function of the pumping unit is to convert the rotational motion of the prime mover into the reciprocating motion of the rod string via the polished rod. It is important to have an appropriate size of pumping unit with the correct size of gear box. There are many pumping units available on the market, suitable in terms of both shape and size.

The gearbox transforms the low torque and high RPM from the prime mover, into the high torque and low RPM needed for the pumping unit. The usual reduction ratio is 30:1 (i.e., it reduces the RPM by 30 and increases the torque by 30).

Counterweights are surface equipment that helps reduce the torque supplied by the gearbox. As indicated by their name, they always perform in the opposite (counter) direction. They provide help to the gearbox on the upstroke by releasing potential energy, while during the downstroke they are lifted with the help of rods and accumulate potential energy during this lifting. The essential idea behind the counterweight design is to balance the unit at the point when the upstroke and downstroke torques are equal.

The polished rod is another important part of the system. It is the only section of the rod string that is visible, and connects the rod string and the pumping unit. The polished rod has a smooth surface that insures that the stuffing box is not worn off. The stuffing box provides a tight seal around the polished rod in order to prevent fluid leakage.

2.2 Rod String

As mentioned before, the rod string is a connection between surface and subsurface equipment. The main function that rods conduct is to transmit the oscillating movement of the polished rod to the pump. Thereby, this component of the SRP provides the necessary power to lift the oil. The rod's motion follows wave equations, and the fact that rods constantly experience stretching and compressing cycles leads to the fatigue. Proper rod design can reduce or even eliminate the costs of repairing or replacing rods.

Sucker rods are usually steel or fiberglass pipes with a length of 25ft or 30 ft (37.5 ft for fiberglass). The rod strings discussed in the thesis are steel. Information about rods installed in the wells is provided in Appendix A.

The rod's motion is usually presented in a wave equation. The string's movement follows the law of harmonic vibrations of systems having one degree of freedom [6]. The free harmonic vibrations that rods experience are defined by a natural frequency. The motion of the pumping unit, in turn, also causes vibrations; these are called forced vibrations and characterized by the forced frequency. The plunger movement is a result of these two frequencies and is corrected with a system damping factor. Damping (or friction) coefficient is a function of fluid and system properties (higher in wells with great water cut, water salinity, gas and foam presence, buckling, etc.).

The law of harmonic motion implies that the weight of a model is constant during the entire cycle. In the pump, the weight varies for downstroke (weight of the rods minus friction) and upstroke (weight of the rods plus fluid and friction). As indicated by Kendrick [6], it is not of great importance for systems with high SPM, but has great influence on systems with low SPM. It is therefore essential to note SPM. The superposition of induced natural and forced frequencies influences the

rod's behavior, the dynamometer card shape and the frequencies range [6]. SPM and natural vibrations are related by the formula:

$$(1) \quad \text{SPM} = \frac{60R}{T},$$

where R denotes the ratio of T/T_1 , and T being the period of natural vibrations in seconds, and T_1 is the period of forced vibrations in seconds.

There are three variables that describe the plunger motion: forced vibrations of pumping unit, natural vibrations of the system and damping coefficient. The formula given by S. Timoshenko [70] describes the resultant vibration:

$$(2) \quad d_3 = \frac{d_2}{\sqrt{\left(1 - \frac{T^2}{T_1^2}\right)^2 + \frac{T^2}{T_1^2} u^2}},$$

with d_3 denoting the half plunger stroke in inches, d_2 the half polished rod stroke in inches and u is the damping coefficient. Natural vibrations T are defined as:

$$(3) \quad T = 0.3195\sqrt{d_s},$$

with d_s as the static stretch, which is equivalent to the fluid weight and 1/3 of the rod's weight.

The forced vibrations period is calculated as:

$$(4) \quad T_1 = \frac{60}{\text{SPM}}.$$

This information is essential to know in order to design the SRP system in such a way that the plunger does not vibrate with its greatest amplitude, i.e. in resonance. It is ensured when the periods of previously mentioned vibrations are equal. In order to guarantee the SRP's proper design and exploitation, the ratio T/T_1 must be less than 0.5.

The value of the damping coefficient is the most difficult to obtain for solving this set of equations. It is clear that the damping factor is related to the physical properties of the fluid (viscosity, density, gas presence and water content). To calculate the damping coefficient, experiments need to be conducted in the laboratory. In the absence of the damping coefficient data for this thesis, it is taken based on recommendations from Kendrick [6], where $u=0.3$ for the crude oil with some presence of gas, and $u=2.5$ for the fluid, which is mostly water with a small amount of gas.

As shown in equation (1), the stroke length at the polished rod is longer than at the plunger. This fact is explained by the rods stretching under the load. For this thesis, it is interesting to investigate how much both the natural and forced frequencies impact on the overall sound. To calculate the natural period T, it is useful to assume that the ratio of d_3 to d_2 is less than 1%. The range of T can be calculated for different d_3 to d_2 ratio values. In addition, it is assumed that the damping coefficient of the oil and water mixture is calculated in the linear manner. T is calculated for

different damping coefficients u . The wells discussed in the thesis operate with various SPMs. The dependence of T on the SPM is also examined here.

For ease of calculation, a rod factor ρ is introduced to describe the difference between d_3 and d_2 . Knowing that $d_2 \geq d_3$, $d_2 = d_3 (1+\rho)$, the solution of the equation (2) results in:

$$(5) \quad \left(\frac{d_2}{d_3}\right)^2 = \left[1 - \left(\frac{T}{T_1}\right)^2\right]^2 + \left(\frac{T}{T_1}\right)^2 u^2.$$

Introducing

$$r^2 = \left(\frac{d_2}{d_3}\right)^2$$

and

$$x = \left(\frac{T}{T_1}\right)^2$$

results in the simple quadratic equation

$$(6) \quad r^2 = 1 - 2x + x^2 + xu^2$$

with the resolution

$$(7) \quad x_{1,2} = -\frac{u^2 - 2}{2} \pm \sqrt{\frac{(u^2 - 2)^2}{4} + (r^2 - 1)}.$$

As the requirement states $x \geq 0$

$$(8) \quad x = \frac{2 - u^2}{2} + \sqrt{\frac{(u^2 - 2)^2}{4} + \frac{4(r^2 - 1)}{4}}.$$

The natural period T

$$(9) \quad T = \frac{60}{\text{SPM}} \left[\frac{2 - u^2}{2} + \sqrt{\frac{(u^2 - 2)^2}{4} + (r^2 - 1)} \right];$$

Replacing r with ρ , where $r=1+\rho$, the previous equation results in:

$$(10) \quad T = \frac{60}{\text{SPM}} \left[\frac{2 - u^2}{2} + \sqrt{\frac{(u^2 - 2)^2}{4} + \rho(\rho + 2)} \right].$$

Now it is possible to calculate T for each SPM, ρ and u . For example, Table 1 presents calculation results for SPM=3.5: depending on the water content and different ρ , the period is calculated.

Table 1: Period calculation results for SPM=3.5

Water u	Oil u	SPM	Parameter ρ								
			0,10%	0,20%	0,30%	0,40%	0,50%	0,60%	0,70%	0,80%	0,90%
2,5	0,3	3,5	0,10%	0,20%	0,30%	0,40%	0,50%	0,60%	0,70%	0,80%	0,90%
100%Water	0% Oil	$u=3$	0,372	0,526	0,644	0,744	0,832	0,912	0,985	1,053	1,118
95% Water	5% Oil	$u=2$	0,398	0,563	0,690	0,796	0,891	0,976	1,054	1,127	1,196
90% Water	10%Oil	$u=2$	0,429	0,606	0,743	0,858	0,959	1,051	1,135	1,214	1,288
85% Water	15%Oil	$u=2$	0,466	0,659	0,807	0,932	1,042	1,142	1,233	1,319	1,399
80% Water	20%Oil	$u=2$	0,512	0,724	0,887	1,024	1,145	1,254	1,355	1,448	1,536

Figure 3 presents these results graphically. These calculations are performed for each well and different SRMs in order to understand the relationship between T and u.

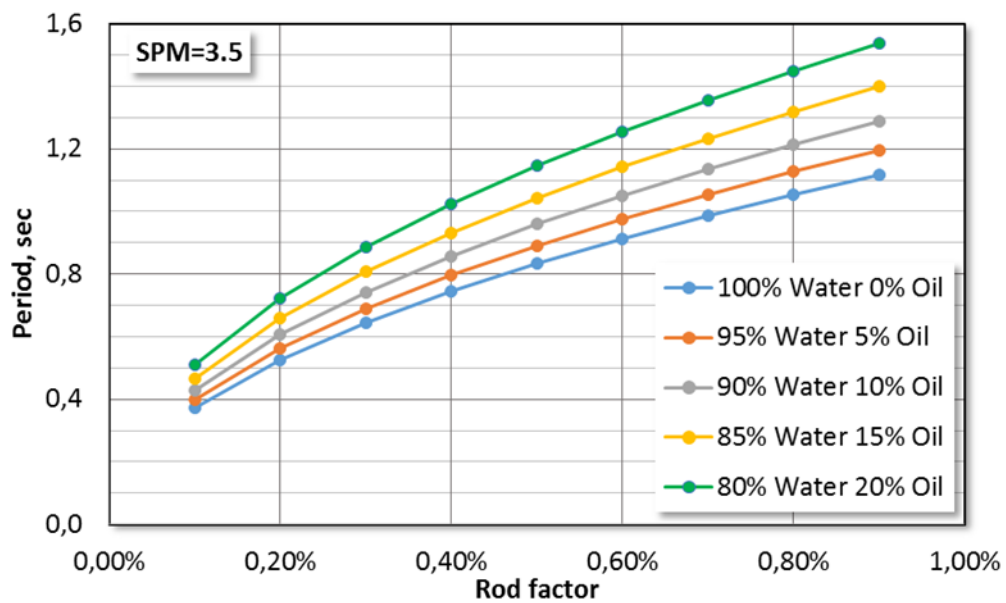


Figure 3: Natural period at SPM=3.5

The dependency of T from the rod factor shows that for the same SPM with increasing of ρ , the natural period decreases, thus the corresponding frequency (that is inverse to the period) increases. Period T is directly proportional to the damping coefficient: with the increasing of water content (and thus increasing of the u) the natural period increases. This, however, results in decreasing of the natural frequency, which is logical as when the damping coefficient increases the rod's frequency decreases (see Figure 6)

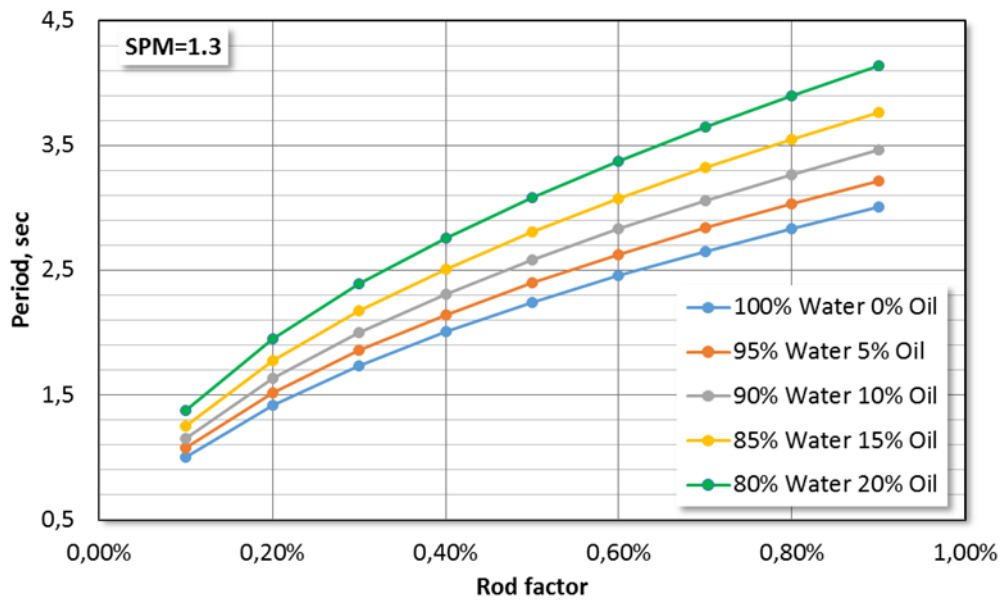


Figure 4: Natural period at SPM=1.3

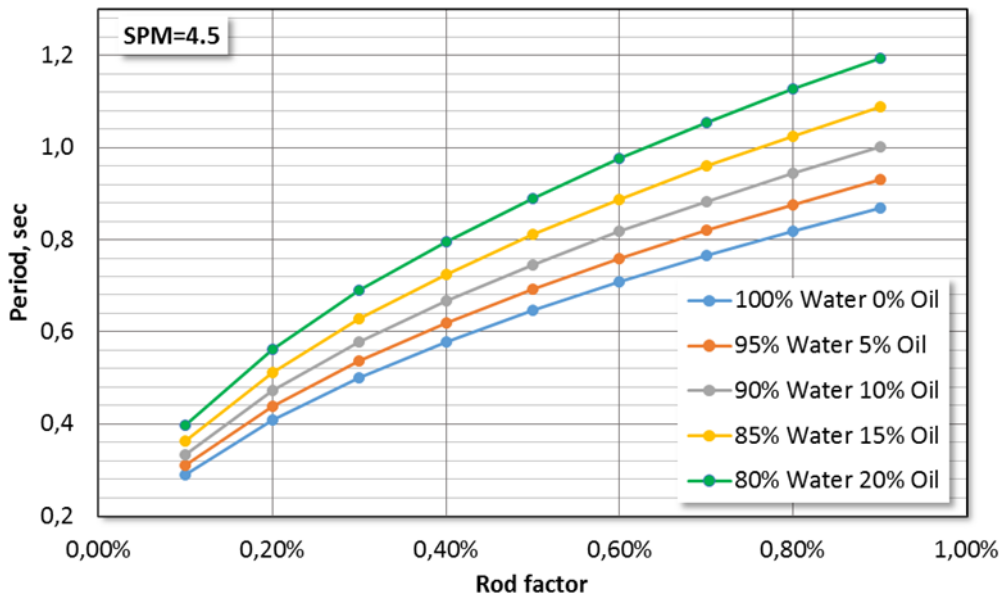


Figure 5: Natural period at SPM=4.5

To observe the relationship between T and SPM, Figures 4 and 5 are presented. They depict periods at the SPM=1.3 and SPM=4.5 correspondingly. The figures show that at a lower SPM, natural periods are larger and at the higher SPM, T is lower. This means that increasing of SPM increases natural frequency (see Figure 6 and Figure 7).

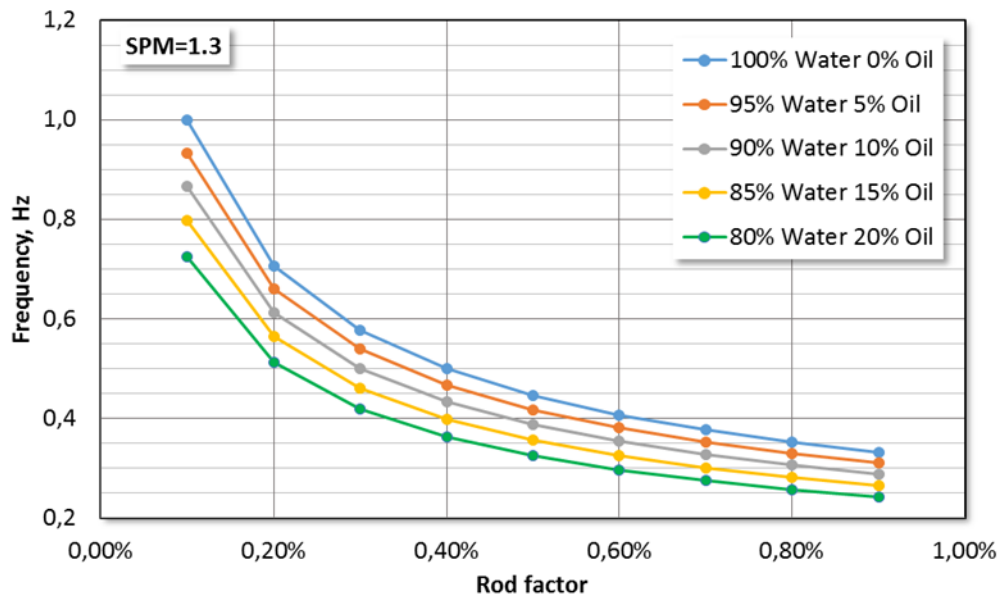


Figure 6: Natural frequency at SPM=1.3

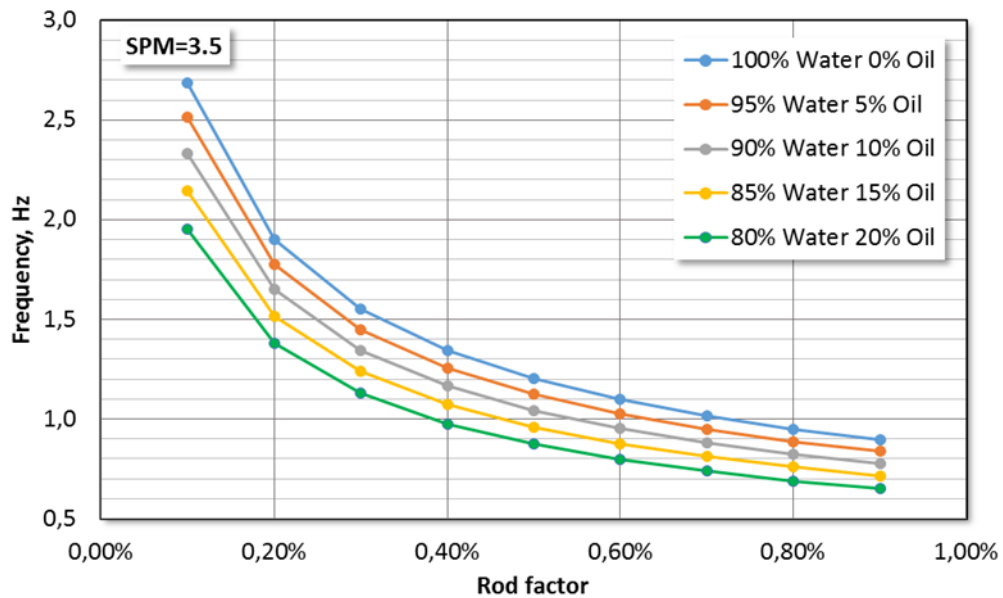


Figure 7: Natural frequency at SPM=3.5

Forced frequency (F_1) in turn, only depends on SPM as shown in equation (4). Figure 8 shows that increasing SPM results in increases of the forced frequency. Calculated natural frequencies have very small values within the range of 0 to 4.5 Hz, whereas forced frequencies lie within 10 to 50 Hz.

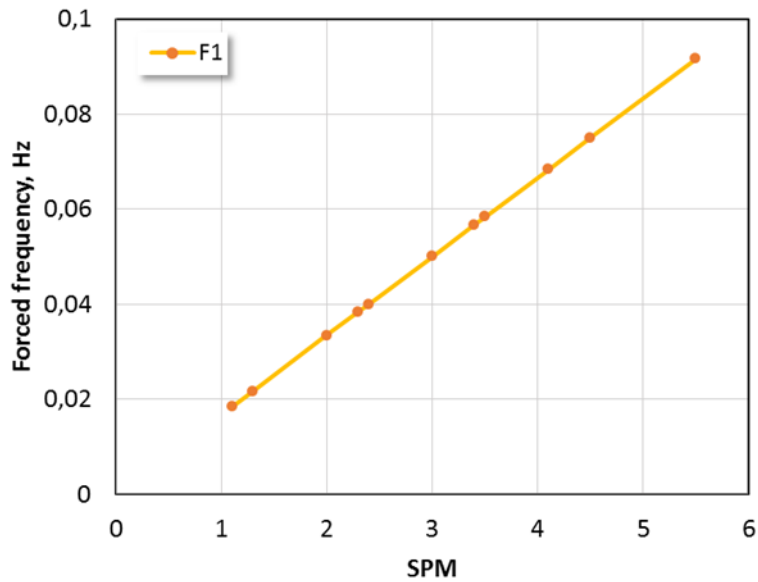


Figure 8: Forced frequency F1 as a function of SPM

2.3 Pump Components

Downhole SRP works on the positive displacement principle, where a piston (plunger) moves up and down in a cylinder (barrel). The barrel has two valves that are situated on the valve seats (Figure 9). One of the valves, normally a ball-valve, is located at the pump inlet (standing valve, SV). It is attached to the tubing and limited in its movement. The SV works as a suction valve. Another valve is the travelling valve (TV), functions as a discharge valve and moves along with the plunger. Both valves serve as check valves and their opening/closing cycle provides displacement of the fluid to the surface. The working principle of the SRP is given on page 25 of Chapter 2.4, How Sucker Rod Pump Works.

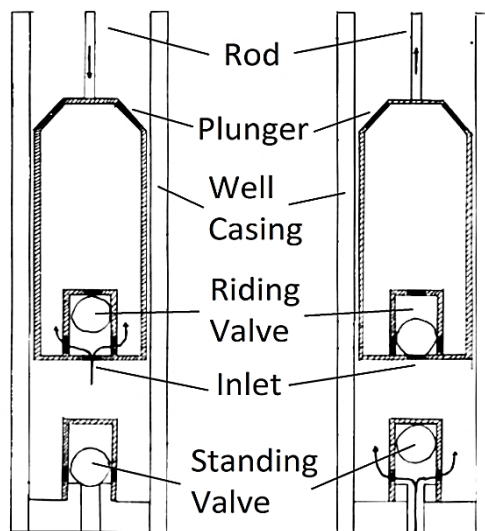


Figure 9: Sucker rod pump, after Tan, 2008 [71]

2.3.1 Barrels

Rod pump barrels are manufactured in different designs: normal, heavy-wall and thin-wall. Heavy-wall barrels are integrated into the tubing string. They meet the total tubing string stress at the setting depth. Heavy-wall barrels possess good retention of shape. A disadvantage is related to the decreased effective plunger area which is smaller due to increased wall thickness. This, in turn, decreases daily production.

Thin-wall barrels are characterized by lower dimensional stability; hence they are shorter in length comparing to the heavy-wall barrels. The smaller wall thickness also makes them susceptible to high differential pressures. The SRP discussed in this thesis are equipped with normal barrels.

2.3.2 Plungers

Subsurface pump plungers are available as

- metal plungers,
- soft-packed plungers.

Metal plungers have no additional sealing elements, therefore the sealing effect is ensured by carefully adjusted tolerance between the plunger and barrel. The plungers can be either pin end or box end, with non-grooved or grooved running face.

Soft-packed plungers contain a sealing element, distinguished depending on its type: ring-type sealing arrangement, cup-type, or combination of ring and cup seal. The sealing is produced from different types of material either leather, rubber-impregnated fabric, or various plastic or ceramic rings, depending on the type of media. The SRP plungers in this thesis are the metal type.

2.3.3 Valves

The pumps use predominantly ball valves, with only a few using ring type valves. The choice of valve material depends on the medium to be produced. Valves with different material combinations, hardness classes and configurations are being used. The most used materials are stainless steel and ceramics. The material of ball seats and the ball-seat combination plays an important role (e.g. stainless seat and ball, ceramic seat and ceramic ball, stainless seat with tungsten carbide insert and stainless ball, etc.). Seals are divided by ball size, i.e., valve seats with a regular ball (normal ball diameter) and valve seats with an alternative ball (smaller ball diameter). All wells discussed in the thesis are equipped with stainless steel balls and ball seats.

2.3.4 Additional Components

Additional components (or accessories) of SRP can also include all kinds of elastic sealing elements, sucker rod catchers, plunger couplings, and rod rotators amongst others. On the observed wells, no additional equipment is used. The SRP well equipment information is provided in Appendix A.

2.4 How Sucker Rod Pump Works

Two main pump valves (TV and SV) are working in the principle of differential pressure. They are one-way check valves, opening when the pressure below is greater than that above the valve. There are the upstroke and the downstroke. On the upstroke, the travelling valve (TV) closes and moves

up, pulling a column of fluid which is equal in volume to the cross sectional area of the plunger (Figure 10). At this point, the fluid load lies on the plunger and sucker rods. On the downstroke the TV opens (when the pressure in the pump chamber is greater than the pressure from the hydrostatic load on the top of the valve); the fluid load is then transferred to the tubing string, pump barrel and standing valve SV. The load carried by the rods is a complex value, composed of the number of loads such as [34]:

- fluid load lifted by the pump;
- pump intake pressure (to give the net load).

During normal pump operation, the plunger of the pump is in the down position and begins moving upward (upstroke) which creates differential pressure across the TV. The valve moves against the pump discharge pressure P_{dis} . This pressure is the sum of the hydrostatic fluid column from the pump setting depth to wellhead P_{hy} , wellhead P_{wh} and pressure losses P_{loss} . That differential pressure causes the TV to close, and a low-pressure area is formed in the void space where the plunger had been. Therefore, a pressure differential forms across the SV. The higher pressure outside of the pump, P_{intkr} forces the SV to open. This allows the higher fluid pressure in the well to be forced into the low-pressure area within the pump, thus filling the void space within the pump chamber with the fluid.

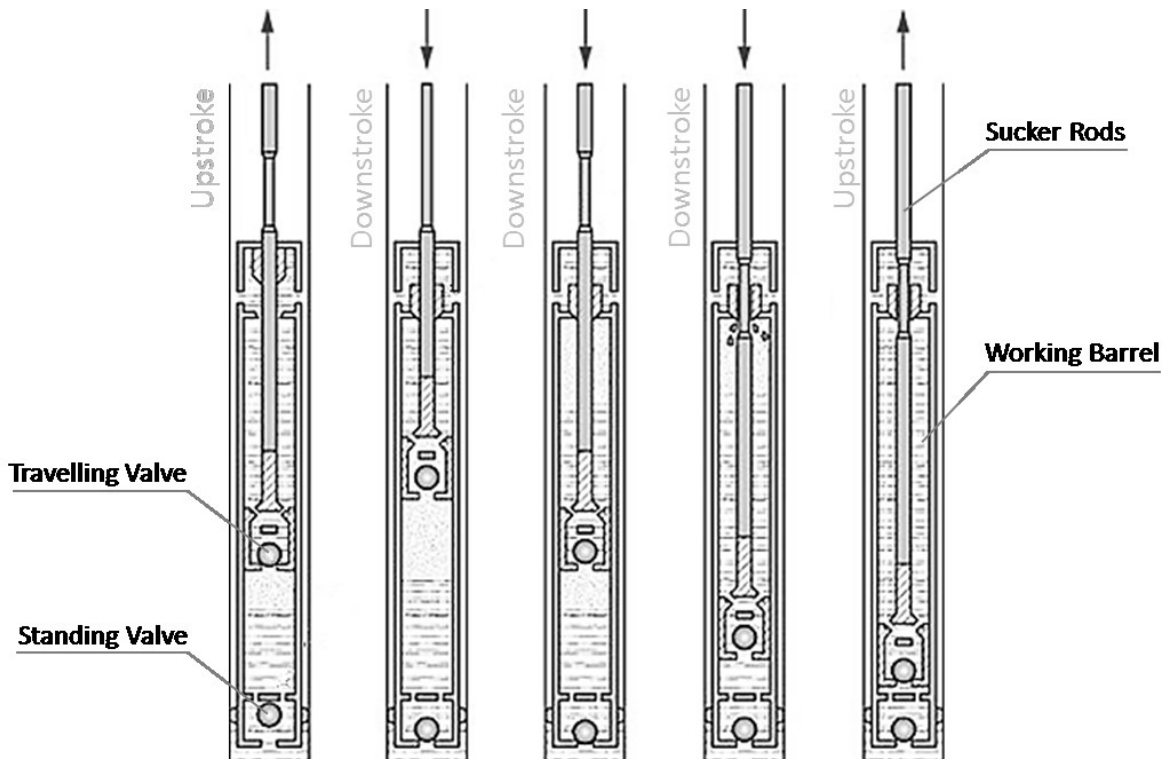


Figure 10: SRP components and pumping cycle, after Lea, 2003 [22]

When the plunger reaches the top of the stroke and starts downward, the pressure inside the pump exceeds the pressure outside the pump, and the SV is forced to close. As the plunger continues downward, it attempts to compress the fluid, thus causing a pressure differential $\Delta P = P_{comp} - P_{dis}$ between the pump chamber and the production column. When the plunger is travelling

downwards, P_{comp} (pressure inside the pump barrel) causes a force F_{up} , which pushes against the bottom of the travelling valve, attempting to open it. When this force is great enough to exceed the force pushing on the travelling valve from the fluid column above the pump P_{down} , the traveling valve opens. Thus, the fluid within the pump barrel is being transferred through the open TV into the production column of fluid above the pump. When the pressure reaches the bottom of the pump, the differential pressure ΔP diminishes to zero, the TV closes and the plunger starts going upwards again, creating a low pressure P_1 within the pump barrel. This opens the SV and allows the fluid from the well to enter the pump.

This is the constant cycle of the sucker rod pump. The regular series of both the fluid load and magnitude change is the major cause of the sucker rod pump system failure. Other factors such as gas pound, fluid pound, corrosion and abrasion only accelerate and promote failures.

2.5 SRP Kinematics

SRP movement comprises of two types of motion: rotation of the crank transformed into progressive motion of the polished rod. The polished rod motion is influenced by the geometry of the pumping unit and torque to speed characteristics. Kinematic laws of the SRP are well researched and their description can be found in many sources like Svinos [58], Knapp [27], among others.

Gray [16] was the first who approached the exact kinematic behavior of the SRP. In his paper he studied the effect of the kinematic factors on the pumping system via applying analogy to the pumping unit from the four-bar linkage, which is normally used in the mechanically driven mechanisms. The involved elements are: the pitman, the crank arm and the walking beam. The four connection points are: the center bearing, the crankshaft, the crank pin bearing and the equalizer bearing (located on the pitman to walking beam connection). An equation to calculate polished-rod motion is presented as follows [16]:

$$(11) \quad S(\theta) = \pm L_5 \left[\cos^{-1} \left(\frac{\frac{L_1^2 + L_2^2 + L_3^2 - L_4^2}{2L_2L_3} + \frac{L_1}{L_3} \cos(\theta R + d)}{\sqrt{1 + \frac{L_1^2}{L_2^2} + 2 \frac{L_1}{L_2} \cos(\theta R + d)}} \right) + \sin^{-1} \left(\frac{\frac{L_1}{L_2} \sin(\theta R + d)}{\sqrt{1 + \frac{L_1^2}{L_2^2} + 2 \frac{L_1}{L_2} \cos(\theta R + d)}} \right) \right],$$

where

$$(12) \quad d = \frac{\pi}{2}(1 \pm 1) - \cos^{-1} \left[\frac{L_2^2 - L_3^2 + (L_4 \pm L_1)^2}{2L_2(L_4 \pm L_1)} \right].$$

In equation (11), the sign \pm shows its applicability to the class 1 (+) and class 2 (-) units (Figure 11). Parameter d (phase angle in rad), defined by equation (12), is the crank angle shift. To determine it, the condition of $\theta = 0$ at the bottom of the polished rod stroke must be fulfilled. For the calculations, angular velocity is assumed to be constant.

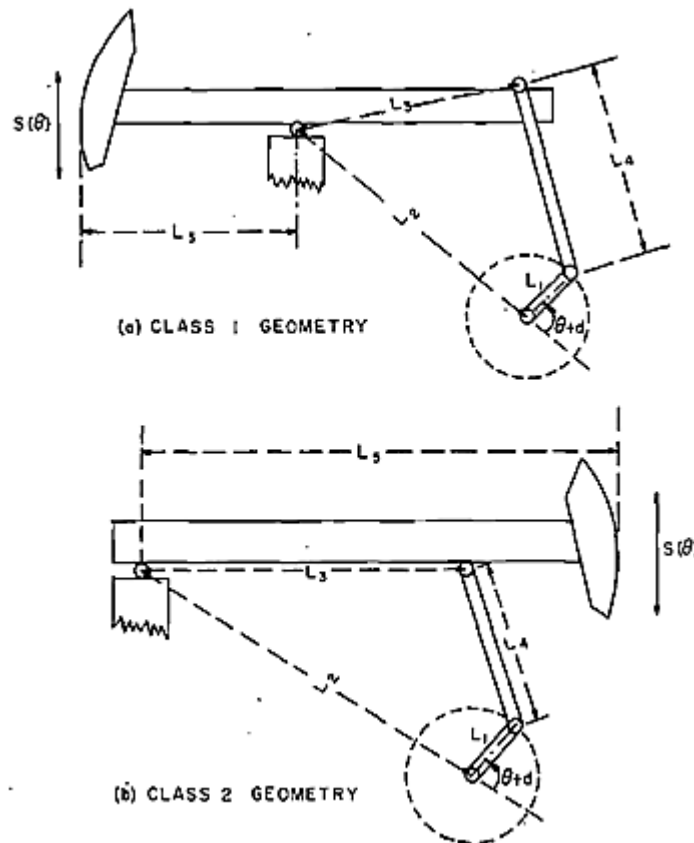


Figure 11: Sucker rod pump types, after Gray, 1963 [16]

Assumptions and conventions for these equations:

- the sign for $S(\theta)$ is positive when the polished rod moves upwards;
- θ is the crank angle (rad), measured from the most lowest polished rod position;
- θ ranges from 0 to 2π for the calculations. Positive direction coincides with the direction of the crank sweep;
- direction of rotation is defined by the factor R , where $R = +1$ indicates rotation of the crank towards to the Sampson post, and reverse rotation corresponds to $R = -1$.

Gibbs [15] defines the following equations to obtain polished rod position versus crank angle θ :

$$(13) \quad u(0, \theta) = L_5 \left[\sin^{-1} \left(\frac{L_1 \sin \theta}{h} \right) + \cos^{-1} \left(\frac{h^2 + L_3^2 - L_4^2}{2L_3 h} \right) \right],$$

where

$$(14) \quad h = \sqrt{L_1^2 + L_2^2 + 2L_1 L_2 \cos \theta}.$$

Grays' calculations are accepted by API and with slight modifications are included into the API SRP Spec.11E [69]. The harmonic motion model and other models based on crank and pitman assumptions, manage to describe the polished rod motion in an acceptable way. Even so, the exact kinematic models describe the motion of polished rod in the most correct manner. Figure 12 and Figure 13 depict differences in these models.

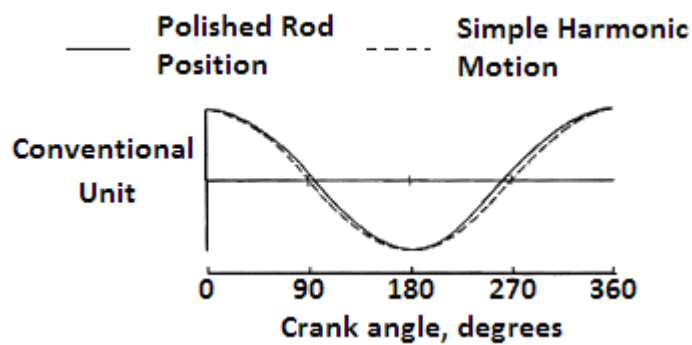


Figure 12: Polished rod motion of conventional units, after Nind, 1981 [41]

Figure 13 shows that the origin of both the up and downstroke is shifted from the crank angles 0 and 180 degrees respectively. This shift is predicted by the presented models and defines crank angle range, which varies for different pumping unit models. Tackas [59] presents formulas that calculate the ranges of the crank angles for units of different geometries.

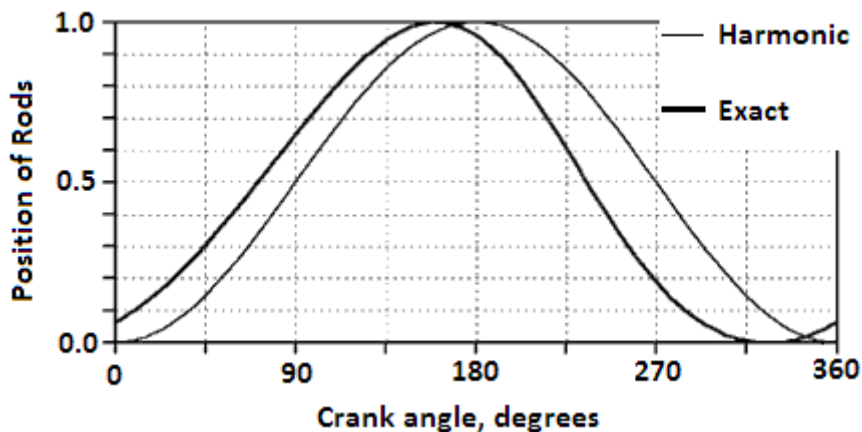


Figure 13: Polished rod motion of conventional units, after Tackas, 2003 [59]

2.6 Sucker Rod Pump Advantages and Disadvantages

Sucker rod lift system advantages [17]:

- high system efficiency;
- optimization controls available;
- economical to repair and service;
- positive displacement/strong drawdown;
- using upgraded materials can reduce corrosion concerns;
- flexibility – ability to adjust production through stroke length and speed;
- high salvage values for both surface unit and downhole equipment.

The disadvantages of the SRP are limited to: relatively low production volume (less than 1,000 barrels per day) and them being often incompatible with deviated wells.

2.7 Sucker Rod Pump Failures

Failures are unwanted events in an operational well, which result in a drop in production rate, downtime and damaged equipment and therefore need to be avoided. A variety of mechanical problems can occur with the SRP system during operation. The need to identify these problems quickly and accurately is essential in order to minimize operating costs and downtime and maximize production.

According to Rischmüller [17] the major sources of pump failure are divided into the following groups of damage:

- inside of the plunger/barrel assembly;
- at the valves;
- in the pump seating arrangement.

To identify damages in the plunger/barrel assembly, it is necessary to note that, in general, any premature wear on the barrel or plunger is related to an incorrect fit. The proper clearance can only be determined by the field tests. Jammed plungers result from an excessive amount of solid particles in the pumped medium; or caused by secondary foreign substances, usually particles which appeared due to the changing of the pump.

Excessive wear on cups or sealing rings of soft-packed plungers is often an indicator of an excessive pressure difference at the plunger. A fracture in sucker or plunger rods, as well as inexperienced handling of pumps during assembly, may cause mechanical damage to the sealing and running faces of the plunger and/or barrel.

Valve failures are mainly caused by excessive or uneven wear due to erosion or corrosion events, resulting from solid particles which have penetrated between the seat and ball. The ball valves which are very heavy, may lead to deformation of the ball face and/or seat face and consequently to bursting the seating ring. The valves and/or valve guides can become clogged by rubber particles or other foreign matter during production due to wear and tear.

2.7.1 Common Rod Problems and their Solutions

In principle, rod failures can be distinguished as forced fractures and fatigue fractures. In practice, most cases of premature failure result from fatigue fractures [17].

2.7.1.1 Causes for rod failure

The type of rod string failures caused by mechanical surface damage is predominantly damage to both threaded connections and to the rod's body. This damage mainly originates during handling and assembly of the rods and during the operation when the rod string moves inside the tubing. Furthermore, any surface damage caused by hammer blows, application of wrenches, improper storage on unprotected steel racks, or knocking against each other because of unsatisfactorily securing rods during transportation, may cause fracture in rods and premature failure of rod strings.

- **Rod string failure caused by flexure of rods.** Any bending of the rods changes the material structure and produces a concentration of stress at these points. Such a fracture is detectable due to the fact that the surface of fracture is not perpendicular to the rod axis. Another cause leading to the flexure of rods is helical buckling.
- **Rod string failure caused by reverse bending stresses.** The motion of the pumping unit induces vibration in the sucker rod string. Since the area of threaded points is more rigid than the rod body, such fatigue fractures occur predominantly near the couplings. These flexures can reach a point where the rods diameter changes and the load carrying cross section of rods or couplings is being reduced. These reverse bending stresses produce increased material stresses in the rod (tensile range) which allow the formation of fatigue cracks.
- **Rod string failure caused by corrosion.** Corrosion is an electrochemical process, which is characterized by the flow of an electrical current due to potential differences of individual materials and is proportional to metal removal at the anode. The occurrence of corrosion causes several types of failures: surface damage (e.g. wrench nicks, hammer marks, scores), insufficient material homogeneity, increased material stresses due to localized plastic deformation, damages to corrosion inhibiting coating and lubricant residue.

2.7.1.2 Buckling

Buckling is the response of the sucker rods to the compressive loads in the string. It is not influenced by the buoyancy force or hydrostatic pressures increasing with the depth, and can only be caused by forces applied to the rods by the pump or external forces. The events that intensify buckling are: the flow through the traveling valve on the downstroke, friction between the plunger and the barrel on the downstroke, dynamic effects in the rod string and tight spots in the tubing.

The degree of buckling depends on both the magnitude and the direction of forces acting on the string. As shown in many sources, e.g. [21] and [27], the effective stress is the parameter that leads to the buckling. In many cases, although the lower part of the sucker rods is in compression, it does not buckle until additional force is applied. To eliminate causes of rods buckling, sinker bars (heavy bars), which tend to keep the rods in tension, are included to the downmost part of the rod string. The main negative consequences of buckling are: scratching in the tubing leading to the walls thinning and extra loads being put on the rods.

2.7.1.3 Rods wear

Wear, flexing fatigue, unidirectional bending fatigue and stress-fatigue failures indicate compressive rod loads, deviated wells, fluid pound, gas interference, highly stressed sucker rods, improperly anchored tubing, pumps tagging bottom, sticking pump plungers, unanchored tubing, or any combination of the preceding [5]. Wear leads to reducing the cross section of the metal parts, exposing the metal surface to corrosion and causing joints to fail through impact and shoulder damage. Wear on the sucker rod string is defined as the progressive removal of surface metal by contact with the tubing [53]. A deviated (or crooked) wellbore usually induces wear that is equal in length, width and depth. The rod string that rubs the unanchored or improperly anchored tubing during fluid pound results in angled wear patterns. Corrosion/abrasion wear usually happens in the middle of the rod body. Wear accelerates the rate of corrosion by removing the inhibiting films and exposing the new metal surfaces to corrosive production fluids and gases. Specially designed hardened materials do not wear quickly and they leave a ridge of material when the rest of the coupling wears.

2.7.2 Sand Problems

Basically, there are two main factors that can cause sand production: the reservoir rock formation is insufficiently consolidated or the flow rate of the pumping medium is too high. The negative impact of the sand on the pump is rapid abrasive wear of the plunger, the barrel and valves, jamming of the plunger, or "cementing" of the pump into the seat or into the tubing string.

The following measures can be employed for the pumps protection [17]:

- installation of a slotted liner or a sand filter;
- utilization of a gravel pack;
- protective measures at the pump;
- solidification of the sand at the formation (consolidation).

2.7.3 Free Gas

Fluid that contains free gas is one of the major problems in oil production, as it releases free gas which leads to production difficulties later. It has the most apparent effect on the pump's efficiency. Efficiency here means the ratio of the fluid volume delivered with each stroke to the volume of effective plunger displacement. Moreover, appearance of free gas directly contributes to higher lifting costs, as well as indirectly accelerating the deterioration of surface and subsurface equipment. The problem of free gas in the pump is also called gas lock.

As explained in Chapter 2.4, SRP works by the principle of differential pressure. Any delay in opening or closing one of the valves reduces the pump volumetric efficiency. The pump efficiency is a function of the pumped free gas/liquid ratio. Presence of free gas affects the pump volumetric efficiency by losing part of the pump stroke in the up and down cycles as follows:

(1) The amount of free gas enters the pump on the upstroke and occupies a percentage of the area vacated by the plunger - depending on the amount of the free gas. On the upstroke the standing valve does not open (i.e. the fluid does not enter the pump) until the formation pressure exceeds the pressure between the standing and travelling valves. If this space is occupied by the

gas, the pressure in that area falls gradually as the plunger moves upward. The standing valve does not open until part of the stroke is lost due to gas compressibility (Figure 14, right).

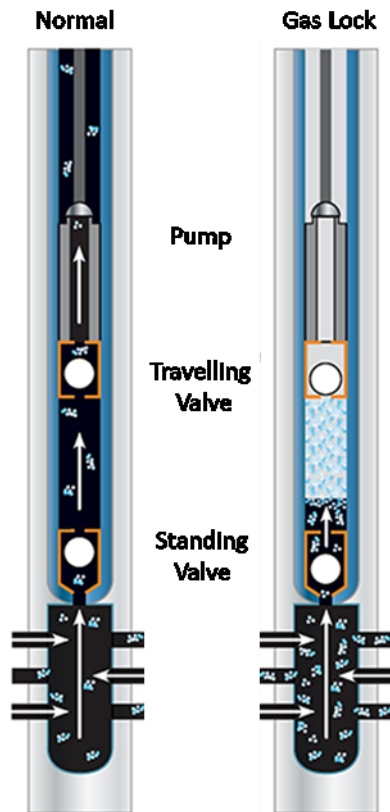


Figure 14: Free gas example, after Kudu Industries Inc.

(2) On the downstroke, the pressure in the pump chamber is insufficient to open the travelling valve. As result, the plunger moves downwards a certain distance, depending on the amount of free gas in the barrel, until enough pressure builds to open the valve. In this operation, part of the downstroke is absent. In the event that the necessary pressure difference is not reached, the TV does not open and the pump is “gas locked”.

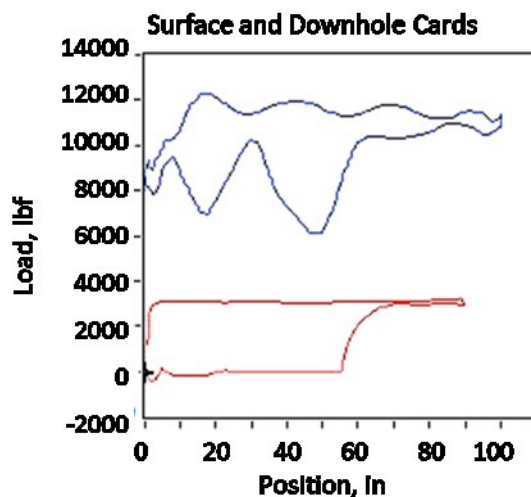


Figure 15: Surface and downhole card of a pump with the free gas, after Sage Technologies, Inc.

In order for the well to produce at optimum efficiency, the presence of the free gas has to be identified and reduced. A dynamometer card of the pump operating with the free gas is shown in Figure 15.

There are two main recommendations of how to produce a well with high GOR. The first is to achieve the highest pump volumetric efficiency. The free gas then is prevented from entering the pump by gas separation (gas anchors). The second approach is to handle the gas through the pump by applying correct pump design, which allows the travelling valve and standing valve to operate properly (multiphase pumps, special design SRP for gas handling).

2.7.4 Paraffin Precipitation

Paraffin precipitation is one of the major problems occurring in fields of RAG. It cuts oil production, shortens the rod's life and results in downtime. Paraffin appearance is defined by the cloud point, which determines the potential of the fluid to develop paraffin precipitations, and is the temperature at which the first crystals of wax appear [9]. Pressure and pressure drop have high influence too: as pressure decreases, the melting point also decreases. This effect is related to a fluid property called solubility.

The process of paraffin build up can be explained as follows. It precipitates from the oil if there is a change in the equilibrium conditions. A reduction in temperature is the most common cause, but there are many other factors influencing paraffin precipitation. Once a pressure difference is introduced into the well after drilling, the melting point of the reservoir fluid is changed, and orthorhombic shaped waxes are formed and carried in the oil. These wax crystals trap oil molecules and create a gel matrix which traps other wax crystals [45]. When the temperature decreases, the gel structure hardens at the tubing walls. Wax aggregation over time leads to a reduction in the tubing diameter and thus, a decrease in production. In cases of severe paraffin problems, the sucker rods might become jammed. To prevent this, RAG injects special inhibitors that change the physical structure of paraffin. Treated in this manner, paraffin and asphalt particles tend to adhere less to metal surfaces. To fight paraffin precipitations, well treatments are conducted regularly. These treatments are: hot water treatment (when hot water is pumped into the well to melt and wash away paraffin), and condensate treatment (to change the chemical composition of the oil and dissolve paraffin and asphalt). Both of these methods are currently used in RAG. Other methods to prevent and fight paraffin precipitations are: use of different solvents (ethyl benzene, benzene, BETX, etc.) and suspenders (e.g. Paraspere).

2.7.5 Knocking Travelling Valve

The knocking down valve is also named the ball dance [47]. The term ball dance describes a situation where the plunger is forced into the barrel and results in striking the TV. During each stroke, the valve opens and closes repeatedly. The ball can land to the left, then to the right the next time, seeming to "dance" on its seat. As the travelling valve is knocked severely by the fluid flow, it frequently chips both itself and the entire sealing surface. Once the seal is chipped, the sealing between the ball and the seat is lost; the pump must then be pulled out and repaired. Increasing the ball mass is one option to reduce the occurrence of the ball dance; this is because a ball of a larger mass requires larger forces to displace it [47].

2.7.6 Pumped-Off Well

Pumped-off is a common operational state for a well during its production life. This state refers to a situation when the SRP operates so fast that the dynamic fluid level drops below the pump intake. The two figures below show how a pumped-off (POF) operational state can be recognized with the help of dynamometer cards. Figure 16 corresponds to the pump with the high DFL.

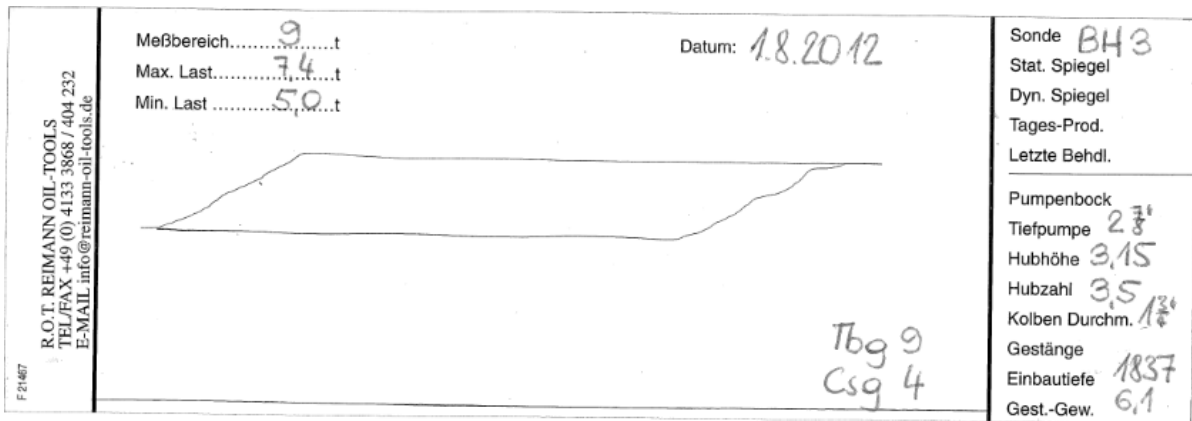


Figure 16: DC of normal operating pump with SPM 3.5

The DC shown in Figure 17 is taken at the moment when the well is pumped off. The main indicator of the POF state is that the shape of the dynamometer card has a missing lower right-hand corner, but two horizontal features are still parallel.

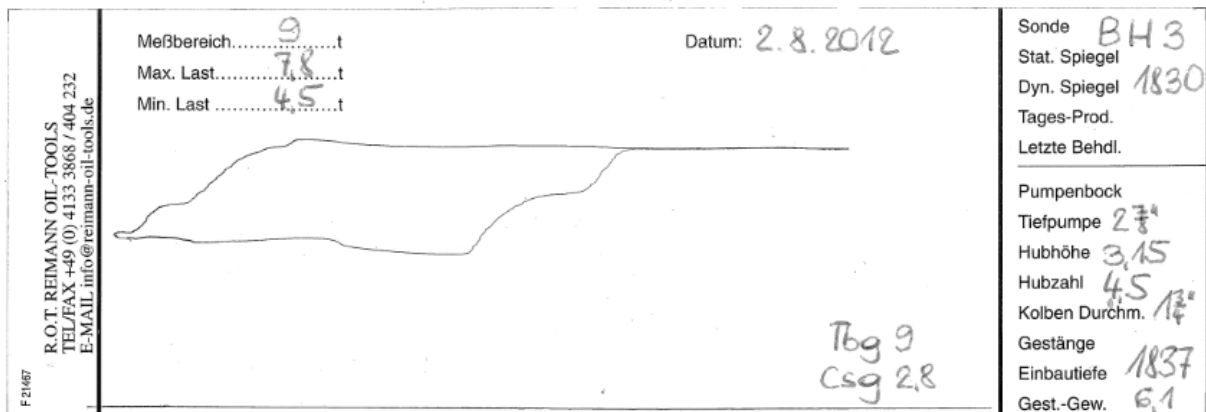


Figure 17: DC of the pumped-off well with SPM 4.5

On one hand, the pump-off operating state applies excessive wear and tear on the rod pumping equipment while wasting power. On the other hand, a well reaches maximum production when the pump lifts up all volume that the reservoir supplies. A specialized tool, the pump-off controller (POC), is used. It operates by stopping the unit when the DFL at the level where the pump does not produce fluids anymore. The major disadvantage of the POC is that it cannot reflect the downhole situation in real time, and it reacts after the incident has already happened.

Since the POC is primarily used as an on/off type of control, the constant attempt to overcome the coefficient of static friction (when starting and stopping the rod string) causes extreme wear and tear to the rods and causes them to break sooner. The rod string experiences the highest stresses

during this period. Using the approach to predict the pumped-off situation by applying knowledge about how pump sound changes as the well becomes pumped-off can save money, operational equipment and ensure wellbore integrity. Corresponding DC and sound data will be used for the analysis in order to obtain sound features that indicate pumped-off state.

2.8 Production Data

The major focus of this thesis is to find a correlation between a well state and its sound. A well's production history records all changes in the well. It includes all registered events, failures and system changes that can be important to the research. Well history is built from the RAG production reports and conversations with the field engineers. All production data is sorted out and labeled according to several indicators: events, observations, rules and snapshots.

- Events are occurrences that are initiated around and inside the SRP system. The following indicators are referred to as events: paraffin (indicated by production engineers), scheduled and forced well and pipeline treatments (hot water treatment or condensate treatment in order to illuminate or prevent paraffin precipitations), change of the pump or the pump jack (any equipment in general), or the Murag sensor exchange.
- Rules are related to the production information and describe the system design. Examples of rules are: SPM number, pump type, pump installation depth, pump motor type, pump jack type, Gond-40 sensor type, identified leaking valves, oil and gas production rates, DFL, casing and tubing pressures. Rules are applied to a number of sound files and describe the operating conditions under which the SRP is being operated and sound recordings are being collected.
- Snapshots are the system conditions captured at a specific moment in time. Examples of the snapshots are: pump switched on or off, well being pumped-off, DC taken at certain time moment, measured SPM. The time of sound recordings is three minutes ahead of the time at the RAG production systems. This important fact is taken into account for the data correlation. In order to adjust times of all sampled data, the time tolerance (1, 2, 3, and 4 minutes) is introduced. It assumes different time shifts applied for the data acquisition.
- Observations are manually created labels used to describe sound files. For QC reasons and to better understand the nature of sound, thousands of files are analyzed and characterized. The principle of file differentiation includes visual and audial assessment. In order to optimize this process and make it standardized, observations (labels) are created. As result, each sound file is represented by a set of descriptors. This will be described more fully in Chapter 4.6.2, Labels for Quality Control.

All production information is fed into the managing file Audio Collector and actively used for data processing.

2.9 Audio Collector File

The Audio Collector file is one of the main working instruments created in “.xlsx” format. This tool serves as the principal file manager. It gives an overview of sound data, allows data management and visual interpretation. The Audio Collector contains lists of all available sound files, their characteristics, calculated statistics, labeling and different plots. With the aid of the Audio Collector

it is possible to count the number of files in different states for different time frames, correlate them with the production and workover operations, SPM and others.

Figure 18 to 20 portray a summary of each well according to the production events and provide the data presentation in the most favorable way. The figures provide a complete overview of the wells, obtained sound recordings and production states. The Audio Collector creates libraries of sound files for each well, which contain links to all other types of data (audio, dynamometer cards and others).


In all the figures, the abscissa presents the dates of the research from January 2011 till August 2013; the right ordinate axis indicates the sampling frequency in kHz and the duration of the sound recordings in seconds. Events and Rules are grouped in the upper part of the figure. For well BH-003 they include: pipe treatment on 30 November 2011, pumped off operational state on 07 August 2012, well treatment on 04 March 2011. Available DCs are marked with the sign  and also contain DC interpretation. The figure also contains information about changes in the sampling frequency of the recordings (F_s , red solid line), where it is from diminished 48 kHz to 24 kHz in order to decrease recording memory. Sound files recording length (RecdLen, dark blue solid line and dark blue spots) changes several times. Large red dots at the bottom represent SPM information. As shown, SPM changes many times: from 4.3 in January 2011 to 3.4 in July 2011, 3.3 in January 2012 down to 3.1 in August 2012 and 4.4 in June 2013. The figure contains information about the pump, motor and jack type. For well BH-003 they stay the same during entire observation period.


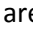

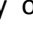
Figure 19 shows the production history of well BH-009. Well treatments () , pumped-off well condition () , pipe treatments () and observed paraffin precipitations () are marked and dated correspondingly. The production history of this well is enhanced with different events, which introduce more operating states for comparison. The sampling frequency of the recordings is maintained at 48 kHz until reduced to 24 kHz in November 2012. Recording length varies from month to month and is noted with a dark blue solid line (as in Figure 18). SPM value for this well keeps at 3.5. QC information is also presented and shows that almost 50% of files are classified as good quality (useful). Similar to Figure 18, Figure 19 contains history of the well from January 2011 till August 2013.

Figure 20 contains summarized production and recordings information from well V-041. Contrary to the other wells, V-041 experienced changes to the surface and downhole equipment as follows: the pump is changed on 12 March 2012; the pump motor and the crank are replaced on 07 May 2012; the Murag is substituted on 23 January 2012; all of which might lead to changes in the sound recordings. If there are significant changes, the files before/after need to be treated and analyzed separately. Well V-041 has the greatest amount of DC (54 in total), which are taken in different pumping conditions. For example, several of the measurements are taken when the well is pumped off, or the TV leaks. The sampling frequency is the same as in to the other two wells and in November 2012 reduced from 48 kHz to 24 kHz. There are some variances in the recording length (dark blue dots), but mostly stay the same. The QC overview shows that about 50% of the files are recognized as not usable. The SPM of the well changes several times: from 2 (in 2010) to 5.5 (in March 2012), then to 1.3 and 2.1 (in May 2012) and increases to 3.1 in August 2013.

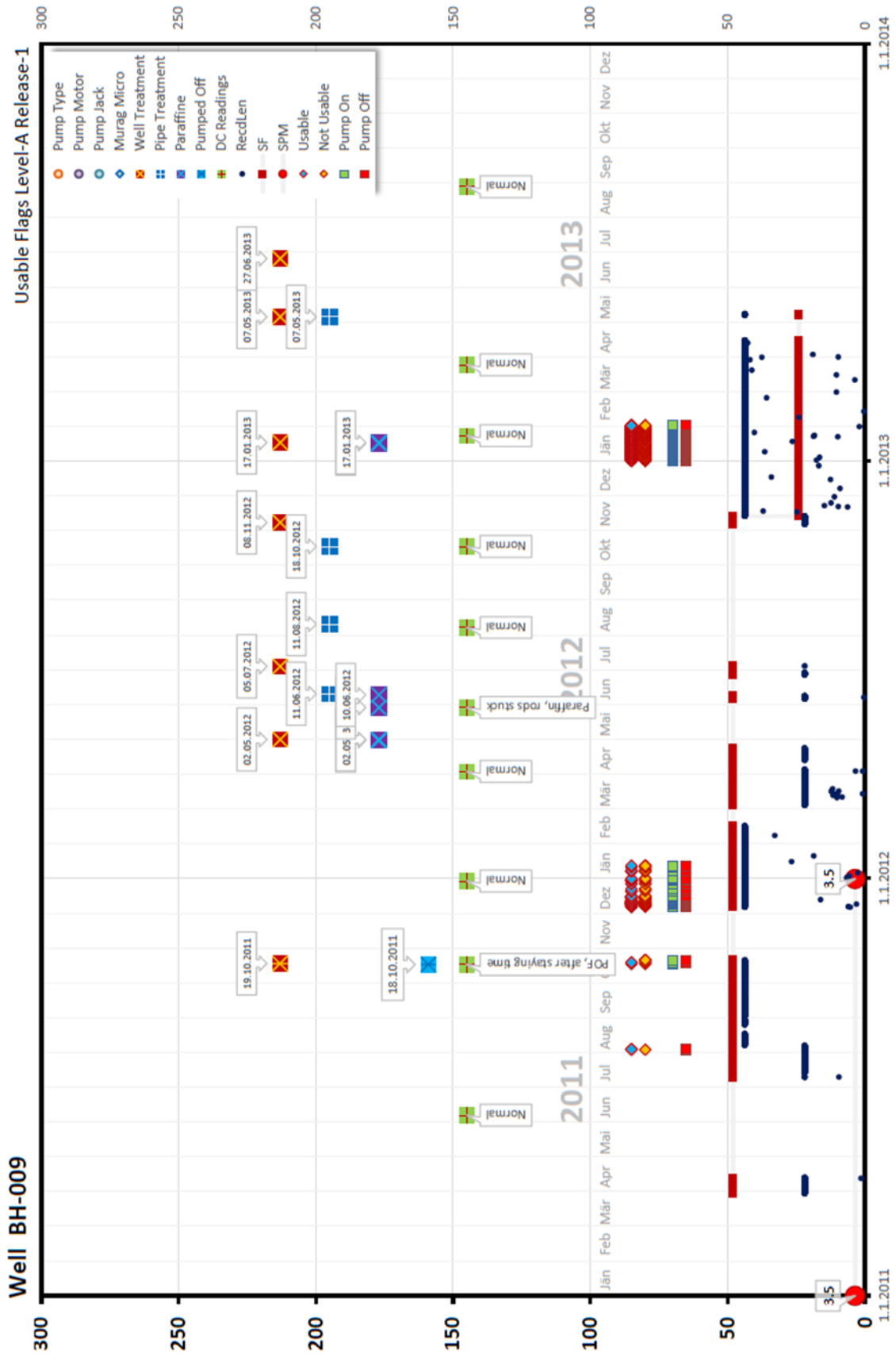


Figure 19: History of well BH-009

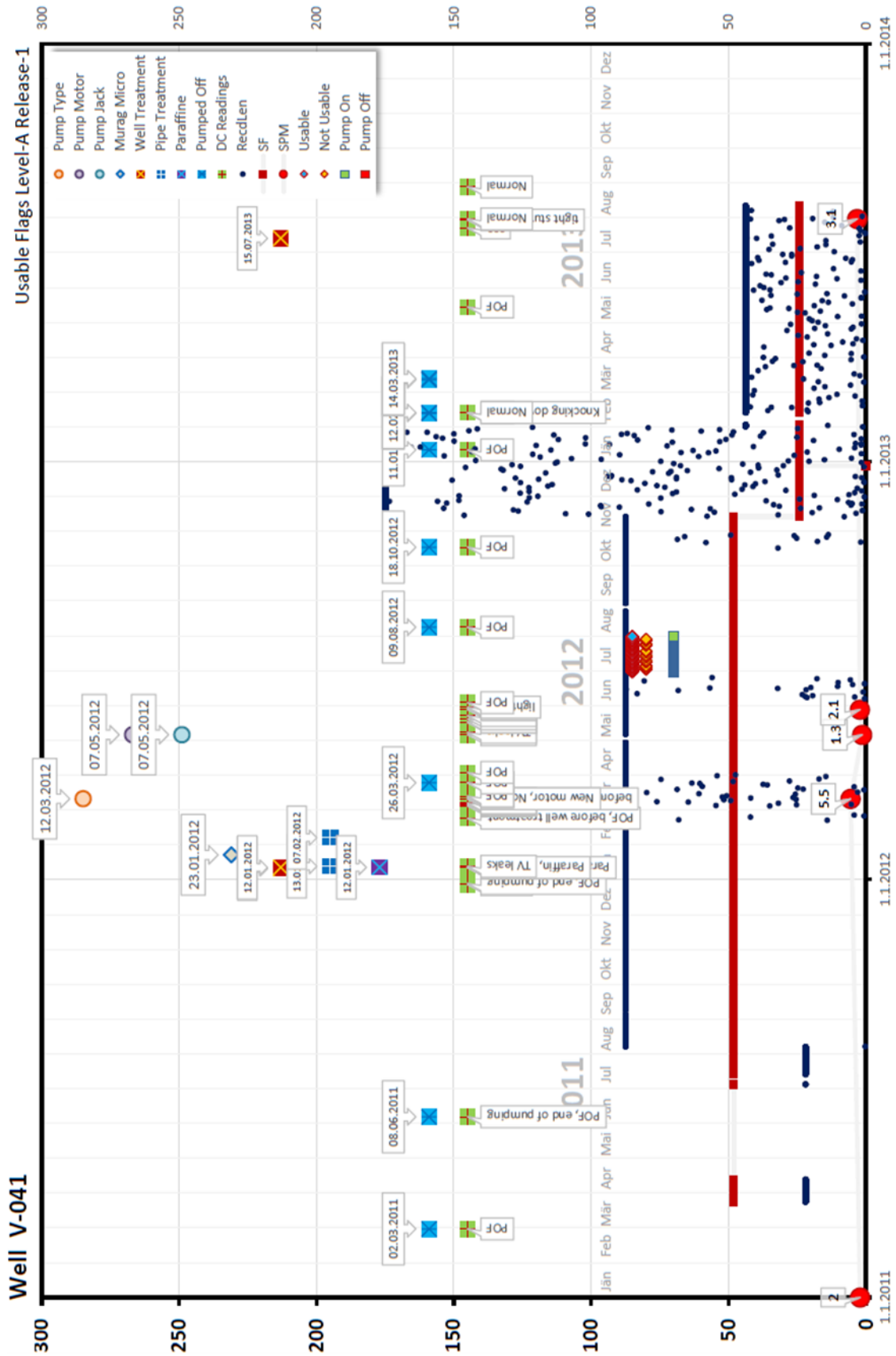


Figure 20: History of well V-041

In addition to the information shown in Figures 18 - 20, the tables in Appendix B, Appendix C and Appendix D, offer production information collected for each well in a more enhanced form. These tables contain information about completion, exact dates of equipment change (pump, Murag microphone, others) and a list of dates and times when the pumps are switched off and on. Information about the well's depth and trajectory, size of casing and tubing, diameter of rods and size of pump, is essential to search for patterns in sound behavior similarity. The type of tubing used in the three wells is different: BH-003 has polylined (polyethylene lined) tubing and wells BH-009 and V-041 are equipped with the steel tubing. It is expected that the sound damping coefficient is different depending on the type of tubing. In general, all completion data (such as well depth, pump depth, tubing diameter, etc.) are of importance and will be counted in further research in order to find patterns for well depth and sizes versus produced sound.

3 Dynamometer Cards

Dynamometer cards (DC) are well-known and widely used in the petroleum industry. DCs are a robust method to identify the SRP state and monitor pump and well behavior, as they can indicate the operational condition of the system (broken pump, valve leakage, fluid pound, gas lock, etc.). DCs acquired for this research illustrate various pumping conditions: pumped-off, paraffin, leaking travelling valve. The research theory assumes that changes in the SRP state (and, hence, in DC) lead to changes in emitted sound and this relationship can be captured. The sound recordings are correlated with the dynamometer cards over the pumping cycle (stroke). For this correlation, the DC data need to be properly prepared to include: DC acquisition, digitization, DC quality control and DC features extraction. This chapter discusses these steps in detail, including how to depict DC data in the most suitable way to reach the thesis goals.

3.1 General Information

Dynamometer cards are the written interpretation of the dependence of the load taken with the rod string to the plunger displacement. Figure 21 demonstrates a theoretical load cycle (for elastic sucker rods), which is considered as an ideal dynamometer card. This image shows a DC corresponding to unanchored tubing and pumping liquid without gas. In the figure: MPT – maximum plunger travel; EPT – effective plunger travel; F_0 – differential load on plunger (fluid load).

In the figure, the MPT is the maximum length of the plunger movement with respect to the length of the pump barrel during one stroke. The fluid load F_0 is a force caused by differential pressure acting on the pump plunger. The differential pressure acts across the travelling valve on the upstroke and is transferred to the standing valve on the downstroke. The differential pressure is the difference between the pressure caused by the tubing fluids and the pressure in the wellbore.

From point A to point B, the fluid load is fully carried by the tubing. Once the rod gradually transfers point A to point B, the load also transfers as the rods stretch to take up the fluid load F_0 . The standing valve begins to open at A, allowing the fluid to enter the pump when the pressure in the pump drops below the intake pressure. From points B to C the rods carry the fluid load along, then the TV closes at C. The plunger starts moving downwards and the TV remains closed until the pressure inside the pump is slightly greater than the pump discharge pressure. From C to D, gas in the pump (if present) is compressed as the plunger goes down to increase pressure on the fluid pumped from the intake pressure to the static pressure in the tubing. Once the fluid in the pump is compressed, the fluid load is gradually transferred from the rods to the tubing. At D the pump

discharge pressure is equal to the static tubing pressure and the TV opens. From points D to A, the fluid in the pump is displaced through the TV into the tubing. The tubing carries the fluid load when the SV is closed. The effective plunger travel (EPT) is the length of the run of the plunger when the full fluid load is acting on the SV. This is the description of one cycle of the pump run with an unanchored tubing (EPT<MPT).

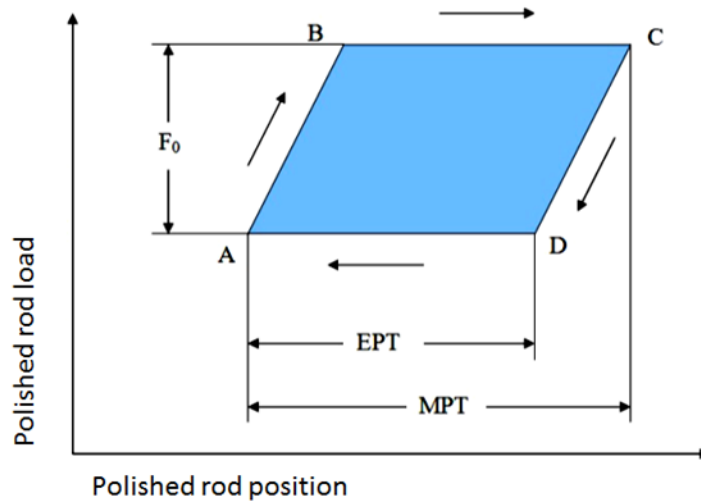


Figure 21: Ideal dynamometer card

At the same time as extracting the DCs, the valve checks procedure is normally obtained to determine the condition of the valves. Valve checks are applied for both TV and SV. Examples of how DC reacts on different operational states and problems in the pump are shown in Chapter 2.7, Sucker Rod Pump Failures.

3.2 Dynamometer Cards Acquisition

The DC acquisition is held by RAG field engineers according to the schedule of the company. Mostly, DCs are collected with the help of a mechanical dynamograph in analog form (example is shown in Figure 22). There are few DCs acquired in the digital form.

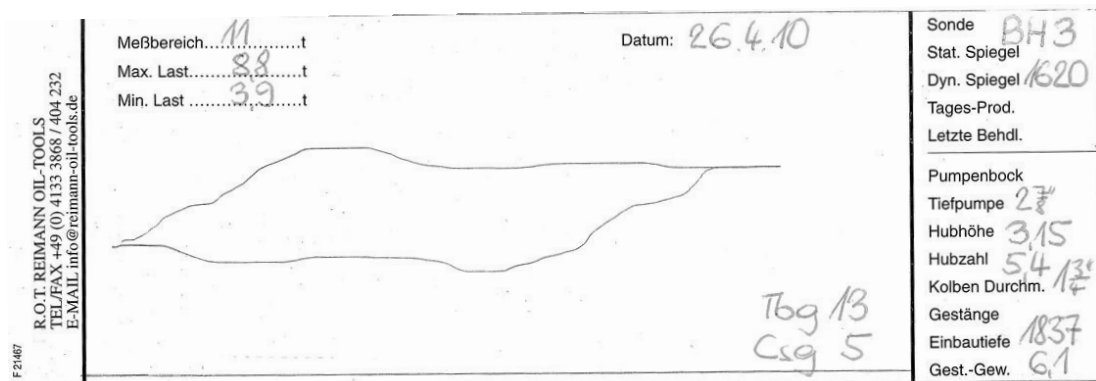
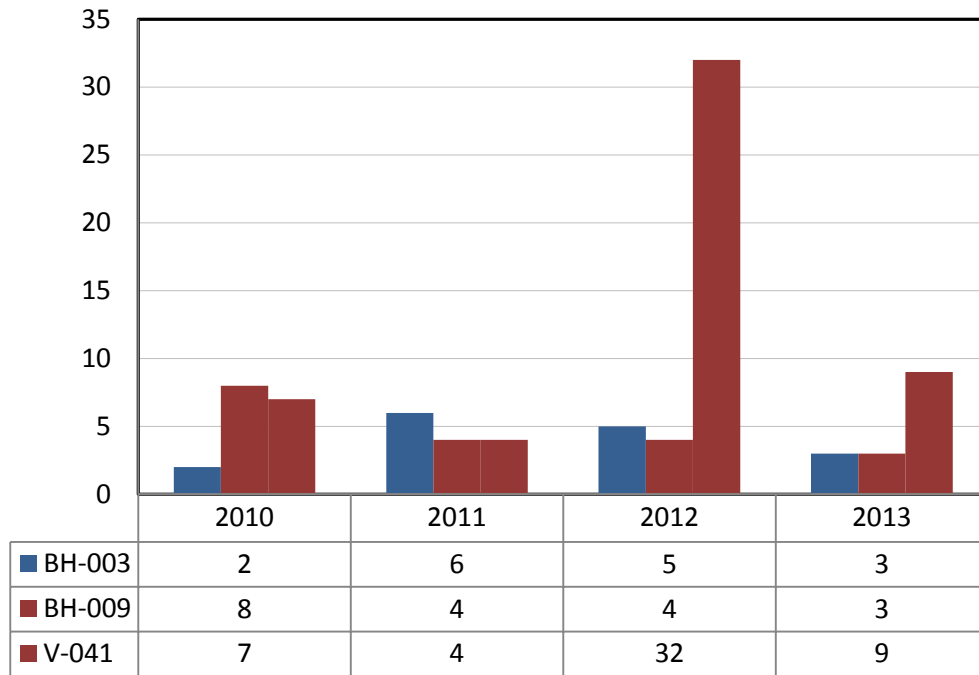


Figure 22: Example of analog dynamometer card from the well BH-003

Table 2 contains information about collected DCs. Appendix E on page 121 encloses interpretation of DCs regarding well and pump states together with their notation used in this work.

Table 2: DC amount per well, per year



For the goals of the research, the ideal case would be to have one DC per sound file recorded simultaneously. In this case a dynamometer needs to be always available at the well or permanently installed. In practice, it is possible with the use of special rod pump controllers or automated well managers, WM (e.g. S.A.M., or L.W.M. from Lufkin), which are widely available on the market. Such equipment can assure higher quality of the DC data, and WM can be coordinated with the Gond-40.

3.3 Harmonic Motion of the Rods

Chapter 2.4, How Sucker Rod Pump Works, discusses the harmonic nature of the SRP motion. To check whether the existing pumping units in wells BH-003, BH-009 and V-041 follow this law, the equations of Gibbs [15] and Gray [16] are applied to their geometry. Table 3 includes information about pumping units. For wells BH-003 and V-041, which are equipped with the Lufkin Conventional pumping units, corresponding information is extracted from the official catalogues of the Lufkin Company “2008/2009 General Catalog Lufkin” [72]. Parameter L_2 (orange solid line in Figure 23) is not given in the catalog and can be calculated as:

$$(15) \quad L_2 = \frac{H - G}{\sin \alpha}$$

with

$$(16) \quad \alpha = \arctan\left(\frac{H - G}{l}\right).$$

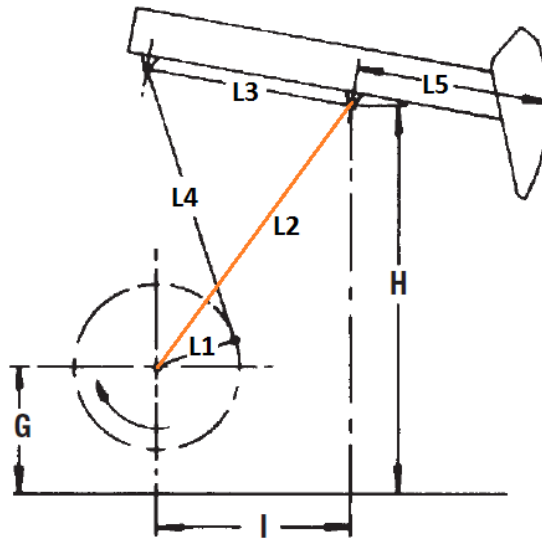


Figure 23: Geometry of the Lufkin Conventional pumping unit, after Lufkin [72]

The pumping unit in well BH-009 is manufactured by another company and the geometry is taken from the design sheets provided by RAG.

Table 3: Geometry of the pumping units

Well	Unit	L1, in	L2, in	L3, in	L4, in	L5, in	H, in	G, in	l, in
BH-003	C640D-365-144	41	158.7	120.0	148.5	180	262	111	120
BH-009	SBS D-1074	-	-	105	-	108.3	185.4	-	114.2
V-041	C320D-256-120	36	144.6	111.1	132	155	232	96	111

Equations (11) through (14) calculate polished rod position versus time. These data are plotted against theoretical harmonic motion and all of them are compared to each other. Figure 24 indicates that the pumping unit of well BH-003 follows the harmonic motion, although it is slightly shifted. Calculation results of Gray and Gibbs equations coincide.

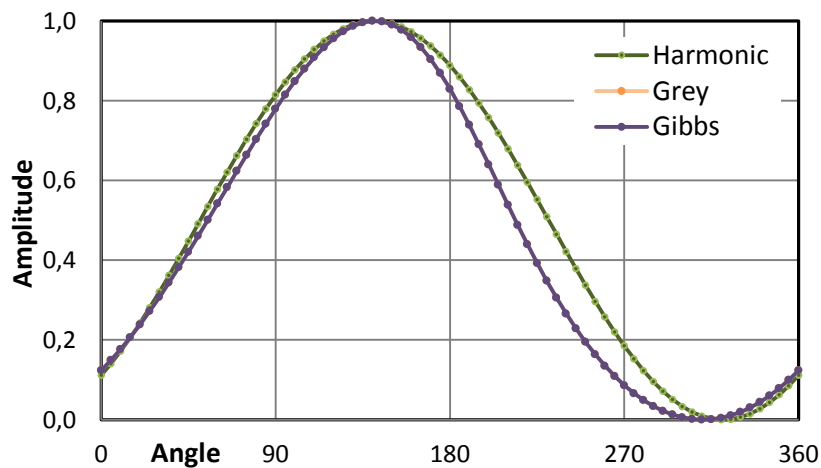


Figure 24: BH-003 polished rod vs crank angle motion

The polished rod motion behavior of the calculated exact kinematic models is similar to the exact motion shown in Figure 13 in Chapter 2.5, SRP Kinematics. Thus, pumping units of all pumps obey laws of harmonic motion as shown in Figure 24 and Figure 25. This assumption is taken for further DC processing.

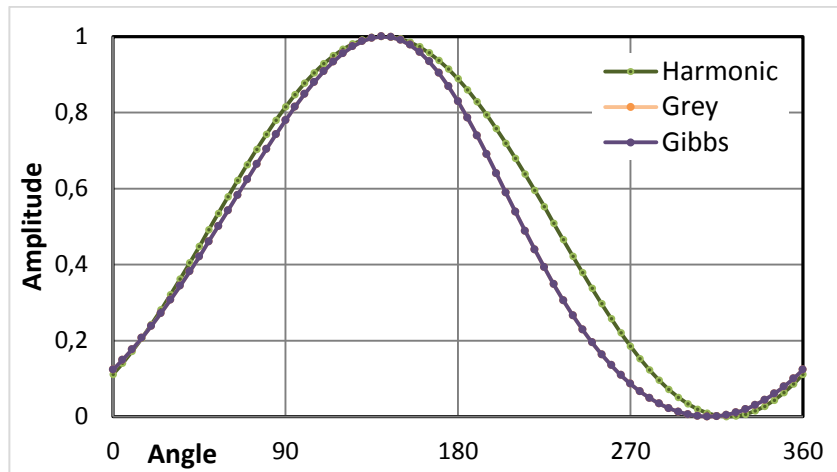


Figure 25: V-041 polished rod vs crank angle motion

3.4 Dynamometer Card Preparation and Quality Control

DCs for the thesis are supplied in the analog form (Figure 22). To facilitate the work, all DCs are digitized. Digitization of the DC means that the acquired cards are transformed into load versus stroke in the form of relative coordinates (Figure 26). The max and min loads are given by the analog DC. The procedure of the digitization points out a presence of tilted x axis (stroke position), as seen in Figure 26. After digitization the DC data are rotated around its center (0, 0) to achieve the straight abscissa.

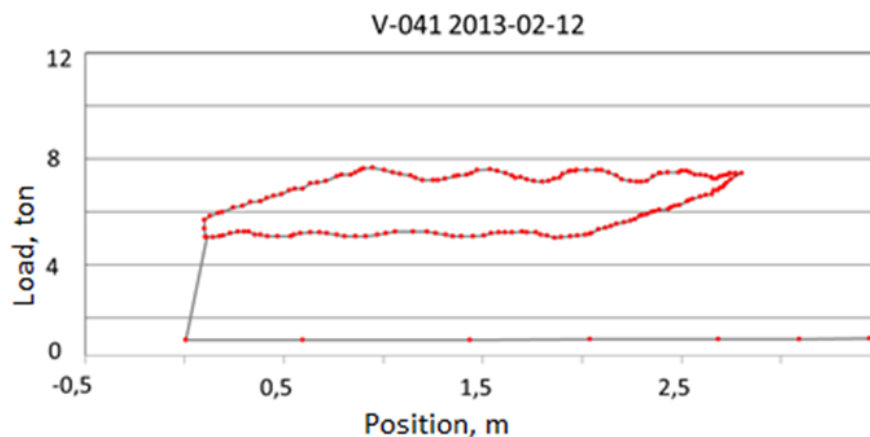


Figure 26: Example of digitized DC

Rotating of digitized DCs change the image tint and provokes errors in max and min load values. In many cases, both of the new values have an induced error. To correct the digitization process the least sum of errors (for x and y axes) approach is assumed. All DCs are checked and those with the

sum of absolute errors less than 5% are accepted. Figure 27 shows an example of the final DC after digitization and correction.

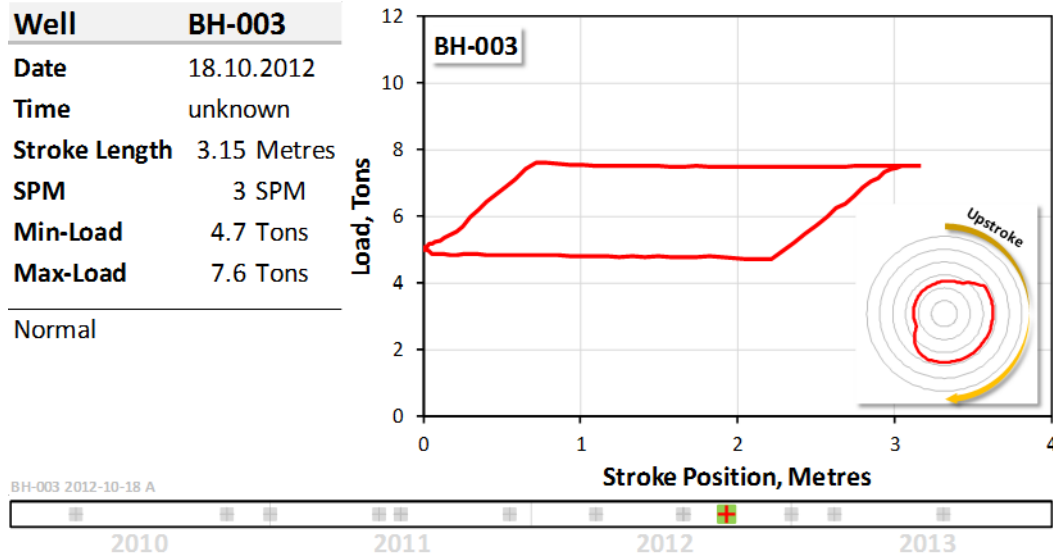


Figure 27: Example of digitized and corrected DC

After the DCs digitization and correction, they are interpolated in order to standardize DC data to 120 points. This number is chosen according to the settings of digital dynamometer and considered to be sufficient. DC visualization as load versus displacement flared-out graph (shown in Figure 28) is advantageous ways of DC interpretation when correlating DC and sound data.

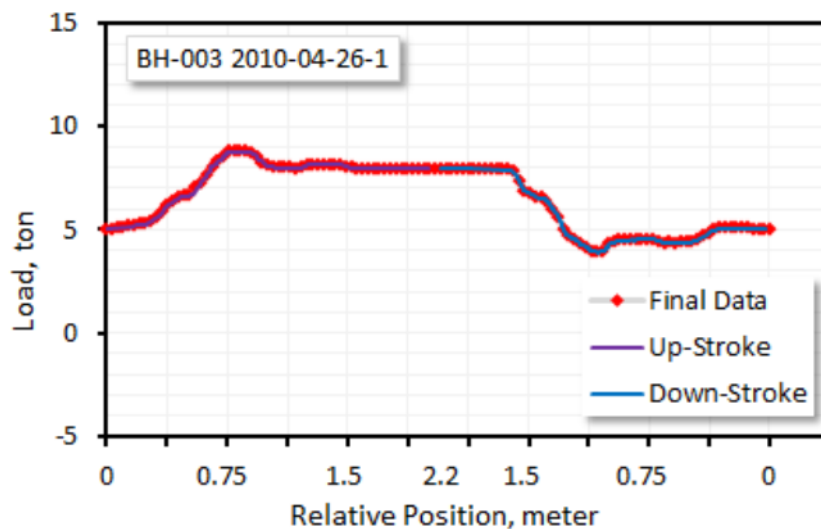


Figure 28: Load vs position flared-out example

Polished rod position can be presented both as a function of the crank angle by equation (13) and as a function of time. Because many sound features are presented in the time domain, it is useful to present a DC in the time domain, in the form of load versus time. Figure 29 shows correlation of DC with the polished rod harmonic behavior. They are overlaid to show the loads' distribution over the stroke.

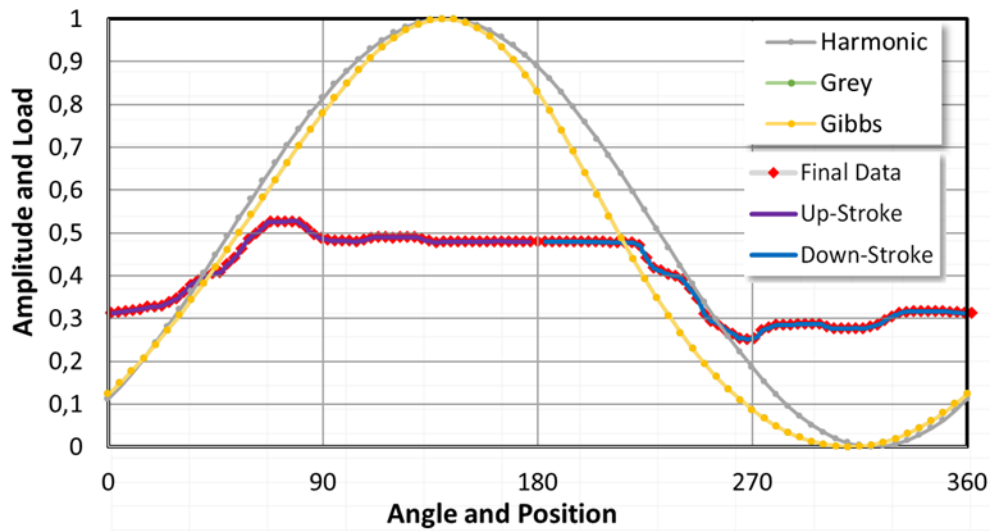
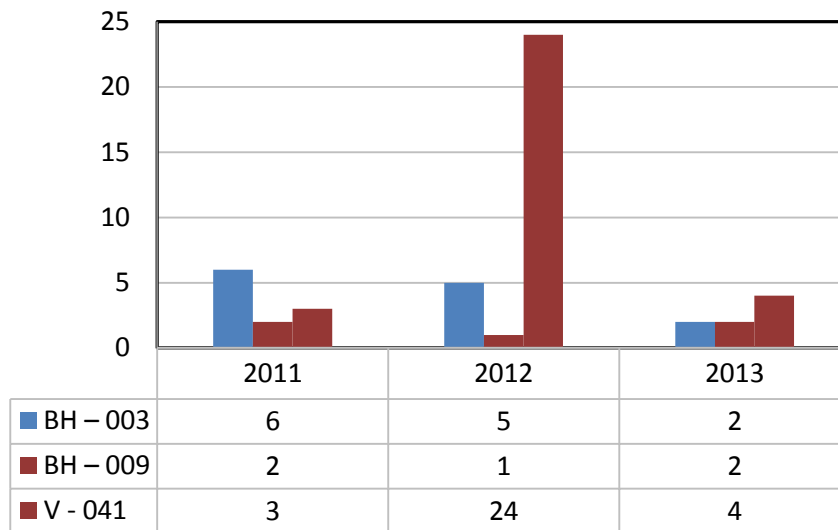


Figure 29: Overlaid harmonic movement of the polished rod and flared-out DC card

Table 4 presents total amount of DC for the entire duration of the research.

Table 4: DC final amount per well, per year



3.5 Dynamometer Card Features

Similar to features of the sound data, DC features portray DC in the best way. DC features calculation does not require additional information and based only on the collected cards. The final stage of the thesis correlates sound features obtained in Chapter 4, Sound Data, with the DC features calculated in this chapter. DC features are computed separately for the upstroke and for the downstroke. Figure 30 and Figure 31 illustrate the principle of features calculation.

One of the features that describe DC is stroke energy. The stroke energy can be presented as an integral of the DC line along its path. As the load is resultant of acting forces on the polished rod, DC energy is related to this force:

$$(17) \quad E = \int_L F \cdot dl,$$

with L being the trajectory of the load from $l(t_1)$ to $l(t_2)$. $l(t_1)$ corresponds to 0 on the x axis, and $l(t_2)$ corresponds to the stroke length L . The stroke energy is measured in N.m.

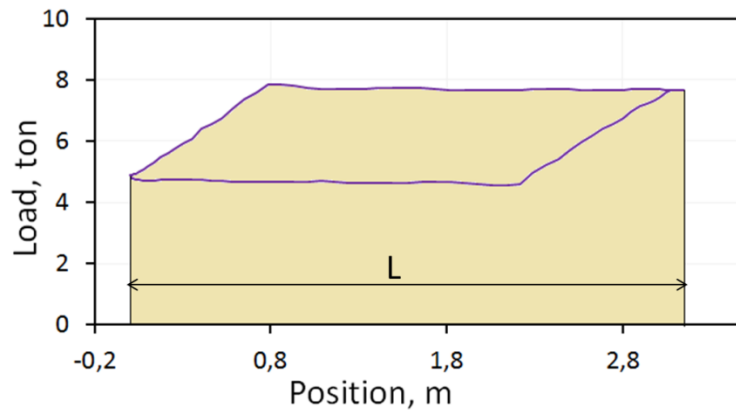


Figure 30: Upstroke notation

The average force, another DC feature, is calculated from the DC energy: it is the energy consumed during the up/downstroke divided by the stroke length. The average force is measured in N.

$$(18) \quad \bar{F} = \frac{E}{L}.$$

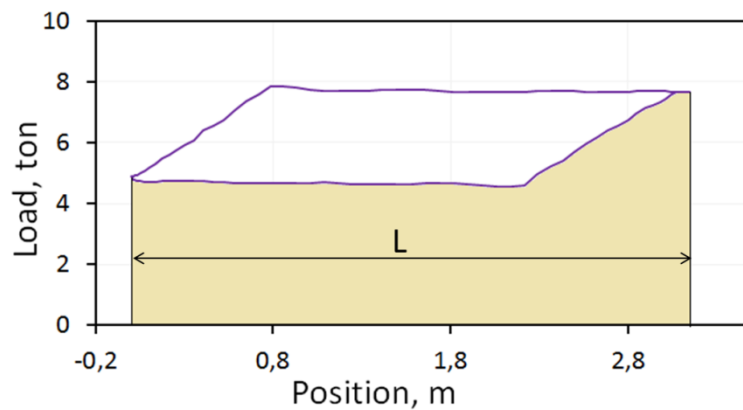


Figure 31: Downstroke notation

The DC power (P) is another measure of the DC. The stroke power is the energy consumed per unit of time. Like energy and average force, power is calculated for the up and/or downstroke. P is measured in W.

$$(19) \quad P = \frac{E}{t}.$$

Different shapes of DCs that correspond to different pump states have different values of features. The set of the DC features comprises of these six characteristics: E_{up} , E_{dn} , F_{up} , F_{dn} , P_{up} and P_{dn} . Each DC is accompanied with these features for further computations.

4 Sound Data

Using a sound application to analyse a well and sucker rod pump system is challenging. At the same time, the application of acoustics is already well-established as a robust technique in many scientific and industrial fields. Its use has shown excellent results in areas such as military service (application of radars, sonic weapons, underwater acoustics), medicine (psychoacoustics, ultrasonic), music (singing, music therapy, music synthesis), construction (vibration control, isolation, noise control). The use of acoustics can be advantageous: acoustic data are relatively easy to collect; processing techniques are well-described and easily accessible.

Audio processing systems usually include two stages [20]. The first stage is the incoming signal preparation which leads to decreasing information. The second stage employs features extraction for files/signal classification. The classification is directly related to the features extracted in the first stage.

Before executing the final step and correlating sound and DCs, the acoustic data needs to be prepared. For that sound recordings undergo the following procedures: acquisition, preparation, data quality control and sound features extraction. This chapter discusses these steps and gives an insight into the techniques and methods that are applied to the sound in all steps of sound processing. Sound data acquisition is the first part in the chain of data processing; after that, recordings go through the sound preparation and data quality control. These steps are vital in the sound processing. A lot of time and effort is invested to obtain the most suitable, robust and automated solutions. The last part of the chapter talks about sound features, why they are created and how to extract them. This is the final sound data preparation step before correlating them with DCs.

4.1 Sound Data Acquisition

When working with data, it is vital to ensure that all the data used is properly collected. Appropriate choice of data acquisition, instruments and techniques, diminishes the likelihood of errors appearing. Defining methods of data sampling, transportation and storage correctly, is essential for any research and helps maintain its integrity. A well-defined data acquisition process ensures accurate data sampling in a repetitive and automated manner.

The sound data discussed here are the SRP and well noise recordings sampled once every hour. The decision on how often to record the SRP sound is crucial, as this affects measurements precision, error elimination and statistical validation. At the beginning of the research, the procedure of sound

recording was not standardized. Sound files were recorded every hour and they were not correlated to the stroke. In autumn 2011, the method of the sound collection was optimized, so that each sound recording is activated by a trigger installed on the base at the moment when the counterweight passes next to it. The recording process starts with the downstroke and finishes automatically after a pre-defined length of time. The length of the recording is chosen in such a way as to be longer than one stroke. This improvement helps standardize the data and ensures they are sampled in a similar manner. This way of sound data recording is repetitive and automated, ensuring the best chance of creating similar conditions for the data collection process. It also simplifies the procedure of correlating sound, DC and the polished rod position. Sound data are written in the “.mat” format and can be easily transformed into other types of data (like “.wav” used to play sounds) without any loss of information.



Figure 32: Murag surface installation

Sound data for this research are recorded with the help of a device called Murag. This tool was designed by a German company, Meodat [12], specifically to measure DFL. Gathered recordings are

sent to the station and stored in the Murag server. These sound recordings are always available to download for future work.

The built-in microphone supports the idea to check the application of the Murag box for sound recording. The Murag unit comprises of two parts: Gond-20, used for DFL measurements, and Gond-40, used for the sound recordings. The entire construction is enclosed in a box and attached to the opened casing valve as shown in Figure 32. The connection between the Murag (the blue-colored box in the figure) and the valve is threaded. Gond-40 is basically a sensor that allows sound recording. There is an anomaly with the Murag system, which is that the two sections cannot function simultaneously, i.e. when Gond-20 performs its task, Gond-40 is switched off. This anomaly causes a problem in using Gond-40 for sound collection and results in many damaged files. This contradiction is discussed in more detail in Chapter 4.6, Sound Data Quality Control.

Meodat engineers indicate that the sensor installed in the Gond-40 registers structure-borne sound together with the airborne sound. Waves that propagate in the solid bodies (structures) and radiate as sound, are called structure-borne sound. This moves within solids with a fixed velocity, which is defined for each material by its structural mechanics (e.g. density, Young's modulus). Unlike airborne sound, the structure-borne sound consists of three types of waves: bending, longitudinal and transverse [51]. The behavior of waves can be described with a set of equations [29] and greatly depends on the material properties. Material property of sound transmission is a function of the sound loss factor, which is an indicator of how much of the sound energy is transformed into heat rather than sound. In other words, loss factor is a measure of material ability to dampen a structure-borne sound. The following set of equations explains the nature of the loss factor.

The pressure level at the point $x = 0$ travelling to $x = \Delta x$ decreases by $\Delta L \Delta x$

$$(20) \quad \Delta L \Delta x = 10 \cdot \log \frac{p_{\text{eff}}^2(x=0, \omega)}{p_{\text{eff}}^2(x=\Delta x, \omega)},$$

thus, pressure decreases proportionally to the exponential function:

$$(21) \quad p_{\text{eff}}^2(x=\Delta x, \omega) \propto p_{\text{eff}}^2(x=0, \omega) e^{-m \Delta x}.$$

In order to include the damping into the wave propagation, the equation can be rewritten as

$$(22) \quad p(x, \omega) = p_a(\omega) e^{-i \underline{k} x} = p_a(\omega) e^{-i k x} e^{-m x / 2},$$

where $\underline{k} = k' + i k''$ is a complex wave number, $k' = \omega/c$ is a real wave number, $k'' = -m/2$ and m is constant [28].

Considering the fact that damping is a loss in the system, and losses can be presented as a loss factor η , the complex wave number then is [28]

$$\underline{k} = k \left(1 - i \frac{\eta}{2} \right).$$

Loss factors can be found in special literature in forms of tables for different structures and media (e.g. in Stevenson, [56]). For example, the loss factor of steel is $\eta_{\text{steel}} = (0.2-0.3) \times 10^{-4}$. For the metal structures the loss factor in general is negligible.

A metal-to-metal bond of the entire system allows Gond-40 to record the structure-borne sound created by downhole mechanical parts and transmitted through casing, tubing and casing media. Different media and their chemical composition, mixing and foam formation, influence sound damping and sound transferability. Although sound behavior in different media and media influence on the recording qualities is not the subject of the thesis, the information about their relationship is given here to show the connection between them.

The acoustic velocity is related to the change in pressure and density of the substance. It is expressed by the formula:

$$(23) \quad c = \left(\frac{dp}{d\rho} \right)^{\frac{1}{2}},$$

where c is the velocity of sound, m/s; dp is change in pressure, Pa; $d\rho$ is change in density, kg/m^3 . Speed of sound in gases, fluids and solids is generalized by the following formula (Hook's law):

$$(24) \quad c = \left(\frac{E}{\rho} \right)^{\frac{1}{2}},$$

where E is bulk modulus elasticity, Pa. In equation (24), the sound travels faster through media of higher elasticity and lower density. In cases where the media is incompressible, the speed of sound is infinite. For comparison, the speed of sound in air is 331.2 m/s and in water it is 1435.4 m/s (at 0°C and 1 bar). In steel, due to less compressibility, the speed of sound is equal to 5960 m/s.

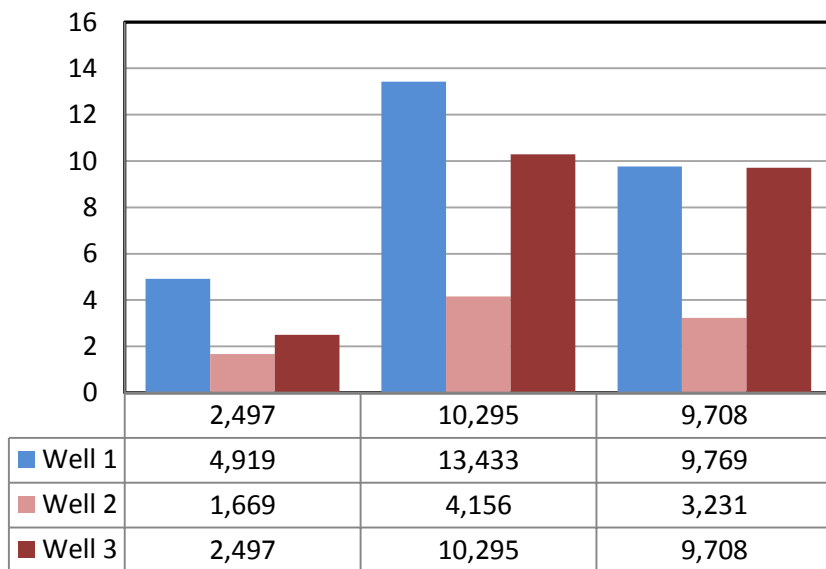
The DFL is basically a non-compressible (or very low-compressible) fluid column, which also presents a sound damping system. Apparently, the height of the DFL has an influence on the quality of collected sound, as well as the fluid's physical properties and chemical composition that can change throughout the production time. As shown in [60], the damping coefficient of water is ten times less than that of oil (with viscosity of 960 cP). In addition, gas and fluids have different orders of damping coefficient. In cases where the fluid is of higher GOR, the damping coefficient increases. The phenomenon of damping is assumed to be independent of frequency, but this assumption does not hold for all temperatures, humidity of the medium, material itself and frequencies. This needs to be the subject of further research in the future.

After three years of constant data recording a significant amount of data was collected, resulting in total about 60,000 files. Figure 33 gives an overview of the sound recordings for each well. The number of available files varies from month to month for each well; in some months the files are absent. This can be explained by workover operations, either a shutting down in the Murag, Gond-40 microphone displacement (V-041 in January 2012), or some other maintenance jobs that require Gond-40 to be switched off. Well BH-009 has months with no sound recordings which, of course, complicates correlation of the sound and DC to the production events.

Table 5 summarizes the amount of sound files acquired during period from August 2011 till August 2013.

Figure 33 gives an overview of the sound recordings for each well. The number of available files varies from month to month for each well; in some months the files are absent. This can be explained by workover operations, either a shutting down in the Murag, Gond-40 microphone displacement (V-041 in January 2012), or some other maintenance jobs that require Gond-40 to be switched off. Well BH-009 has months with no sound recordings which, of course, complicates correlation of the sound and DC to the production events.

Table 5: Number of sound files per well, per year



Not all of these files are of a quality acceptable to allow further processing. Chapter 4.6, Sound Data Quality Control, explains about data quality and QC techniques used to distinguish files into usable and not usable.

4.2 Sound Data Preparation

Before extracting features, sound files need to be correctly prepared. Sound preparation aims to decrease the size of recordings, improve their quality by noise reduction, and preserve the sound informational value. The preparation process ensures more efficient sound handling and facilitates features extraction. To perform this task, signal processing methods and techniques are applied. Bias removal (to diminish noise), down-sampling (to reduce size of files), windowing (to avoid aliasing) and others are described in this chapter.

The sound data preparation is the first step in the chain of sound features calculation. The raw signals are firstly decomposed into their frequencies, or transformed from the time domain into the frequency domain using the well-known Fourier Transform (FT). Subsequently, the sound data are ready for the features extraction performed in both domains. These features will be used in further stages to distinguish between different SRP states, perform data quality control, model DC features, and monitor and predict SRP well behavior.

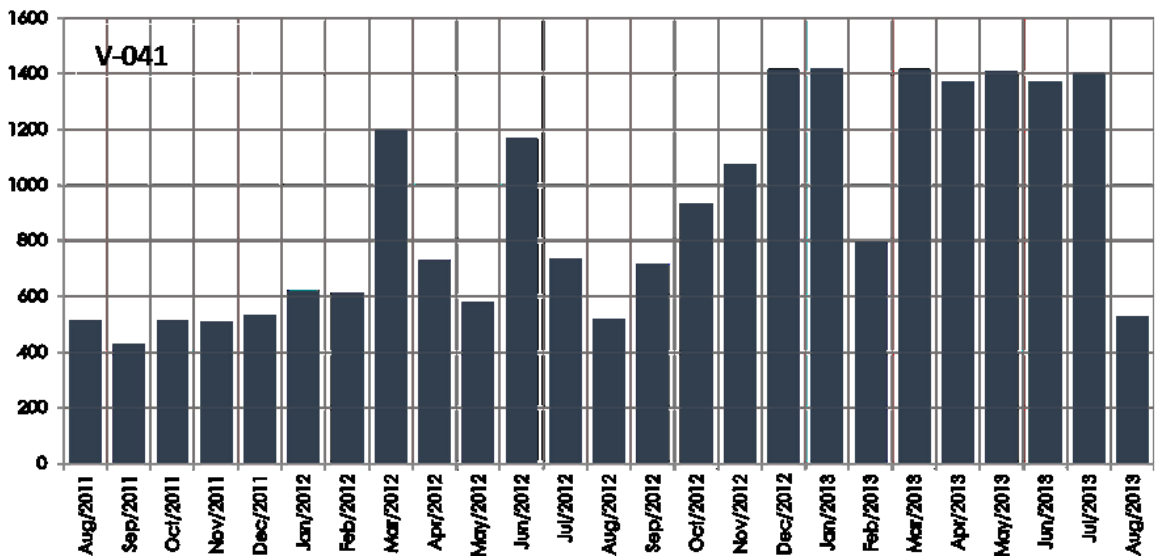
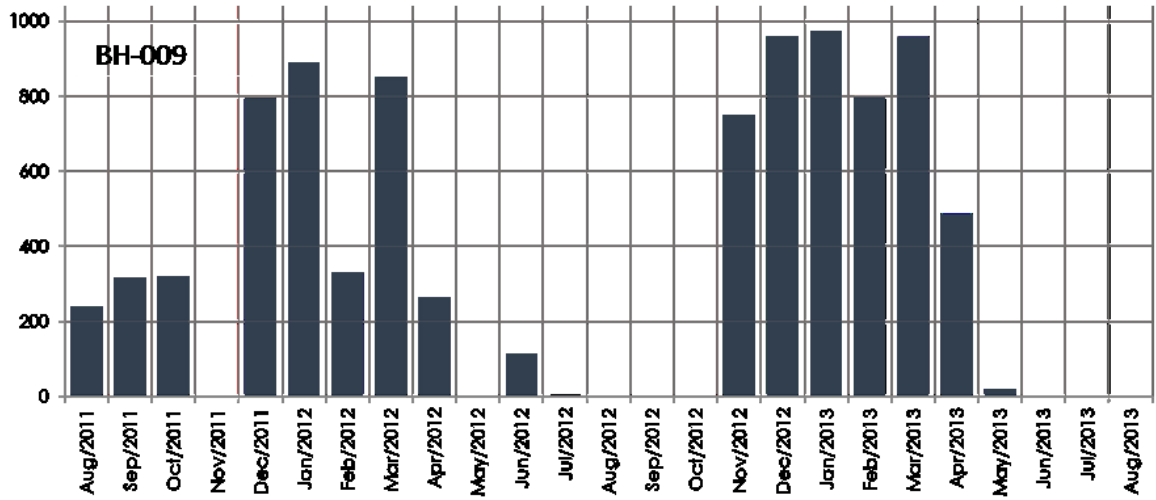
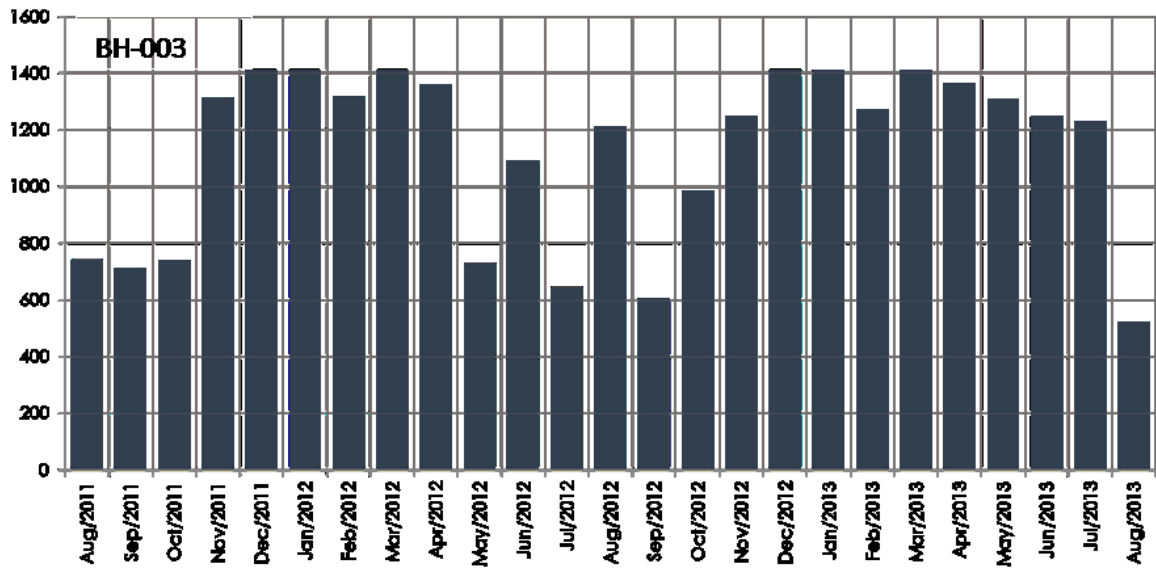


Figure 33: Number of sound files per well

4.2.1 Bias Offset Removal

Bias offset is the signal displacement from zero. It means that the signal is not centered abscissa, i.e., its average is not zero [30]. The cause of the DC offset is usually a predefined voltage offset in the signal chain before the signal is converted from analog into digital form. For instance, this voltage can come from hardware, software, an editing practice or imperfections of A/D conversion. It could also come from the sound card. In general, bias offset is very small, but may cause problems when working with the sound. Bias of a signal needs to be removed in the early stages of the editing process.

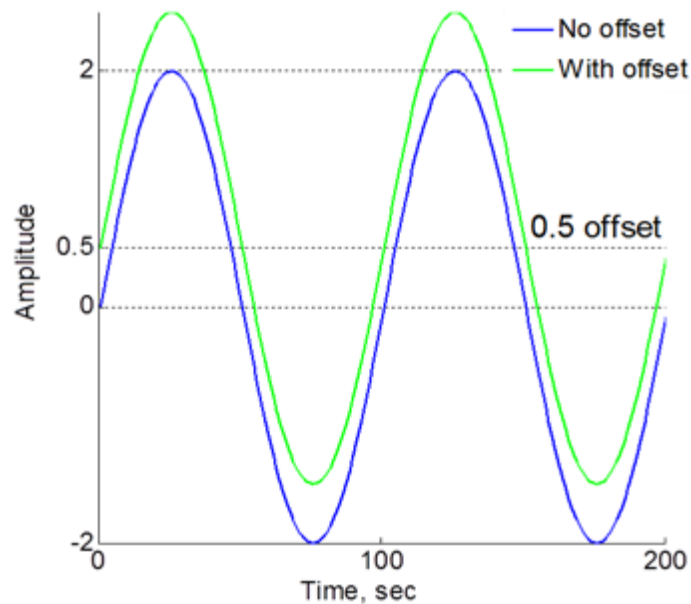


Figure 34: Example of a sound file before and after the bias removal

For a non-real-time signal of fixed length, the procedure of bias removal applied in this research is straight forward [30]:

- 1) compute the average of N samples (can be length of the entire file as performed here);
- 2) subtract the average value from each sample;
- 3) received samples are the data without bias offset (or infinitesimal bias offset).

This simple and effective scheme has only one limitation: it cannot be applied for real-time signals. An example of bias removal is shown in Figure 34.

4.2.2 Fourier Transform

Every signal contains information that can be accessed in the time and the frequency domains. Signal characteristics in the time and the frequency domains are considered interchangeable and are equally important. A complex acoustical signal is a set of several waves characterized by different frequencies and amplitudes. The task of signal analysis (digital signal processing) is to define the content of data, perform reliable measurements and show how the information-bearing elements are related to each other.

The man, who introduced the Fourier Transform (FT), was the French mathematician Joseph Fourier, after whom it was named. He was always interested in heat propagation. Initially, this passion pushed him to derive an equation for heat propagation, and finally in 1807, to solve it with the method today known as Fourier Transform.

The application of FT is essential in many scientific fields. It is a powerful tool used to solve engineering problems; for example, it can be implemented to solve sophisticated mathematical equations that describe dynamical processes of heat, light or electrical energy; FT allows extracting components of complicated signals that permits a correct interpretation of experimental data from astrology, chemistry, medicine and other scientific disciplines [2].

Transformation of a signal from the time domain into the frequency domain is a frequently used data rearrangement method. Transformation helps display signals' properties that are not visible in one domain by displaying them in another domain where they are. It is this property of transformation which permits using sound features in both domains for more comprehensive and complex analysis.

The underlying idea in the FT calculation is that any periodical function can be presented as a sum of sines and cosines of: different amplitudes A , periods T and frequencies ω . This way of signal description is called a time representation. After applying the FT, the signal results in its frequency representation, showing how the magnitude of the signal changes.

The lowest frequency of the signal is called a fundamental frequency, or first harmonic. All other frequencies (harmonics) composing a signal are the multiples of the first harmonic. An example of a function $S(t)$ that consists of harmonics $C_i(t)$ is shown in Figure 35. The lowest sketch in this diagram is an illustration of the main FT principle: the spectrum of the sum function is the summation of the spectra of its harmonics.

One of the advantages that FT possesses is its flexibility. It can be applied for both: continuous (Continuous Fourier Transform) and discrete signals (Discrete Fourier Transform, DFT). The continuous FT treats continuous signals or functions. The DFT has its application with discrete functions and signals, i.e., after continuous function/signal discretization is applied. In other terms, it is employed for the digitally sampled signals [14].

Fast Fourier Transform (FFT) is another example of FT computation that was introduced by J.W. Cooley and J.W. Turkey [61]. FFT gives the same results as other methods, but the computation time is much reduced due to the fact that it uses fewer calculations to analyse the data. FFT is calculated in window-based manner; each window has a length that is multiple of 2^n , which basically makes the FFT work faster. Alternative transformations of the signal from the time into the frequency domain use wavelets [3] and are not considered here.

Almost all signals that occur are analogue. These signals are continuous and defined with the help of sine waves:

$$(25) \quad f(t) = \sin(2\pi t).$$

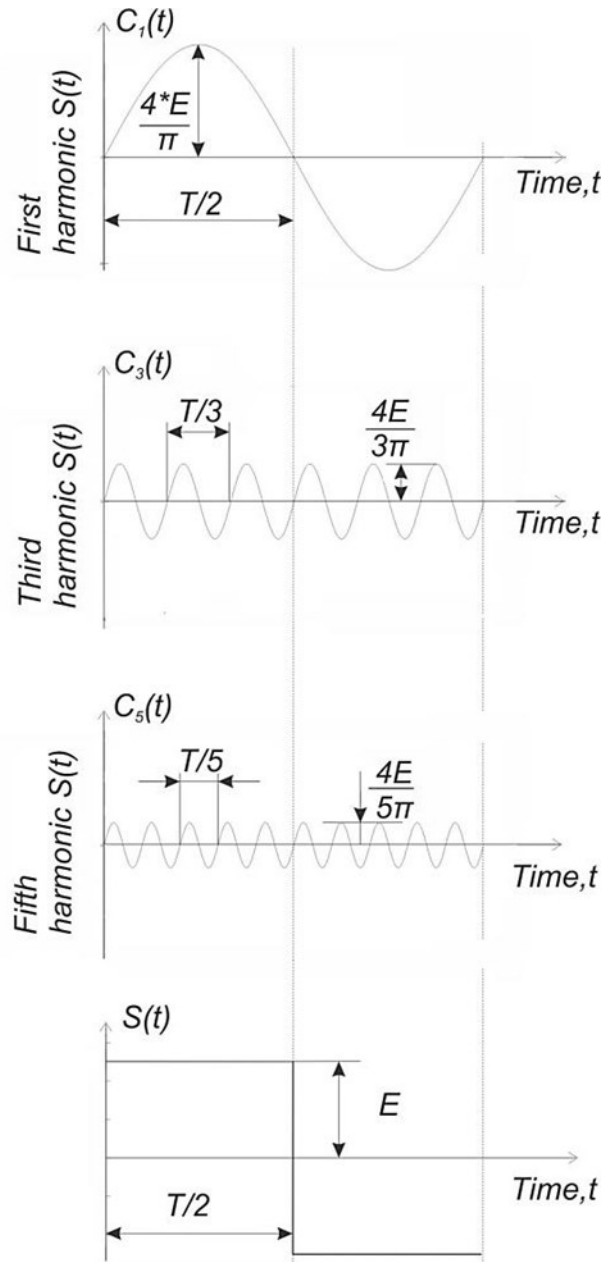


Figure 35: A rectangular impulse as a sum of harmonics

To apply a transform means that the signal changes its representation without changing its characteristics. Physically, the signals are described in the time domain by a function of time $f(t)$. In the frequency domain, the signals are defined by the amplitude F (a complex number that also contains a phase information) as a function of the frequency ω , that is $F(\omega)$ [63]. There is a relationship between functions $f(t)$ and $F(\omega)$, which is described by the FT equations shown below. The FT of a real-valued function in the time domain $f(t)$ is defined as:

$$(26) \quad F(\omega) = \int_{-\infty}^{\infty} f(t) e^{-i\omega t} dt .$$

The application of the inverse FT allows transforming signal back to the time domain

$$(27) \quad f(t) = \frac{1}{2\pi} \int_{-\infty}^{\infty} F(\omega) e^{i\omega t} d\omega.$$

Both functions, $F(\omega)$ and $f(t)$ are related to each other and reversible, i.e.

$$(28) \quad F(\omega) \Leftrightarrow f(t).$$

They are referred to as Fourier Transform Pairs. The complex number that lies in equation (26) is a number where both real and imaginary parts are sinusoids. Here it is necessary to remember that sinusoids are merely a special case of a polynomial function. Euler's formula describes the exact relationship as following:

$$(29) \quad e^{i\omega t} = \cos\omega t + i \sin\omega t.$$

FT is complex-valued, and its imaginary and real components are complete and orthogonal. Thus, $F(\omega)$ can be presented in the form:

$$(30) \quad a(\omega) + ib(\omega).$$

This leads to another way of FT representation through the magnitude and phase as shown in:

$$(31) \quad F(\omega) = |F(\omega)| e^{i\Phi(\omega)}.$$

$|F(\omega)|$ is called Fourier (amplitude) spectrum and defined as:

$$(32) \quad |F(\omega)| = \sqrt{\Re^2[F(\omega)] + \Im^2[F(\omega)]} = \sqrt{a^2 + b^2}.$$

Phase of the corresponding frequency component can be expressed as:

$$(33) \quad \Phi(\omega) = \tan^{-1} \left(\frac{\Im[F(\omega)]}{\Re[F(\omega)]} \right) = \tan^{-1} \left(\frac{b}{a} \right).$$

Phase angle is generally ignored in many computational applications, and only amplitude is needed. In applications where phase angle information is essential, higher order statistical computations are applied [32].

All three methods of FT representation shown here are used in this research. The choice of method depends on the initial data and required output data. Dirichlet conditions describe the particular conditions a function $f(t)$ has to fulfil in order to be expanded as FT. They are summarized as follows; the function must:

- be periodic;
- be continuous and single-valued (some possible exceptions on a number of discontinuities);
- have a finite number of its minima and maxima within one period;
- fulfil that its integral over one period converges.

The Fourier series converges if all the aforementioned requirements are met.

Signals have a unique property, described with the *Parseval's theorem*, which states that the total energy of the signal in the time domain is equal to the signals' energy in the frequency domain. It is formulated thus:

$$(34) \quad \int_{-\infty}^{\infty} |f(t)|^2 dt = \frac{1}{2\pi} \int_{-\infty}^{\infty} |F(\omega)|^2 d\omega.$$

4.2.3 Sampling Theorem and Decimation

Audio signals used for this work are recorded with the sampling frequency F_s of 48 kHz. Such high sampling frequency results in an enormous number of data points per file. As an example, for a signal of 30 seconds length there are $48,000(\text{Hz}) \times 30(\text{s}) = 1,440,000$ data points. Having this amount of samples per file increases computational time and used memory. A method called decimation, or downsampling, is used to lessen the number of data points without reducing the quality of the signal.

As previously stated, sampling frequency defines how often a signal is being sampled per time period. Thus, the function $f(t)$ that describes the signal is not continuous. Instead, it is discrete and presented in the form $f(k\Delta t)$, where k denotes the integer index of the sample. A constant Δt is the time interval between two samples and depends on F_s in the form of relationship

$$(35) \quad \Delta t = \frac{1}{F_s}.$$

The sampling theorem is often referred to as the Nyquist sampling theorem and shows that any signal with bandwidth B Hz can be properly presented if taken at a sampling rate of $F_s > 2B$. This theorem is related to the Nyquist frequency F_{Ny} . Nyquist frequency is one half of the sampling frequency and is the maximum frequency that can be recorded with a given F_s . FFT is symmetrical around zero and limited with the Nyquist frequency. Because the signal is discrete, the FFT computation assumes that the signal is periodic and repeats itself with the period $2F_{Ny}$.

The process of decimation decreases the F_s , i.e., both the number of samples and the Nyquist frequency by a decimating factor, which must be an integer number. Decimation implies that the FFT length is also reduced by the decimation factor.

In Figure 36 the decimation factor is equal to two. In the time domain the original signal y and the decimated signal x are related thus

$$(36) \quad y[n] = x[Mn],$$

with $M=2$ in the given example. In the frequency domain:

$$(37) \quad Y(\omega) = \sum_{k=0}^{M-1} X\left(\frac{\omega - 2\pi k}{M}\right).$$

The decimation process is concluded by performing Inverse Fourier Transform, where decimated FT is fed into equation (27). The output is the desired decimated signal in the time domain.

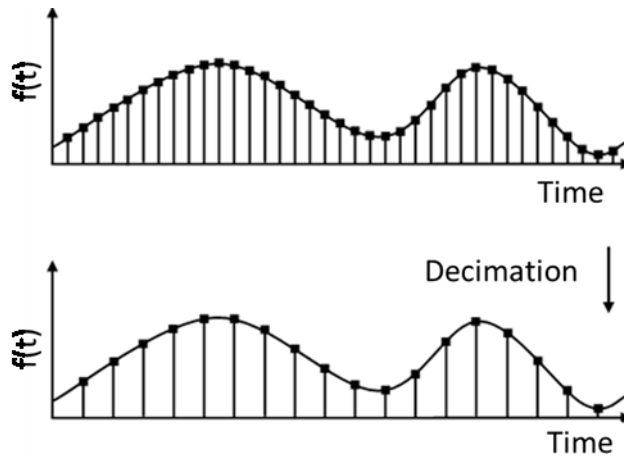


Figure 36: Decimation in the time domain, after Matlab R2014a Documentation

As the FFT length after the decimation becomes smaller, it moves along its axes towards to 0 Hz. Then the FFT values are reduced by the new value of $F_{Ny,new}$, FFT tends to fold its values to the new range of FFT thus creating unwanted peaks from the frequencies of the higher order [19]. This feature is known as aliasing and is a serious complication when performing decimation. Often, there is no aliasing in the original signal, but decimation can cause the signal to develop it. Figure 37 demonstrates the effect of decimation in the frequency domain.

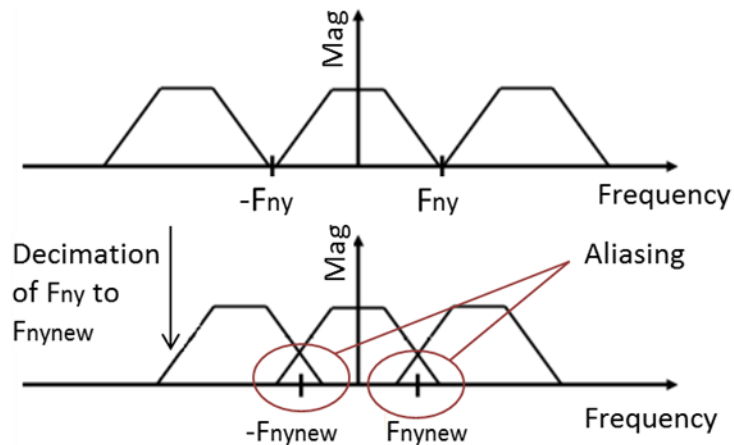


Figure 37: Effect of decimation in the frequency domain, after Matlab R2014a Documentation

To eliminate this problem the signal is filtered with a so-called “anti-aliasing” filter before downsampling (Figure 38). It allows the signal spectra to avoid overlap at F_{Ny} . The filter is a lowpass type that passes all frequencies lower than F_1 and cuts off all frequencies higher than F_2 . F_1 and F_2 are two pre-defined frequencies that are called transition bands, and provide gradual frequencies attenuation.

If the decimation is done in the frequency domain as presented here, FFT values for the frequencies higher than new F_{Ny} are equalized to zero by convoluting with a rectangular-shape function so that:

$$(38) \quad W = \begin{cases} 1 & \dots & 0 < k < N-1, \\ 0 & \dots & \text{otherwise.} \end{cases}$$

Here N denotes the length of the desired FFT corresponding to the decimated F_s . The function W is also known as a window-function and is normal practice when working with the signals. Application of the window-function illuminates unwanted frequencies, and, thus, prevents aliasing.

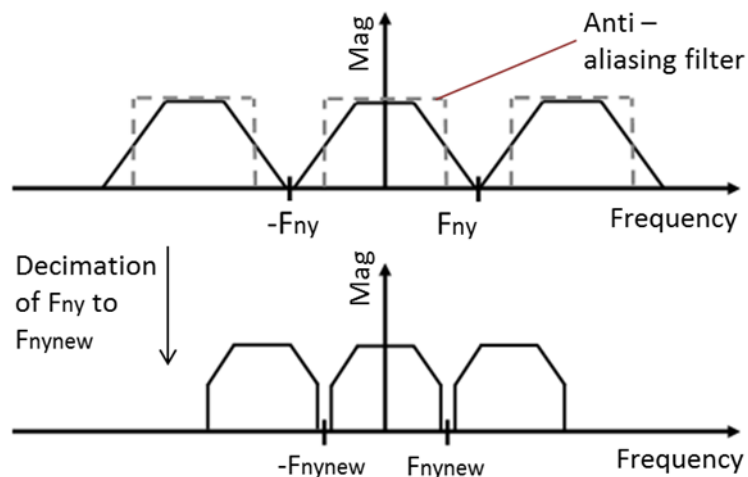


Figure 38: Filter to prevent aliasing when reducing F_s , after Matlab R2014a Documentation

According to the convolution theorem, the convolution of two functions in the time domain corresponds to the multiplication of their transforms in the frequency domain, that is:

$$(39) \quad f(t) * w(t) = \int_{-\infty}^{\infty} f(\tau) w(t - \tau) dt ,$$

and

$$(40) \quad F\{f(t) * w(t)\} = F(\omega) \cdot W(\omega).$$

Here it is important to remember that the window-function (noted as $W(\omega)$) has its response in the frequency domain. An example of this is presented in Figure 39. The window has many side lobes that influence the result of the FFT. It hinders the signals representation in the frequency domain and adds unwanted values in measurements [39].

To decrease this effect, other types of windows can be applied. They are presented in a large number of variations (more on that see in Heinzl, Rüdiger and Schilling [18], Smith [54], Nuttall [42]). The choice of the window-function depends on the sound processing experience, signal features and the objective of the research. The most well-known and frequently used windows are: triangular, rectangular, Welch, Hanning, Hamming, Chebyshev, Blackman, among others. The scope of this research is not concentrated around a window choice, thus the default windows used here are rectangular, triangular and Hanning. These three types are shown in Figure 39, Figure 40 and Figure 41 respectively.

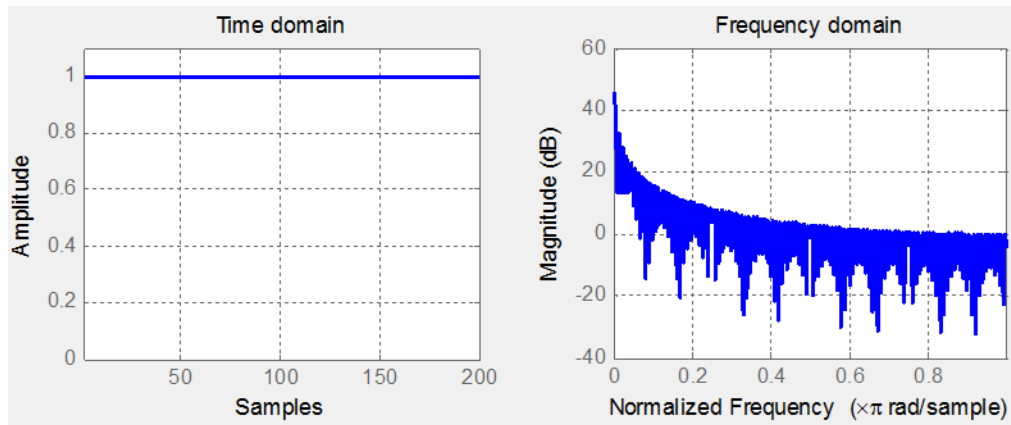


Figure 39: Rectangular window in the time and the frequency domain

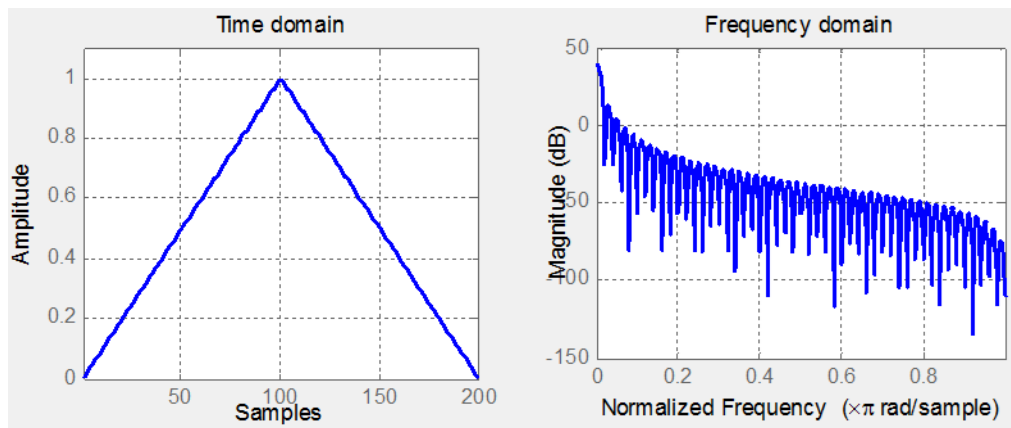


Figure 40: Triangular window in the time and the frequency domain

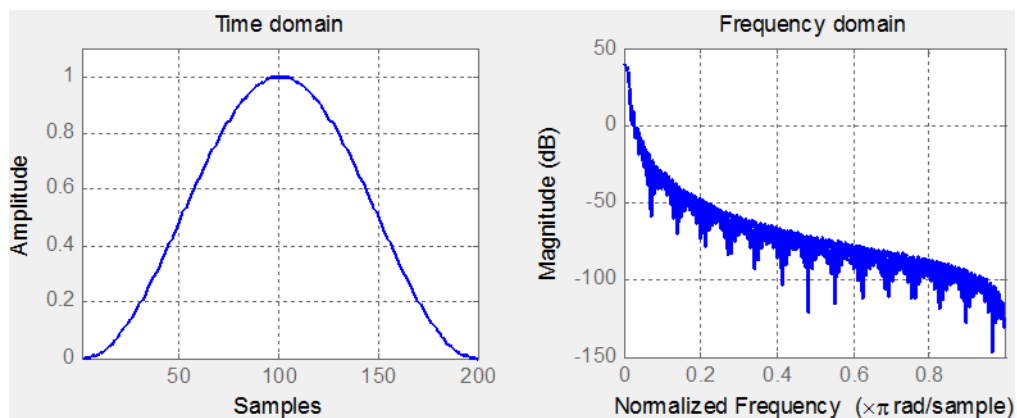


Figure 41: Hanning window in the time and the frequency domain

Table 6 represents mathematical formulas which describe the windows. As shown, the Hanning window has smaller side lobes and it influences the output of FFT the least. Moreover, it has the least influence on the signal retrieval into the time domain. The Hanning window is used to calculate some sound features. The rectangular window is applied in this research for sound preparation and features calculation. The triangular window is used to calculate Mel frequencies and cepstral coefficients. These are specific sound features and will be discussed in Chapter 4.3.16.

Windows are usually applied to a signal in the overlapping mode; this means that each subsequent window is applied after a pre-determined percentage of the length of the window. For the rectangular and triangular windows in this research, the overlap is 50%. Overlapping ensures that all data are trapped with a window and no data points are lost.

Table 6: Equations of window functions

Window	Formula
Rectangular	$w_k \equiv 1$
Triangular	$w_k = \begin{cases} z & \dots & z \leq 1 \\ 2-z & \dots & z > 1 \end{cases} \quad z = \frac{2k}{N}, \quad k=0 \dots N-1$
Hanning	$w_k = \frac{1 - \cos(z)}{2} \quad z = \frac{2\pi k}{N}, \quad k=0 \dots N-1$

At the beginning of the research, it was unknown which frequencies were the most “informative”. Research established that the frequencies of the most interest lay within 0 to 3000 Hz. The decimation factor thus is fixed to 8 and yields $F_{Ny}=3$ kHz. Data quality control and features calculation are performed on the decimated signals in order to decrease computational time and memory.

4.2.4 Power Spectrum Density

Power Spectrum Density (PSD) is one of the most important characteristics that a signal has. PSD determination is acknowledged as a useful and robust tool in signal processing, being successfully used for more than fifty years. PSD is nothing more than an indicator of sound energy distribution over the frequency range and is presented with the help of autocorrelation sequences. Usually, these restrictions are sufficient to analyze a Gaussian signal. When the signal does not obey Gaussian distribution, information about phase behavior might be required. PSD calculation implies that phase relationships are inhibited. The power spectrum density $P(\omega)$ is calculated as:

$$(41) \quad P(\omega) = \Re^2[F(\omega)] + \Im^2[F(\omega)].$$

It is useful to notice that when calculating power distribution, FFT shows it for both positive and negative frequencies. As sound processing in this thesis deals only with positive frequencies, the negative are ignored. The PSD values, except the zero component and the Nyquist frequency, are then multiplied twice in order not to lose the frequency’s energy.

There are several methods to calculate PSD of a signal. They can be classified as: conventional (Fourier), maximum-likelihood, minimum energy, maximum entropy, auto-regressive (AR), moving-average (MA), ARMA, and others, such as harmonic decomposition methods [32]. Each of these methods has advantages and limitations that are considered by both computational difficulty and computational performance. The choice of appropriate method depends on the signal environment ([25] and [26]). Spectrum estimation can be also introduced with the help of linear methods (e.g. the Blackman-Tukey direct method based on FT).

They are, however, weak in sense of resolution [40]. Due to some assumptions made for these methods (like the one that FT assumes the data repeat themselves outside of the calculating window), the spectrum calculated is different to the true one. For instance, peaks that locate relatively close to each other can be presented as one peak that is an integrated version of all the peaks. This results in incorrect spectrum estimation [64].

The PSD can be represented in two different ways, linear or in Decibel (dB). The conversion to dB is done in the following way:

$$(42) \quad \text{PSD}_{\text{dB}} = 10 \log_{10} \left(\frac{\text{PSD}}{\text{PSD}_{\text{max}}} \right).$$

Phase angle is usually ignored in many computational applications, and only amplitude is needed. In the event that phase angle information is necessary, higher order statistical computations might be applied [32].

4.2.5 Hilbert Transform

A signal $f(t)$ and its Hilbert transform $q(t)$ form a complete trace, which is of complex nature [33] and can be expressed as:

$$(43) \quad c(t) = f(t) + iq(t),$$

where $c(t)$ is called the complex trace, $q(t)$ is called the quadrature trace (Figure 42).

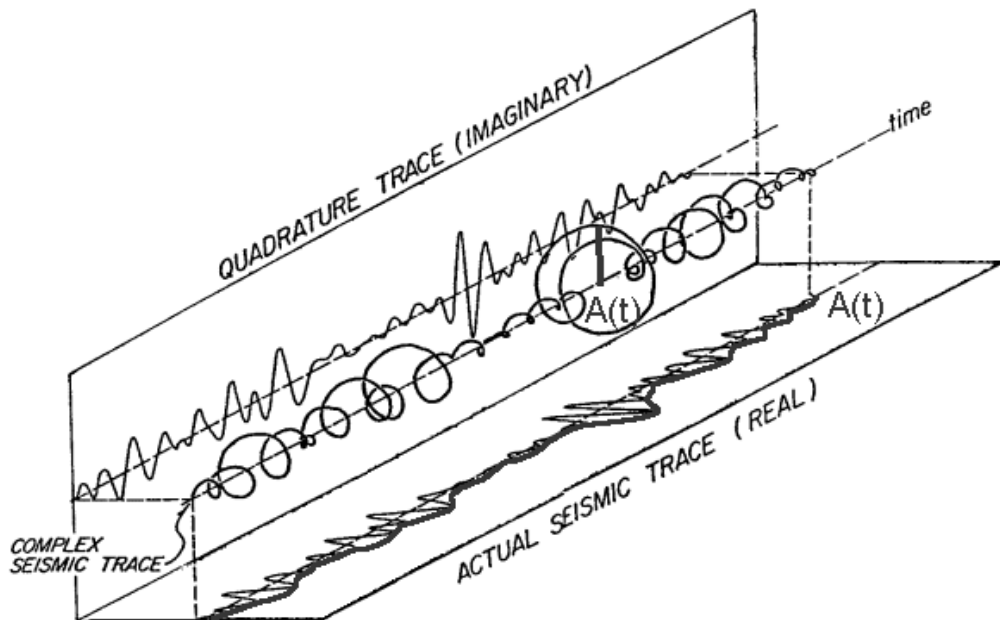


Figure 42: A complex trace and its attributes, after Taner, 1979 [33]

Similar to the signal in the time domain, the complex trace can be presented in terms of the envelope $A(t)$ and the phase $\phi(t)$:

$$(44) \quad c(t) = A(t)e^{i\phi(t)}.$$

Hilbert transform for all t is presented in form:

$$(45) \quad q(t) = \frac{1}{\pi} \text{p.v.} \int_{-\infty}^{+\infty} \frac{f(\tau)}{t - \tau} d\tau.$$

Hilbert transform has an interesting feature of a $\pm\pi/2$ phase shift for the positive frequencies. In the frequency domain it is treated as multiplication with the imaginary unity i . The amplitude therefore does not change.

Similar to Parseval's theorem, the energy of the signal is the same as for its Hilbert transform. This feature is widely used. Moreover, the analytical signal can be also presented in the form of amplitude and phase. The derivative of the phase is referred to as an instantaneous frequency [33] and is used for the signal processing. Instantaneous frequency is found to be informative and is used in this thesis to determine a set of sound features. Chapter 4.3, Sound Features, explains how to obtain the instantaneous frequency and features related to it in greater detail. The quadrature trace is also used to calculate sound features [24].

After the sound data are correctly acquired and prepared, the sound features calculation can be performed.

4.3 Sound Features

Recorded data are sets of numbers that symbolize sound in the digital format. The fact that every signal can be presented in many different ways, introduces sound features developed in this research as characteristics that describe sound in a quantitative manner. The choice of characteristics, i.e. features, is based on their relationship to the signal processing, their demonstrability and physical meaning.

Ideas for sound features created in this thesis, are taken from different areas of sound application. Application of the acoustics in seismic technology, speech recognition, music interpretation, radar application among others, is used to define the best set of representative features. In addition, features are analyzed in order to check and improve their applicability for the SRP states recognition. The final version of sound features calculation is composed of both signal processing and statistical methods. This chapter explains the procedures applied to extract sound features.

4.3.1 Features Definition

The purpose of the sound features is to present acoustic data in the most favorable way. Features need to be chosen such that they are efficient characteristics, and, in addition, should ignore any irrelevant information [46]. Only features containing the maximum amount of essential information need to be chosen.

To create and select features is a challenging and time-consuming task. A large amount of research has been done to determine state-defining features, which fulfill criteria of sufficiency and efficiency. There are more than 1600 features, which are created for overall acoustic processing. The majority of them refer to low-level signal features with highly discriminative characteristics and include such properties as spectral centroid, signal energy, signal trace, etc. These features can be extracted from a signal in reliable and simple way with the help of FFT, PSD and Hilbert transform.

The creation of features is an ingenious process and implies no restrictions, except for a basic understanding of their physical meaning and interconnection. It is possible to combine both domains, e.g. divide, multiply, take a natural logarithm of them, apply some statistics and so on. Nonetheless, the combination of mathematical operations applied to features must be intelligible. For example, there is no need to apply a natural algorithm to many of the features that have negative values. Moreover, such features as the z-score, is itself a statistically normalized set. Calculating the standard deviation or the mean value for z-score in this case is irrelevant. The usual process of feature calculation includes the following:

(1) Take a definite length of the file.

Sound features are extracted in the window-by-window manner due to the overwhelming amount of samples in the file. If F_s is equal to 48 kHz, it means there are 48,000 samples captured and stored in each second. Analysis of this amount of data requires more powerful computers, longer computational time and, in the end, might not pay off in terms of the information extracted. The window-by-window method means that a sound file is divided into several windows of a pre-defined length (frame), and features are obtained for each frame individually. Different lengths of frames are used for individual applications. For QC purposes, only one frame with the length of the whole signal is used. For more detailed analysis (data correlation and DC features modelling), initially, the precise length of one stroke is extracted from a sound recording. This is necessary in order to correlate one stroke of the sound with one stroke of the DC data. The file with the duration of one stroke is then divided into frames. The number of frames in the file may be chosen as much as needed, although a higher number increases output information capacity. In the first approach, the number of frames was limited to 15. Possible variations were: 1 frame (entire stroke), 2 frames (file divided into halves: one frame for the upstroke and one for the downstroke), 4 frames (two frames for the upstroke and two for the downstroke), and 8 (four frames for the upstroke and four for the downstroke), i.e., according to the 2^n with $n=0 \dots 3$.

Digitized DC with 120 data points promotes the idea of having 120 frames for the sound features. It facilitates correlation of both types of data. In the final approach, each sound file of one stroke is divided into 120 frames, and sound features for each frame are computed.

(2) Calculate desired feature.

To enhance acoustic analysis, features from both the time and the frequency domains are used. Chapter 4.5, Features and their Notation, explains the logic behind notation and provides a full list of the used features.

(3) Perform statistical analysis on each feature's frame.

Different types of statistics are applied for the features calculation. They include methods from both descriptive and robust statistics and combinations of them. The notation of the performed statistics is always included at the end of the feature's notation.

The following parts of the chapter explain each sound characteristic, which is applied for the sound features calculation, in more detail.

4.3.2 Real Trace

The real trace is a signal itself (or signals amplitude) and obtained in the time domain. The real trace can also be computed using Hilbert transform, equation (43). In the features notation it is referred to as R.

4.3.3 Quadrature Trace

The quadrature trace is the imaginary part of the complex trace. It is computed from the real trace by applying the Hilbert transform (equations (43) and (45)). The quadrature trace is phase rotated by $\pi/2$ and shares the same amplitude spectrum with the real trace. As was noticed before, the quadrature is also used to compute other features from the complex trace, e.g., instantaneous frequency. The quadrature trace in the frequency domain is equivalent to the real trace in the time domain. In features notation it is $q0$.

4.3.4 Signal Envelope

Signal envelope can be presented as:

$$(46) \quad e = \sqrt{r^2(t) + q^2(t)},$$

where $q(t)$ is the quadrature trace and $r(t)$ is the original signal. The signal envelope is also called energy envelope. In features notation, signal envelope is E.

4.3.5 Z-Score

The z-score calculates distance in terms of standard deviation from a data point to the mean. This means that the z-score standardizes the data. It is calculated for each element of the data set (sound files) in such a way that the z-score values have mean of 0 and are scaled so that standard deviation is equal to 1. Apparently, the z-score has the same size as raw data and keeps the shape properties of the initial data (such as kurtosis and skewness). It is expressed by the formula:

$$(47) \quad z = \frac{x - \mu}{\sigma}.$$

The nature of the z-score allows comparing several sets of data of different units. The z-score is calculated for the real trace, quadrature trace and signal envelope.

4.3.6 Instantaneous Frequency

The instantaneous frequency is the first derivative of the phase calculated with the help of Hilbert transform:

$$(48) \quad \omega(t) = \frac{d\theta(t)}{dt} = \text{Im} \left[\frac{c'(t)}{c(t)} \right] = \frac{f(t)h'(t) - f'(t)h(t)}{f^2(t) + h^2(t)}.$$

The instantaneous frequency does not depend on the phase and amplitude, and represents a type of time dependent mean frequency. Another way to compute this is derived in Taner [33]. The instantaneous frequency in the features notation is F0.

4.3.7 Spectral Centroid

The spectral centroid is another measure to characterize the spectrum. It is a middle point of the energy distribution of the signal within a certain band. The spectral centroid is an example of a “center of gravity” (Figure 43).

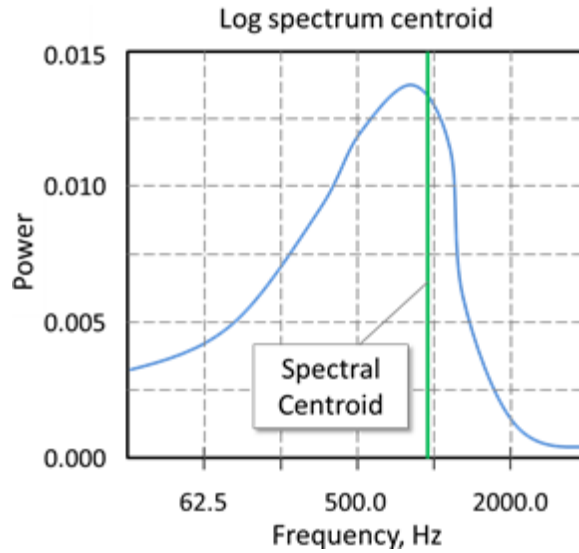


Figure 43: Spectral centroid

Spectral centroid is calculated as weighted mean of the frequencies presented in the signal with their magnitudes as weights (49).

$$(49) \quad SC = \frac{\sum_{n=1}^N f F[n]}{\sum_{n=1}^N F[n]}$$

Where $F[n]$ is the amplitude corresponding to the bin n in the FFT spectrum.

The spectral centroid of a signal is normally higher than expected, as there is much more energy above the fundamental frequency than below. Higher values of the centroid correspond to a higher amount of high frequencies. Spectral centroid frequency is usually used in the speech recognition techniques, and also proved itself as a good indicator for SRP states definition. More information on spectral centroid calculation is in [46].

4.3.8 Temporal Centroid

Temporal centroid is a prototype of the spectral centroid in the time domain: it is a signal’s center of sound gravity obtained in the time domain. The formula for the temporal centroid:

$$(50) \quad T_s^2 = \frac{1}{E} \int_{-\infty}^{\infty} t^2 |r(t)|^2 dt.$$

Here E is the total energy of the signal in the time domain.

4.3.9 Spectral Bandwidth

Bandwidth can be considered as a standard deviation of the spectral centroid. The equation to calculate the bandwidth is

$$(51) \quad BW = \frac{\sum_{n=1}^N (f - f_c)^2 F[n]}{\sum_{n=1}^N F[n]},$$

with f_c representing the spectral centroid. In the same way the bandwidth can be calculated in the time domain.

4.3.10 Roll-off Frequency

Roll-off frequency is a frequency below which 85% of the distribution of the spectrum is concentrated (Figure 44). It describes condition, where the lower frequencies are produced at full amplitude, but as frequencies go higher, they are reduced in amplitude.

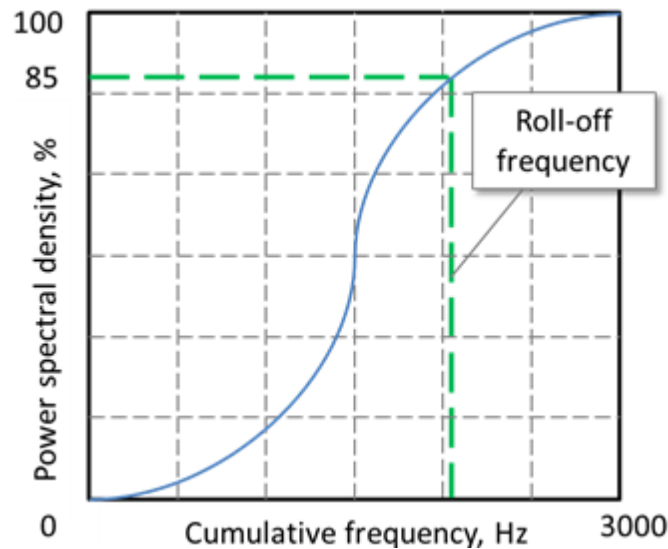


Figure 44: Roll-off frequency

The common specification is 3dB roll-off, or a point where the gain of the amplifier is reduced by 3dB because of bandwidth limitations. As indicated in [57] and [36], roll-off frequency is a low-level signal feature.

4.3.11 BT Product

BT product, which is Bandwidth multiplied by Temporal Centroid, can be a good characteristic of a sound. It is known that BT product represents a richness of a signal. In other words, high BT indicates how large the amount of information that a signal contains. In features notation, BT product is labelled as BT.

4.3.12 Amplitude in the Frequency Domain

Amplitude in the frequency domain is its absolute value and calculated as:

$$(52) \quad A = \sqrt{\Re^2 + \Im^2}.$$

Essentially, the amplitude is related to the sound energy.

4.3.13 Signal Entropy

The signal's entropy can be two types: temporal and spectral. The calculation of the entropy uses histogram-based estimation [79]:

$$(53) \quad E_n = \sum [x_i \log(x_i)],$$

whereby

$$x_i = \frac{v_i}{\sum v_j},$$

and the v_i values origin from the temporal and spectral envelopes correspondingly.

4.3.14 Spectral Skewness

The spectral skewness (S in the features notation) measures the degree of sound asymmetry around its mean value, i.e., the spectral centroid. It is calculated in much the same way as the skewness of any data set:

$$(54) \quad S = \frac{\sum_{n=1}^N (f - f_c)^3 F[n]}{\sum_{n=1}^N F[n]}.$$

4.3.15 Spectral Kurtosis

The spectral kurtosis (K in the features notation) gives a measure of the spectral flatness around the spectral centroid. K is calculated using the formula:

$$(55) \quad K = \frac{\sum_{n=1}^N (f - f_c)^4 F[n]}{\sum_{n=1}^N F[n]}.$$

4.3.16 Spectral Flatness

Spectral Flatness is a method that determines the amount of randomness in a signal [11], i.e., it measures its noisiness or sinusoidality. It also measures the amount of existing correlation structure in the signal. The studied sound sample is compared to the white noise (which has a flat spectrum) in terms of amount of peaks in the power spectrum. In general terms, spectral flatness can be calculated as the ratio of the geometric and arithmetic means of PSD:

$$(56) \quad SF = \frac{\exp\left(\frac{1}{N} \sum_{n=0}^{N-1} \ln x(n)\right)}{\frac{1}{N} \sum_{n=0}^{N-1} x(n)}.$$

Spectral flatness varies between zero (for tonal signals) and one (very noisy signals) [57]. As result, low flatness usually indicates the presence of harmonic components in the sound. Spectral flatness formula, applied to the signal in the time domain, calculates temporal flatness.

4.3.17 Mel Frequency Cepstral Coefficients (MFCC)

Another widely used characteristics' set is mel-frequency cepstral coefficients (MFCC). The MFCC is a good parametric description, as it is level-independent and has low mutual correlations between different features. In general, it is easier to analyze and use it for the features analysis, which are not correlated.

MFCCs are mostly well-known due to their wide application in speech recognition. Firstly, this method was introduced by Davis and Mermelstein [37] in the 1980s and since then it has been state of the art. MFCCs represent the shape of the spectrum with just a few coefficients. Cepstrum is simply an inverse FT of the logarithm of the signal's spectrum. The mel cepstrum, in turn, is the cepstrum calculated over mel bands instead of Fourier spectrum. Equation (57) expresses the conversion of frequency values from Hertz to the mel scale [44].

$$(57) \quad \text{Mel} = 2595 \log_{10} \left(\frac{f}{700} + 1 \right),$$

f is the frequency in Hertz. The use of the mel scale allows for better consideration of middle frequencies of a signal. There is a standard procedure to calculate MFCC that is used in this work also.

1. Divide signal into frames of predefined length.
2. Calculate power spectrum for each frame.
3. Apply mel filter (filter-bank) to the calculated power spectra.
4. In each filter, sum the energies.
5. Take the logarithm of each filter-bank.
6. Take the discrete cosine transform of the result.
7. Record desired coefficients.

After dividing the signal into frames, the calculation of the power spectrum identifies frequencies in each frame. Next, the mel filterbank is applied. The filterbank defines the frequency bands and indicates how much energy is in each frequency region. For instance, the first filter gives an idea of how much energy is located near 0 Hz. As frequencies get higher, the filters get wider. Mel frequencies define exactly how wide filters can be, and answer the question of how to space them. A standard set of filterbanks varies from 20 to 40 and usually includes 26 triangular windows. There is a methodology available on how to calculate spacing.

The next step is to take a logarithm of the data in each frame. This step is explained by the nature of the human ear: it hears in logarithmic scale. The final step includes computation of the discrete cosine transform in order to decorrelate energies. The correlation appears due to the overlapping of filterbanks.

The approach of how to divide the frequency range into bands depends on the desired result. In this research, it is interesting to examine frequency bands and their dependency from the pump and the system states. The division of the linear bands (LB) for the MFCC is presented in Table 7.

Table 7: Frequency range division into linear bands

LB Number	LB Range	LB Number	LB Range	LB Number	LB Range	LB Number	LB Range
1	0-100 Hz	16	750-850 Hz	31	1500-1600 Hz	46	2250-2350 Hz
2	50-150 Hz	17	800-900 Hz	32	1550-1650 Hz	47	2300-2400 Hz
3	100-200 Hz	18	850-950 Hz	33	1600-1700 Hz	48	2350-2450 Hz
4	150-250 Hz	19	900-1000 Hz	34	1650-1750 Hz	49	2400-2500 Hz
5	200-300 Hz	20	950-1050 Hz	35	1700-1800 Hz	50	2450-2550 Hz
6	250-350 Hz	21	1000-1100 Hz	36	1750-1850 Hz	51	2500-2600 Hz
7	300-400 Hz	22	1050-1150 Hz	37	1800-1900 Hz	52	2550-2650 Hz
8	350-450 Hz	23	1100-1200 Hz	38	1850-1950 Hz	53	2600-2700 Hz
9	400-500 Hz	24	1150-1250 Hz	39	1900-2000 Hz	54	2650-2750 Hz
10	450-550 Hz	25	1200-1300 Hz	40	1950-2050 Hz	55	2700-2800 Hz
11	500-600 Hz	26	1250-1350 Hz	41	2000-2100 Hz	56	2750-2850 Hz
12	550-650 Hz	27	1300-1400 Hz	42	2050-2150 Hz	57	2800-2900 Hz
13	600-700 Hz	28	1350-1450 Hz	43	2100-2200 Hz	58	2850-2950 Hz
14	650-750 Hz	29	1400-1500 Hz	44	2150-2250 Hz	59	2900-3000 Hz
15	700-800 Hz	30	1450-1550 Hz	45	2200-2300 Hz		

4.4 Statistical Analysis

Statistical tools used in the thesis are formally divided into three categories: descriptive, robust, and the combination of both. The mixture of these methods gives a wide range of features. Calculation of the sound features' statistics is the last step in the process of features formation and needs to be carried out accurately. During this work, a Matlab file that performs automated features extraction is created. The statistical tool's description is taken from [62] and [23].

4.4.1 Minimum

Minimum (min) is the smallest value in the range of data:

$$(58) \quad x_{\min} = \min(x_k).$$

4.4.2 Maximum

Maximum is the greatest value in the set of data:

$$(59) \quad x_{\max} = \max(x_k).$$

4.4.3 Mean

Mean value is known as the first moment of the data set. The equation below depicts how the mean is calculated [55]:

$$(60) \quad \bar{x} = \frac{1}{N} \sum_{i=1}^N x_i ,$$

with N denoting the number of data samples.

4.4.4 Median

Median is the middle value in the data set, arranged from the smallest to the largest. It is a good indicator of the most typical value of the set with outliers. An outlier is a value in a data set that greatly differs to other data.

4.4.5 Mode

Mode is a value that is most repeated in the data set.

4.4.6 Range

Range is the difference between the largest and smallest values in the data set:

$$(61) \quad \text{Range} = x_{\max} - x_{\min} .$$

These six representatives (min, max, mean, median, mode and range) of the statistics are noted as robust statistics and together form the base of any statistical approach. Figure 45 represents them all in a data set.

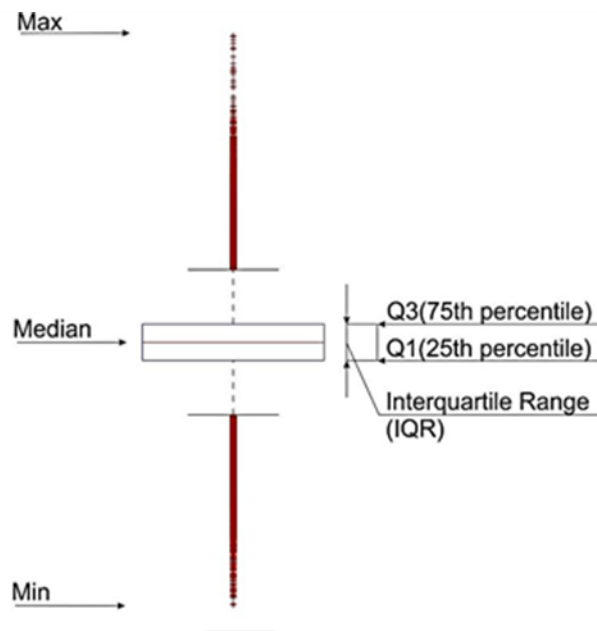


Figure 45: Boxplot example

4.4.7 Interquartile Range

Interquartile range is the measure of data variability. The data are divided into four equal quartiles and the interquartile range shows the difference between the 75 % and 25 % percentiles of the data set (Figure 45). This is a robust method to estimate the data spread.

4.4.8 Percentile

Percentiles of the data values, return percentiles of the values in a data set. It is possible to choose different percentiles. In this research, three of them are used: 1 % and 99 %, 5 % and 95 %, 10 % and 90 %. It reflects how much data are distributed. The median is the 50 % percentile.

4.4.9 Variance

The variance σ^2 is a squared deviation from the mean, averaged with respect to the number of data values. It can be presented as:

$$(62) \quad \sigma^2 = \frac{1}{N-1} \sum_{i=1}^N (x_i - \bar{x})^2 .$$

4.4.10 Average Deviation

Average deviation is the arithmetic mean of the absolute deviation and specified by the formula:

$$(63) \quad x = \frac{1}{N} \sum_{i=1}^N (x_i - \bar{x}) .$$

4.4.11 Standard Deviation

Standard deviation (SD) is the second moment of the data distribution. It is a measure of data spread, showing how far the numbers are from their average. When the data are extended widely, it leads to a large standard deviation; therefore small values indicate compact distributed data. The standard deviation is the square root of the variance and thus denoted as σ .

$$(64) \quad \sigma = \sqrt{\frac{1}{N-1} \sum_{i=1}^N (x_i - \bar{x})^2} .$$

Average deviation and standard deviation are also used in this research for appropriate correlation of DC and sound features.

4.4.12 Root mean Square

The root mean square value (RMS) is a measure of the data magnitude and is the square root of the average of squares. It is particularly useful for data sets with positive and negatives values.

$$(65) \quad \text{RMS} = \sqrt{\frac{1}{N} \sum_{i=1}^N a_i^2} .$$

4.4.13 Skewness

Skewness is the third moment of the data distribution. It characterizes the shape of the distribution and its asymmetry. If skewness is negative, the data are spread more towards the left of their mean value. Positive skewness indicates that data are spread more towards the right.

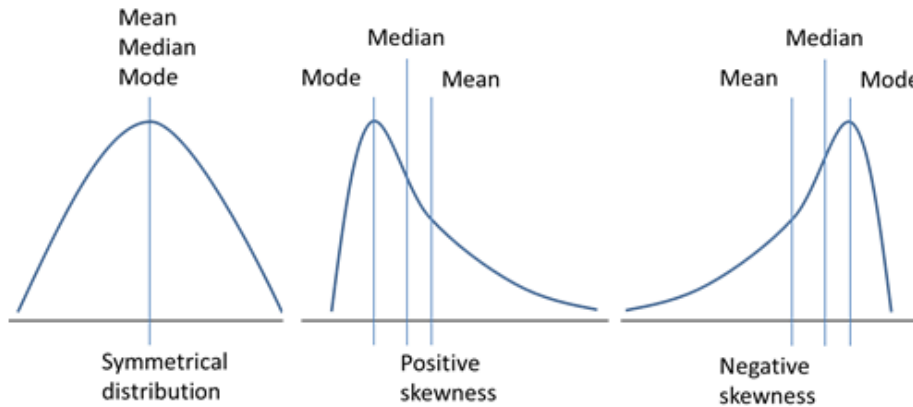


Figure 46: Examples of distributions

Moreover, in the skewed left data distribution, its left tail is longer than its right, and vice versa. The skewness of the normal distribution is equal to 0 (Figure 46). The equation below shows skewness calculation:

$$(66) \quad \text{Skewness} = \frac{1}{(N-1)} \cdot \frac{\sum_{i=1}^N (x_i - \bar{x})^3}{\sigma^3}.$$

4.4.14 Kurtosis

The kurtosis is the fourth moment of the data distribution and shows how outlier-prone the distribution is. It is an indicator of peakedness/flatness relative to the normal distribution. Kurtosis values < 3 indicate flat distributions whereas kurtosis values > 3 indicate peaked distributions. The Gaussian distribution has a kurtosis value of 3 (Figure 47); if kurtosis is greater than 3, the distribution is more outlier-prone than the normal distribution, and vice versa.

$$(67) \quad \text{Kurtosis} = \frac{1}{(N-1)} \cdot \frac{\sum_{i=1}^N (x_i - \bar{x})^4}{\sigma^4}.$$

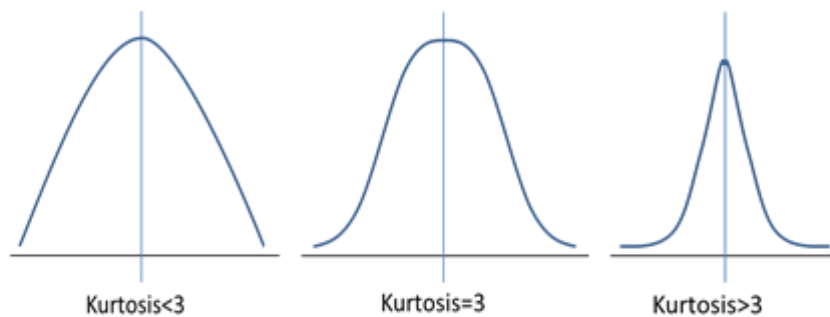


Figure 47: Examples of distributions with different kurtosis

4.4.15 Mean Absolute Deviation

Mean absolute deviation (MAD) is called average deviation of a data set, and is the average of the absolute deviation of the data points. It is the total difference between a data point value and a given point (mean or median of the data set).

MAD of mean is calculated using the following equation:

$$(68) \quad \text{MAD} = \overline{|x - \bar{x}|}.$$

In case median is used as a given point, MAD is called median absolute deviation (MDD). It is calculated as following:

$$(69) \quad \text{MDD} = \text{med}|x - \text{med}(x)|.$$

4.4.16 Trimmed Mean

The trimmed mean value is the mean value excluding some possible outliers. The idea of it is to include only a percentile of the data for computations. One example is to ignore the top and bottom 10% (i.e., total 20%), and use the middle section of data (i.e. 80%)

For this research, the following percentages are used: 25, 10 and 5. The number of the excluded data values k is calculated with the formula:

$$(70) \quad k = \frac{1}{2} \left(N \frac{\text{percentage}}{100} \right),$$

with N being the total number of data samples.

4.4.17 Modified Statistical Methods

The word “modified” here, is the internal term that refers to statistical methods that are created during this research and are not defined by other grouping methods. These methods reflect creative approach in the features creation.

Modified methods include various types of mathematical operations that can be applied to the data sets. However, these operations do not include linear summation and subtraction due to their simplicity. The data can be multiplied, divided into each other, and a natural logarithm can be taken. Furthermore, all these operations are mixed together with other statistical operations. For example, a data set x representing a feature can undergo regular and modified statistical methods like

$$x, \bar{x}, \ln(x), x \ln(x), \frac{\ln(x)}{x}, \bar{x} \ln(x), \ln(\bar{x}), \bar{x} \ln(\bar{x}), \frac{\bar{x}}{x} \ln(\bar{x}), \frac{\ln(\bar{x})}{\ln(x)}$$

Instead of the mean value \bar{x} other statistical measures or combinations can be used.

The process of combining statistical methods is only limited by the understanding of how they are interconnected and influence each other. In addition to linear manipulations, statistical scaling and readjusting are implied. Table 8 represents some of the used combinations in order to show the logic of their creation.

Table 8: Combination of statistical measures and their formulas

Combination name	Combination notation	Formula
Mean to Trimmean	mean/trimmed mean	$\frac{\text{mean}}{\text{trimmean}}$
RMS to Range	rms2range	$\frac{\text{RMS}}{\text{range}}$
Mean to MAD	mean/madmean	$\frac{\text{mean}}{\text{MAD}}$
Median to MDD	median/madmedian	$\frac{\text{med}}{\text{MDD}}$
Mean to Median	mean/median	$\frac{\text{mean}}{\text{med}}$
MAD to MDD	madmean/madmedian	$\frac{\text{MAD}}{\text{MDD}}$

4.5 Features and their Notation

The process of feature creation is iterative and challenging. In the first approximation, 1600 features were created. The initial evaluation showed that there were several features similar to each other (e.g., min value of the real trace and its mode), or their behavior on plots looked similar (mean value of the real trace and mode of the envelope), thus giving a redundant number of features. After thorough features analysis, some of them were eliminated and others added. Thus, the final amount of features is limited to 266. The procedure of features notation is rather creative. The first goal in creating features notation is to make it short, unique and comprehensible. Notation needs to reflect how the feature is created, i.e., it shall include all steps of signal processing and statistical methods.

For example, a file is decimated first and the rectangular window (r) is applied to avoid aliasing. Next, the original trace (R) in the time domain (T) is trimmed by 5% ($t5$), and the range (rng) of the resultant data is obtained. The notation of this feature would be “ $rTR:rng.t5$ ”. The next example is in the frequency domain: $rFE:C.I$. Here the signal is tapered with the rectangular window (r) and the envelope (E) of the sound is calculated in the frequency domain (F). Subsequently, the natural logarithm (I) for these data is taken and spectral centroid (C) is calculated. During the research period, all features are tested in terms of their effectiveness to use in the correlations. Appendix F lists the final sound features.

4.6 Sound Data Quality Control

Data Quality Control (QC) is an integral part of the research and needs to be performed during several stages, e.g., data collection, digitization, preparation and analysis. It is of the main interest of the research to obtain and develop appropriate QC-related procedures before data collection and manipulation. This chapter explains how data QC is performed.

Sound data QC comprises of two steps: data QC and data QC insurance. To define sound data quality, several manual operations are performed. Data QC insurance is conducted with the help of Neural Networks (NN), one of the robust tools for data classification. All these steps are discussed in detail below.

4.6.1 Data Acquisition Quality Control

As data collection methods and techniques heavily influence the quality of the gathered data, one of the main QC-related objectives is to ensure that the recorded data are of an acceptable quality. The sound data must reflect the actual situation in the well, production data must correspond to the observations and events to guarantee the best data quality. QC control of the data collection procedure includes:

1. Murag calibration: this part of data QC is provided by Meodat and includes a continual check of the Murag operating conditions (sensibility, sound intensity, loudness amongst others). In the event that the quality does not correspond to the pre-defined standards, the device is fixed or replaced.
2. Murag software updates: updates are completed by Meodat according to the schedule or in the case of unexpected failures.
3. Statistical significance: several measurements for both sound and DC are preferable in order to reduce the number of statistical errors.
4. Recording conditions: these monitor whether the recordings are done in the same conditions (Murag displacement or different installation, newly installed surface or downhole equipment, noise induced by third parties, rod rotator, chemical injection line (CIL), etc.).
5. Production reports: to utilize full and self-explanatory reports on production data in order to apprehend all necessary information.
6. Experiments instructions: to track the experiments' instructions, in order to provide organized and meaningful procedure monitoring.

The recorded sound data are digitized before being stored on the Murag server. Meodat constructs a set of rules according to which the primary data QC is supervised. Meodat provides sound data naming, details labeling, lists of relevant codes and other details that accompany the recorded data. Production data (such as well completion data, DC and events) are provided by RAG, responsible for the quality of these data.

The procedure of sound recordings check is applied after data are collected. It includes:

1. sound file naming (correct names that include name of the well, date and time when the recording is done);
2. sound file completeness (duration, correct naming, storing directory and references if given);
3. adding missing information manually if needed (names, tags and links);
4. short analysis in order to detect invalid or low quality (and thus unacceptable) sound files (file recording length as an example).

4.6.2 Labels for Quality Control

Data QC involves, at first, filtering out the unusable data. About 60,000 sound recordings are used in this project. The first goal of the data analysis is to define which files are of accepted quality and suitable for analysis, and which files can be categorized as damaged, and thus discarded. This procedure reduces the amount of files to work with and facilitates further steps. Good files, which are applicable for the further analysis, are referred to as “usable” (US). Other files that are damaged and are not qualified for the following processing are called “not usable” (NUS).

In the first approach of the sound QC checkup, more than 25,000 files are manually examined. This helps understanding the nature of the sound and its patterns. Based on the experience collected from manual file to file inspection, efficient labels for the sounds QC are introduced. Labels are sound and SRP system distinguishing characteristics or, in other words, descriptors. They help differentiate the sound files into groups and organize them in the most efficient manner. Manual classification and created labels serve as a base for extended data QC and QC insurance by Neural Network and assist in the acoustical definition of SRP states.

The following sound and system characteristics are used as labels: pump working/pump is shut off, recordings with gaps/no gaps, recordings clipped/no clipped, recordings defined as usable/not usable, recordings with audibly detected drops from CIL/no drops from CIL, peaky/not peaky envelopes of the signal, ordinary/not ordinary signal pattern, dB range. These labels are described in the following sections, and examples given.

1. Pump is working (“pump ON”): the manual files check determines that many recordings have a wave-like pattern in the frequency range 43-51 Hz (Figure 48). It looks like a cycle with repeated wave spikes and troughs. These files appear to have one trait in common, and that is the working pump. The number of cycles, moreover, corresponds to the calculated number of strokes per recording. In the time domain these files do not have common particularities that indicate a working pump. Thus, it can only be diagnosed in the frequency domain.

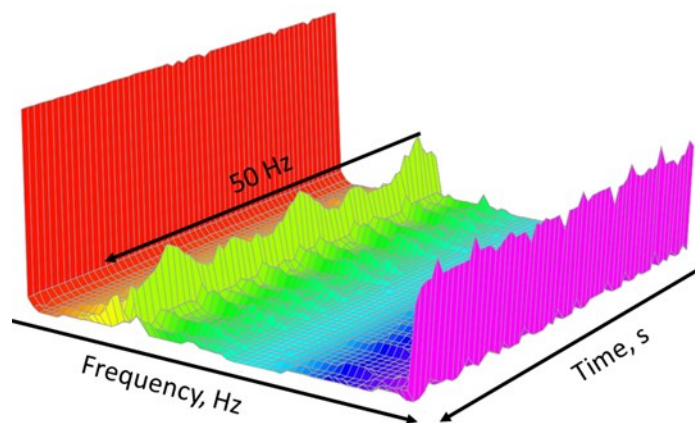


Figure 48: Spectrogram of a sound file with the working pump

2. Pump is switched off (“pump OFF”): to detect whether the pump is switched off, it is necessary to analyze the sound in the frequency domain. Contrary to the previous example, all files with the switched off pump do not have a cyclical pattern in the sound (Figure 49). In this figure, the peaks in the frequency of 50 Hz correspond to the drops from the CIL.

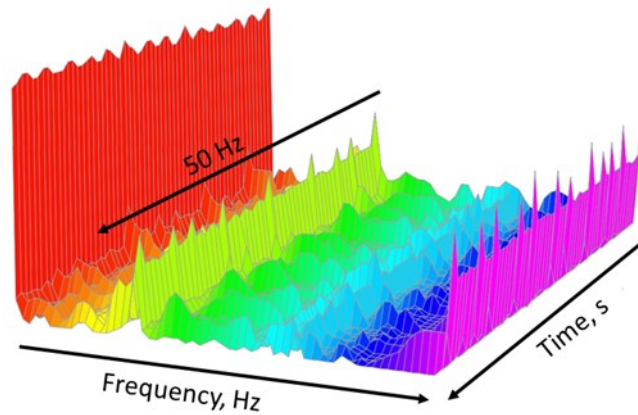


Figure 49: Spectrogram of a sound file with pump switched off

3. Files with gaps: gaps are blanks in the recorded signal caused by switching off the Gond-40 while recording (see Figure 50). When the Gond-20 starts measuring the DFL, Gond-40 is automatically shut down, i.e., no signal is being recorded. Files with gaps have a very significant peak (or many peaks depending on how many gaps are in the recording) in both domains followed by silence (Figure 51).

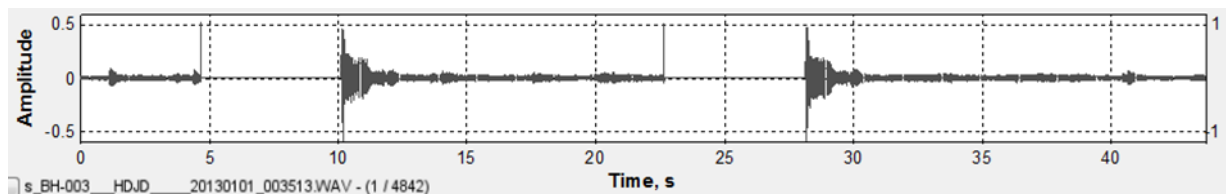


Figure 50: Example of a signal with gaps

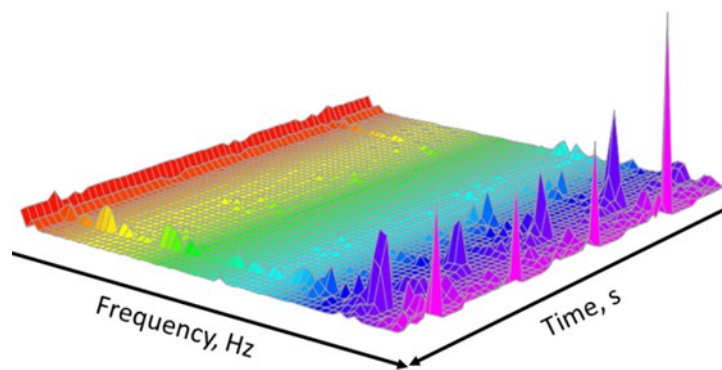


Figure 51: Spectrogram of a sound file with gaps

4. Files without gaps: the examples of files without gaps are presented in Figures 52 and 53. These are files which have continues sound recording without interruption.

5. Clipped files: the volume of this type of signal is so high that the resolution of the microphone is not enough to record the sound correctly (Figure 52). As a result, the envelope of the signal is cut (Figure 53). Figure 54 depicts a spectrogram of a clipped file. The spectrogram looks chaotic due to the high amount of noise.

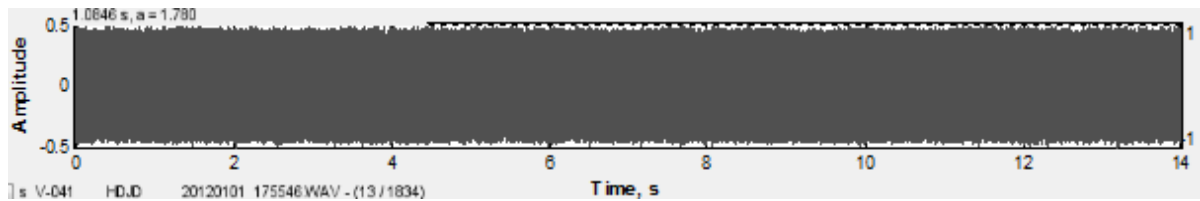


Figure 52: Example of a clipped file

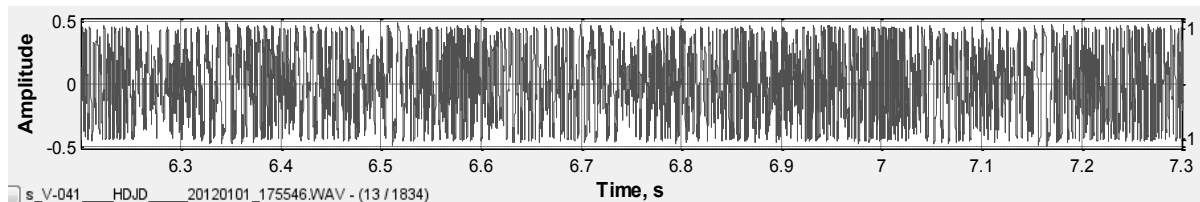


Figure 53: Example of a clipped file enlarged

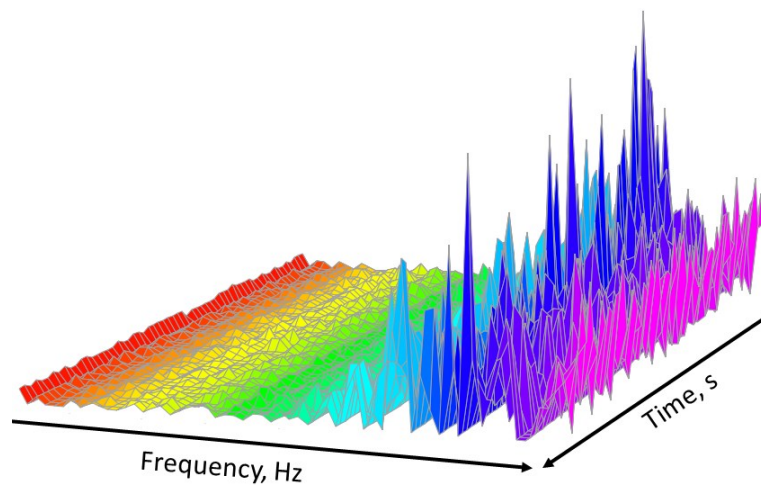


Figure 54: Spectrogram of a clipped sound file

6. Not clipped files: their interpretation in the time domain is as shown in Figure 55. As seen in the figure, amplitude of the signal stays within the frames and is not cut.

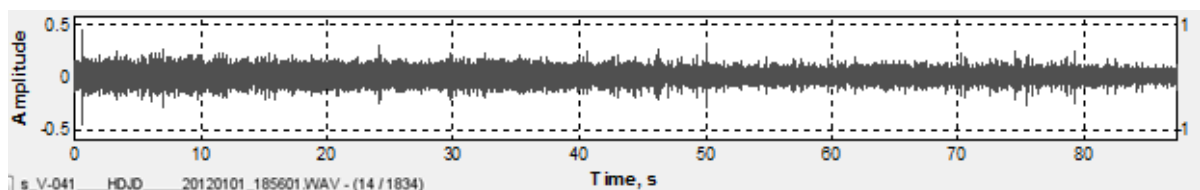


Figure 55: Example of a not clipped file

7. Files with audible drops: these files contain audibly and visibly accessible information about CIL drops. An example of such a file is presented in Figure 56. Figure 49 shows a spectrogram of an audio file with the drops, which are evenly spaced peaks.

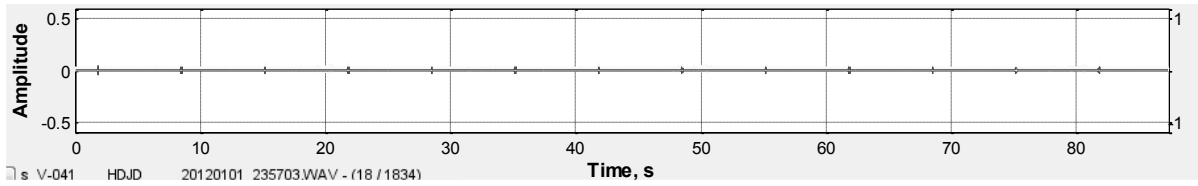


Figure 56: Example of a file with audible and visible drops

8. Stable sound envelope: the envelope of the signal stays the same throughout entire file. An example of this type of file is shown in Figure 55.

9. Changing sound envelope: an example of a file with the changing envelope is shown in Figure 57. Many files display this envelope behavior and the nature of it is unknown.

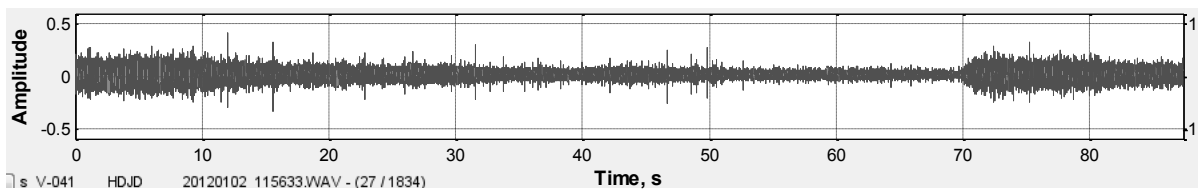


Figure 57: Example of a sound with the file changing envelope

Figure 58 depicts the spectrogram of such file. Apparent changes in the amplitude are also obvious in the frequency domain. Furthermore, the cyclic behavior of the recording at a frequency of 50 Hz in the figure denotes the working pump.

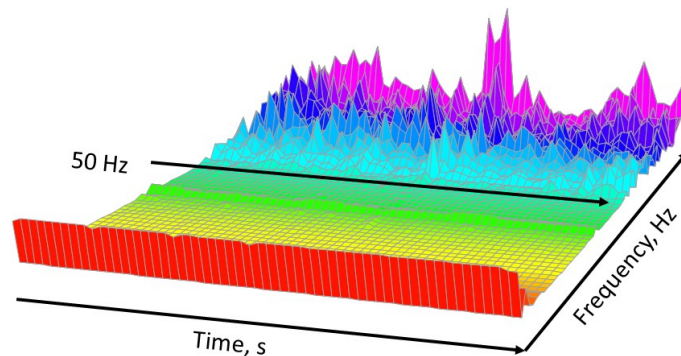


Figure 58: Spectrogram of a sound file with the changing envelope

10. Peaky amplitude: the peaky envelope is a good indicator of the sound type. In many cases sound files look very similar except for peaks in the envelopes. An example of these files is shown in Figure 59.

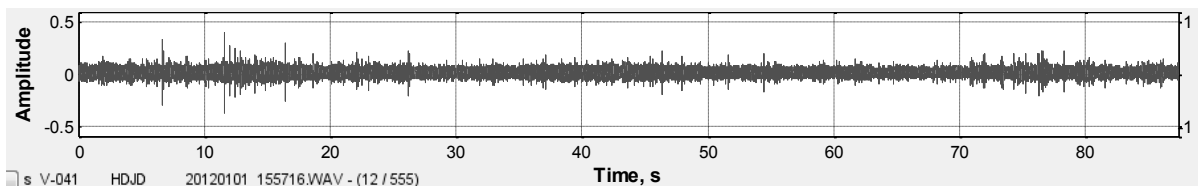


Figure 59: Example of a sound file with the peaky envelope

The spectrogram in Figure 60 has a chaotic structure due to the presence of noise carried by the peaky nature of the sound.

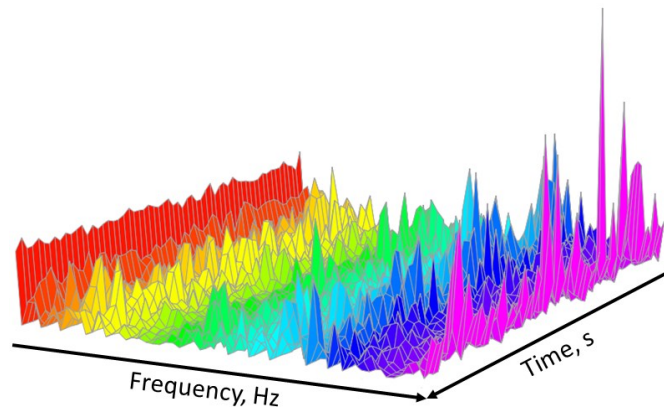


Figure 60: Spectrogram of a sound file with the peaky envelope

These are all labels presented for the sound files description. The next step in files classification is to group the labels into sets that are used to standardize and differentiate sound types. Examples of types/classifiers are: usable or not usable, ordinary files, files with or without gaps, files with or without drops, files with working pump or files with pump switched off. Classifiers of usable and not usable files and standard files are described below.

4.6.3 Usable and Not Usable Files

At the stage of the data QC, the categories “usable” and “not usable” are the most significant. Certain criteria that define a usable or not usable file are established for the data QC. Not usable files are those that:

- (1) have gaps;
- (2) are clipped;
- (3) have alternating envelope;
- (4) are of insufficient length (less than one stroke).

All other files are considered as usable. Within usable files, the signal type can vary: with the pump working or shut down, with less or more capacity of gas in the casing, with audible drops from the chemicals injection line, among others. All these files are considered as usable, and subdivided into other categories which differentiate well states. This assumption is true for all wells. For well V-041, there is an additional rule for a signal to be not usable. In January 2012, the Gond-40 broke down and did not record valuable information: the files were recorded with no sound. Thus, in the period from 16 to 23 January 2012, all files are considered as not usable.

4.6.4 Sound of Standard State

To find a state with properly working system is an attempt to register sound, which in future can be used as a baseline for comparison. This means in practice that sound features of different SRP operating states are contrasted with the features of the standard files. The standard type of sound maintains the same pattern from file to file. In these files, it is possible to hear cyclical loading and rods stretching. These files have no additional undefined or unusual type of noise (15% of data files contain noise of undetected origin). Standard files can be: with drops, without drops, with peaks,

without peaks, etc. They are unique for every well and have different sets of characteristics. A common rule for all wells is that standard state implies visible cycles of SPM. The number of ordinary files varies from well to well and from month to month. In the majority of cases they are 20 – 25% of overall amount of files per month. The set of labels requirements for a file to be standard is composed for each well individually, and it is based on the experience gained during the manual check. A file is classified as standard if the:

- pump is working¹;
- envelope of the signal is constant;
- files have no gaps;
- files are not clipped.

and in addition for well

- **BH-003** if the amplitude is in the range of 18 – 21 dB;
- **BH-009** if the amplitude is in the range of 27 – 30 or 36 – 42 dB;
- **V-041** if the amplitude is in the range of 21 – 30 dB.

4.7 Neural Network for Data Quality Control

Neural network (NN) is a category of artificial intelligence that is designed in a similar way to the human brain and biological nervous system. NN is a genius tool with a wide range of applications. In this thesis, NN is used for sound pattern recognition and files classification through the learning process. Pattern recognition indicates the possibility to find the best representative features for each label: usable, with gaps, etc. The decision to use NN is explained by the substantial amount of sound files that need to be labeled and classified.

The first NN model was suggested by a neuroscientist, Warren S. McCulloch and a logician, Walter Pitts, in 1943. In their paper [49], they initially try to understand how brain could generate very complex patterns by using neurons. Next, they give a simple model of a neuron. This model has many limitations and yet, is a significant contribution to the NN growth. The next important development was done by Frank Rosenblatt. He introduces the concept of perception that is used for the pattern recognition. The NN idea is mostly developed in the 1970s, and during the last decades more calculable theoretical aspects were disclosed.

A peculiarity of NN is its unique approach to information processing. Similar to the human brain, NN has a large number of interconnected working elements (called here: neurons) that work together to solve a problem. NN learns from examples, memorizes and applies acquired knowledge. This is done by creating relationships for the analyzed data.

In NN, a neuron is the basic element. A neuron comprises of four components: input data, weights, summation function and transfer function. Each of the inputs is multiplied with the weighting factors. These factors define which of the inputs are more important than others. Next, the modified inputs are inserted into the summing function. The summing function does not necessarily apply only summation; many other mathematical operations can be applied, including normalizing algorithms and statistics. Moreover, summing functions might be even more complicated by using activating tools in a time sensitive manner. The output of the summation function is fed into the transfer function, which then transforms the number into a real output and, if necessary, scales

it [80]. The received output then is either fed as an input into another processing function, or is ready as a final result.

NN is presented in the form of clustered neurons. These neurons create layers, which are connected with each other. The first layer contains neurons that receive inputs. The last layer provides the output of the NN. The layer between is called a hidden layer and in practice can consist of several layers (Figure 61). All layers and connections between them are thoroughly structured and defined. This approach gives good intuitive solutions, and provides proper functioning of the NN. In many cases, the output results also provide a feedback to the hidden layers. It is important to define the number of hidden layers correctly. If the required number is underestimated, the NN will not completely solve the problem. In contrast, if the NN number is too great, it concentrates around the data learning process and tends to model the noise [8]. Hidden layers of the NN, which contain several layers, are called multilayers. This type of the NN is the most common nowadays. There are also other NN perceptions available. Completely connected perception (CCP) is the most advantageous and uses a completely straightforward network growing process.

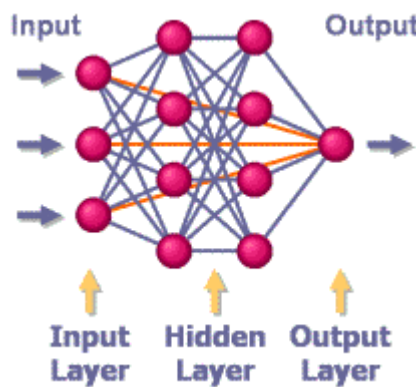


Figure 61: NN structure, after cVision User's Manual, 2009 [8]

NN performs three processes when working with data: learning, testing and validating. Adjustments to NN are corrected in such a way that 60% of the data is used for the learning process, 20% for the testing and other 20% is for the validation. Each process is accompanied with a monitoring tool that calculates errors and plots them. Multilayer NN is trained using a specific algorithm. There are two possibilities for the training: supervised and unsupervised. In this work supervised training is used when both inputs and outputs are given. Unsupervised training is applied when NN is already experienced with the supervised training.

Once the NN is trained, it can be utilized as an analytical tool. To do that, the inputs are given, but there are no defined outputs. NN uses its memory and experience to define the outputs. For this purpose, NN works in the forward propagation mode. One of the advantages of the NN is that it can be also re-trained. This is particularly useful when the network needs to be separated for different inputs.

The application of the NN is included in the procedure of data QC insurance. NN classifies the sound files into usable or not usable, and at the same time, insures that this division is performed correctly. In the first approach, NN is run in sequential forward selection (SFS) manner. SFS allows ranking the considered parameters (i.e., sound features) with respect to their impact on the files

recognition performance [81]. In the learning process, NN uses only sound files with known input and output. For the sound differentiation (QC) sound features are used as inputs (Figure 62). The outputs are the classifications of the sound files, which are given by means of labels (usable or not usable file, gaps or no gaps, etc.). NN, in this case, determines a relationship between input and output, i.e., labels and sound features. Once the connection/dependency is found, corresponding best representative features (BRF) are stored. Subsequently, these features are used to identify the remainder of the not labeled files. The set of BRFs compose a model for data QC. Each well has its own model and BRF are defined for each label and sound descriptor.

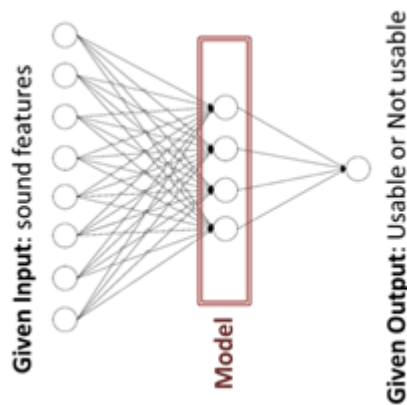


Figure 62: NN learning process

To visualize features efficiency, they are plotted with respect to the error for each NN process: learning, testing and validation. The left ordinate axis shows the error calculated for each NN computational step for each BRF; the right ordinate axis is CCR (calculated cumulative ratio). The CCR shows the percentage of files that are identified correctly.

The best features plotted on the x-axis are grouped by the number of channels (features). In the first left-side group, there are single best features. It means that only one of those features is enough to recognize this particularly label (e.g. “usable”). Starting with feature number nine (rTR:mod) the magnitude of the error increases significantly. Depending on the error allowance, the detection of the BRF is stopped as it becomes inefficient. The second column is the set of features that are best representatives only in combination with the first BRF (rTR:rng in this case). This process is SFS. The third column is the set of features that can show good results only in combination with the best features from the first and the second columns. This column is useful for 3D interpretation. The fourth column is built by analogy to the third one. To sum up, there are some features that are the best representative only by themselves, and some are the best representatives only in combination with others. As the scope of this research is to keep the analysis as simple as possible, only BRF for 1D and 2D presentations are selected.

Figure 63 displays that the first column (single features), has the highest amount of learning, testing and verification errors. The trend of the error curve (for all errors) increases. As seen from columns 2, 3, and 4, there is no significant error reduction, which means it is sufficient to use two features. CCR has similar behavior: its value is the lowest for the single features and close to 100% for features combinations. CCR does not improve drastically if three or more features are used together, thus it is sufficient to have 2D selection.

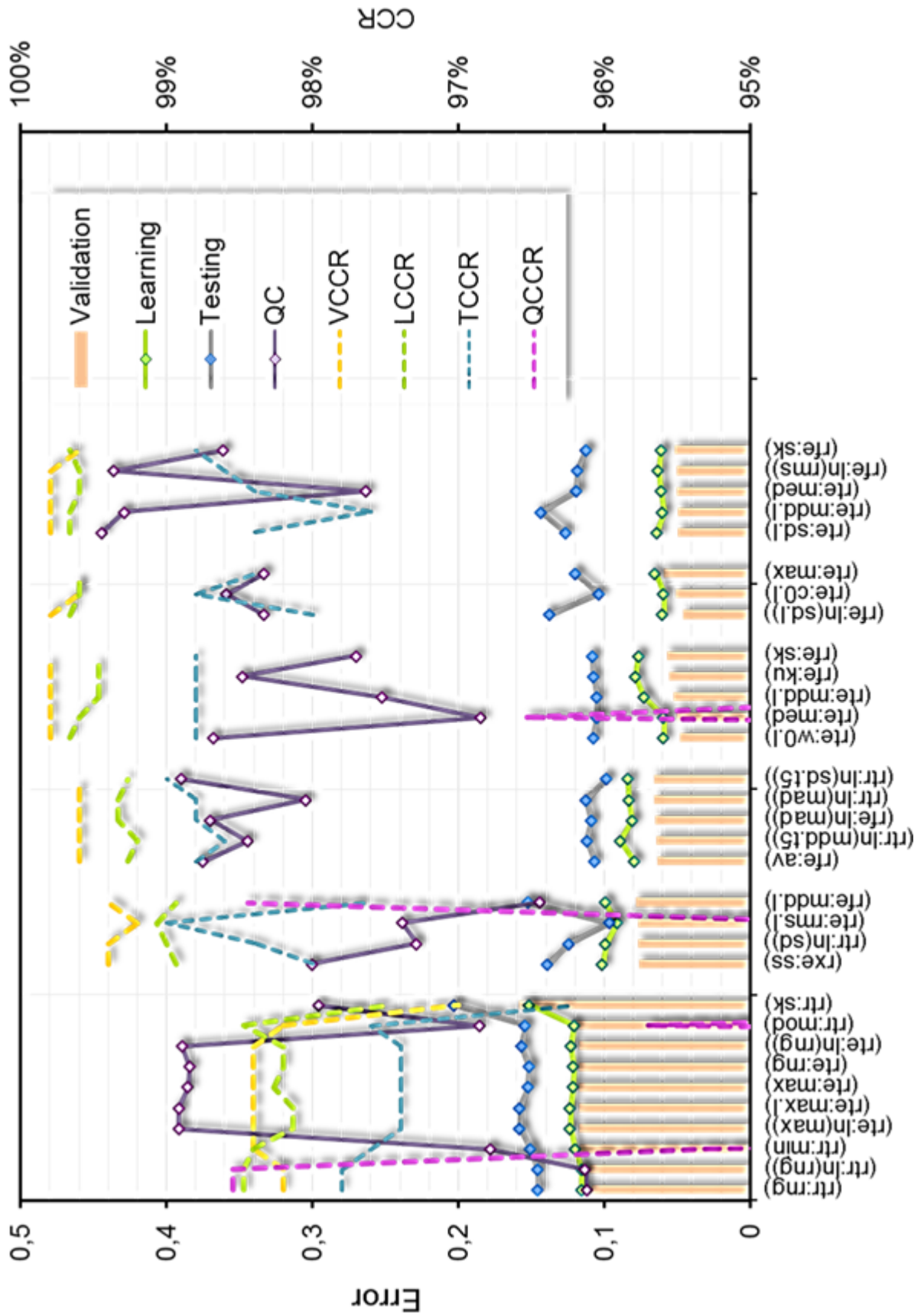


Figure 63: Example of NN output, well BH-009

The first NN run identifies usable and not usable files, and plots the BRF in order to visualize results and evaluate features efficiency. This procedure allows for double checking the initial (manual) data categorization. The example of such a plot is shown in Figure 64, where $rTR:sd.t5$ and $rTE:rng$ are plotted. Yellow dots correspond to usable files, and red to not usable. Strong clustering of the same type of files means that the chosen features are good representatives. NN takes these features for the next step, which is the separation of not characterized files by means of the NN model. In this process, NN uses the calculated sound features of all files, obtained from the previous step model, as inputs. After applying the model, NN provides output for each file: label usable or not usable.

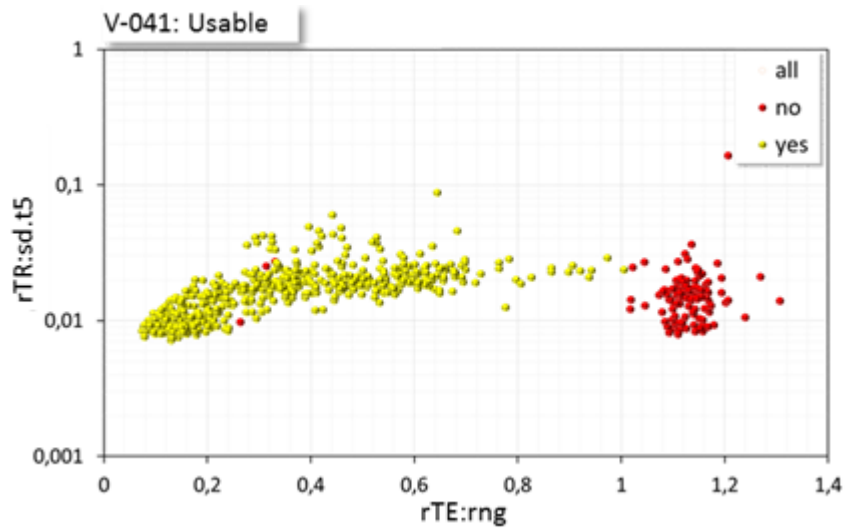


Figure 64: Best representative features for usable files of well V-041

Plots that represent features can also be applied in order to reveal other labels and well states. In Figure 65, $rTR:mn2min$ is plotted on abscissa, and $rTR:min.t5$ is on the ordinate axis of well BH-009.

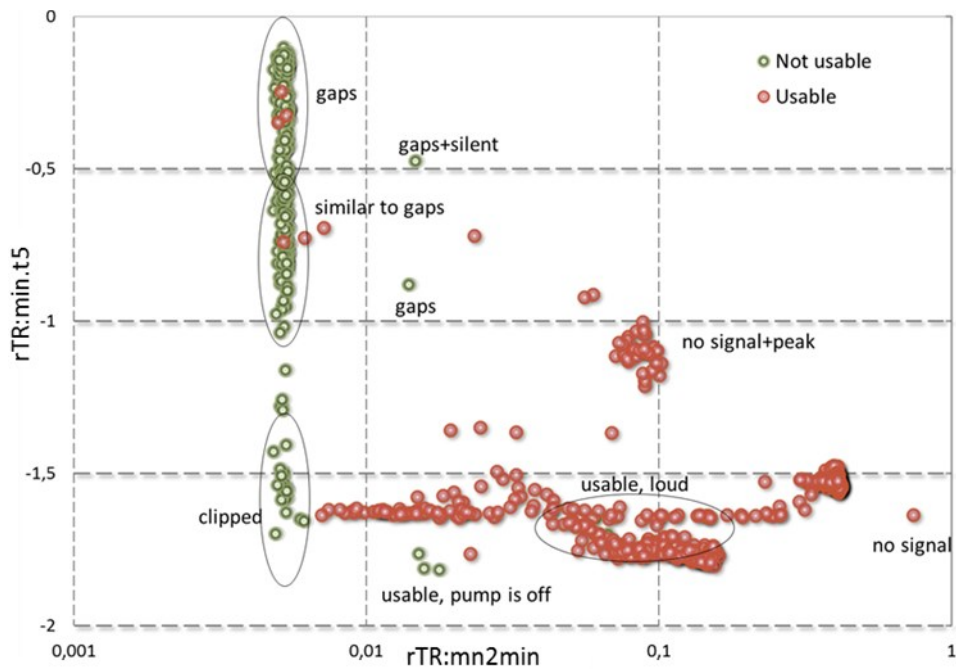


Figure 65: Example of 2D plot

Grouped dots correspond to a specific label (gaps, clipped) or well state (e.g., a switched off pump). Charts can be plotted in either a semi-log or log-log format to provide a clearer demonstration. If mislabeling is identified, it is corrected, and SFS is run again. This procedure is performed for all wells and every label. It is a time consuming part of the work and requires a certain set of assumptions at each iteration step. In the further research, each label will have a set of best presenting features for each well. In the final stage, after all iterative steps are completed, NN identifies features with 100% success in categories recognition. During the QC stage, in many cases the BRF chosen by NN are not the best for a visual check. Tables 9 and 10 present examples of the BRF sets in terms of their efficiency, which is checked manually. Here, the overall performance is estimated from 1 (the best) to 5 (the worst) and colored correspondingly.

Table 9: Estimation of features efficiency for well V-041, label “Standard”

	rFE:ln med	rFE:ln mod	rLB:ln hE04	rFE: W0	rFE:S	rTR: rms	rTR: rng	rFE: mod	rFE: mad
	1	2	3	4	5	6	7	8	9
rFE:ln(med)1	3								
rFE:ln(mod)2	3	3							
rLB:ln(hE04)3	3	3	3						
rFE:W0	4	3	3	3					
rFE:S	5	3	2	2	2				
rTR:rms	6	3	3	3	2	3			
rTR:rng	7	3	3	3	2	3	3		
rFE:mod	8	3	2	2	2	2	2	3	
rFE:mad	9	3	3	3	2	3	2	2	4
rFE:rms.l	1	3	3	3	2	3	3	2	2
rTE:ln(mad)2	3	3	3	3	2	3	3	2	2
rLB:ln(hE08)3	3	3	3	3	2	3	2	2	2
rLB:ln(hE39)4	3	3	3	3	2	3	3	2	2
rLB:CC24	5	2	2	2	1	1	1	1	1
rTE:ln(max)6	2	2	2	2	1	2	2	1	1
rTE:ln(min)7	2	2	2	2	1	2	2	1	1
rTE:ln(mad)8	2	2	2	2	1	2	2	1	1
rTE:rms	9	2	2	2	1	2	2	1	1
rTR:av.t5	10	2	2	2	1	2	2	1	1
rTR:av	11	2	2	2	1	2	2	1	1

For instance, for well V-041, standard files, the feature rFE:S has the highest marks comparing to the others. The same is true for the feature rLB:CC24. It means that both these features (despite the fact that NN did not indicate them as the best representatives) define the standard files the most efficiently. These features are the most beneficial to use to identify this type of sound files.

Table 10: Estimation of features efficiency for well BH-009, label “Usable”

		rTR: rng	rTR: min	rTR: mode	rFE: ln (rng)	rTE: rng	rTE: max	rTR: sk	rXE: SSO.l	rTE: mad
		1	2	3	4	5	6	7	8	9
rTR:rng	1	2								
rTR:min	2	2	2							
rTR:mode	3	1	3	2						
rFE:ln(rng)	4	2	2	2	2					
rTE:rng	5	2	1	1	2	2				
rTE:max	6	2	1	1	2	2	2			
rTR:sk	7	1	1	1	2	1	2	2		
rXE:SSO.l	8	1	1	1	2	1	2	1	2	
rTE:mad	9	1	1	1	1	1	1	1	1	2
rFE:W	1	1	1	1	1	3	3	2	1	1
rFE:F	2	1	1	1	1	2	2	2	1	1
rXE:CC	3	1	1	1	1	2	2	2	1	1
rXE:SS	4	2	2	2	2	2	2	2	2	1
rTE:med	5	2	2	1	4	3	3	2	3	1
rFE:mod.l	6	3	2	1	2	3	3	2	3	1
rTR:ln(rng)	7	1	2	2	2	2	2	2	1	1
rTR:ln(mad)	8	2	2	2	2	2	3	1	1	1
rTE:av	9	2	2	1	1	2	2	1	1	1
rTR:ku.t5	10	1	2	1	2	2	2	2	2	1
rFE:mod	11	1	2	1	1	1	1	2	1	1

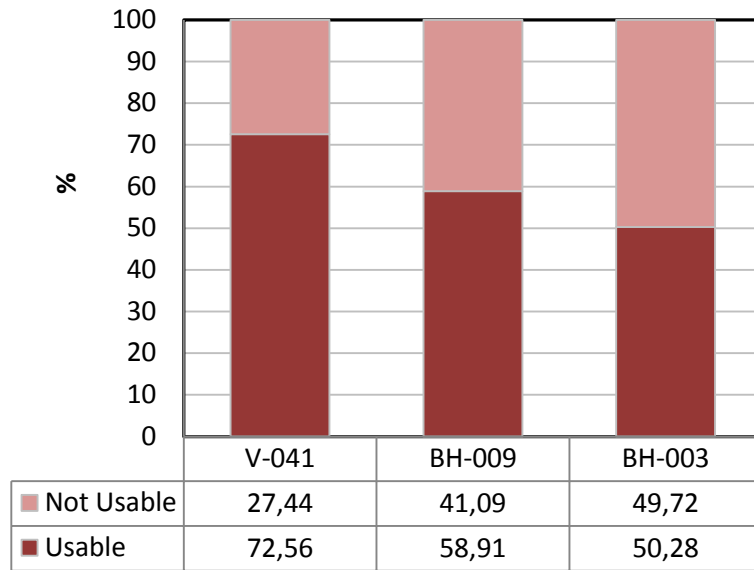
The tables illustrate that the application of only one feature for files differentiation is not always sufficient. There are some pump states that are relatively difficult to identify with the sound features (e.g., standard files for well BH-003). With the help of NN, all sound files are grouped into usable or not usable. Final number of usable files after data QC is shown in Table 11.

Table 11: Final number of usable/not usable data after data QC

Well	Files total	Files usable	Files not usable
V-041	22,500	16,326	6,174
BH-009	9,056	5,335	3,721
BH-003	28,121	14,139	13,982

The lowest percentage of not usable files belongs to well BH-003. This fact can be explained by the method of well completion, particularly by the use of the polylined tubing, which supposedly has higher damping coefficient. Statistically, 60.58% of all files are usable, and, correspondingly, 39.42% are not usable.

Table 12: Percentage of usable and not usable files after data QC



All QC positive sound files are taken to be processed again. Further procedures include computation of the same features, but in 120-window-based manner. Extracted features are stored in the form of a spreadsheet and ready to be correlated with the DCs and DC features.

5 Dynamometer Card and Sound Data Correlation and Results

The final part of the research concentrates on finding the relationship between DC and sound data. This procedure involves two processes each with a different purpose. The first checks the concept that DC and sound are related to each other; in other words, it checks whether sound can reflect load alterations. The correlation and determination coefficients achieved, indicate the strength of the correlation.

The second process is based on the first correlation, which states that DCs and sound are related. Using this assumption, NN uses sound features to model DC features. Collated with the production events, they serve as SRP state indicators and can be used as a monitoring tool.

5.1 Correlation of Sound Features and DC values

The first correlation process aims to prove that DC values and sound features are correlated. This knowledge can help understand how the sound features and the DC load values are related and which features best reflect DC behavior: frequency or time domain features, Mel frequencies, etc. An example of such a correlation is shown in Figure 66, the DC load values of well BH-003 are shown together with the sound feature rLB:CC09. SFM stands for *single feature model*, meaning that a single feature is linearly transformed to fit the DC load values in an optimal sense.

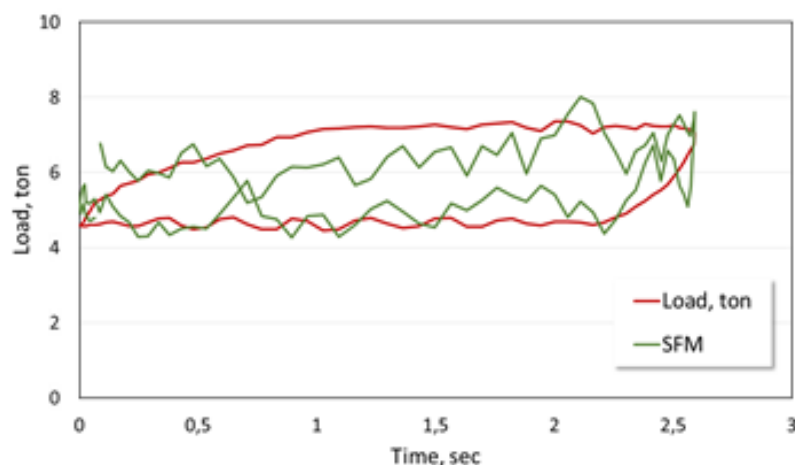


Figure 66: DC and sound features correlation

A standardized method to estimate correlation is to use the Pearson correlation coefficient r . Correlation coefficient measures how strongly two data sets are linearly related to each other. r shows the direction of the correlation and $-1 \leq r \leq +1$. The equation for r :

$$(71) \quad r(x, y) = \frac{\sum(x_i - \bar{x})(y_i - \bar{y})}{\sqrt{\sum(x_i - \bar{x})^2 \sum(y_i - \bar{y})^2}},$$

Where x and y are two ranges of values, \bar{x} and \bar{y} are their average values respectively.

Positive r indicates such a relationship between x and y , so that if the values of x increase, values for y also increase. The maximum r in this case is 1 and indicates perfect fit. Negative correlation means that if the values of x increase, the values for y decrease and the strongest negative correlation is defined with $r = -1$. Correlation coefficient of zero means there is either no, or random non-linear correlation between two variables.

A correlation is described to be strong if r is higher than 0.8, and is weak when r is less than 0.5. A perfect correlation means that all points belong to the same line.

Figure 67 depicts another method of evaluating data correlation. In addition to r , a determination coefficient, denoted r^2 is applied. r^2 indicates how well data sets fit a regression line and are related to each other. It ranges from 0 to 1. The equation that illustrates the regression line is modelled from the data. This plot is created for the same sound file, using feature rLB:CC07. In this example $r = -0.948$ and $r^2 = 0.8993$. This means that 89% of the sound feature variation can be explained by its linear relationship with the DC.

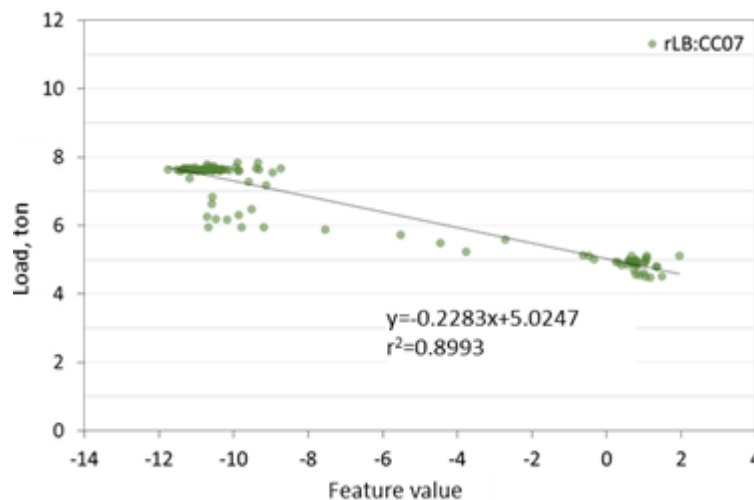


Figure 67: Example of the determination coefficient and regression line

The result of the DC values and sound features correlation is a set of correlation and determination coefficients, obtained for each point of correlation. Figure 68 shows an example of this. The lower part of the graph contains load (red) versus time data points plotted alongside the sound feature (green). In this case it is rLB:CC07. Here it is easy to see how much data coincide, thus indicating strong correlation and high value of r . The upper part of the plot contains two curves and its ordinate limits with -0.9 and 0.9 (for r and r^2 scaling). The green line is the sound feature and the brown line is the determination coefficients. The sound feature curve is being moved along the DC

to obtain the r^2 . Values of r^2 change and have their peak at the marked point. Feature lines in both subfigures have been 180° rotated, which indicates the negative correlation.

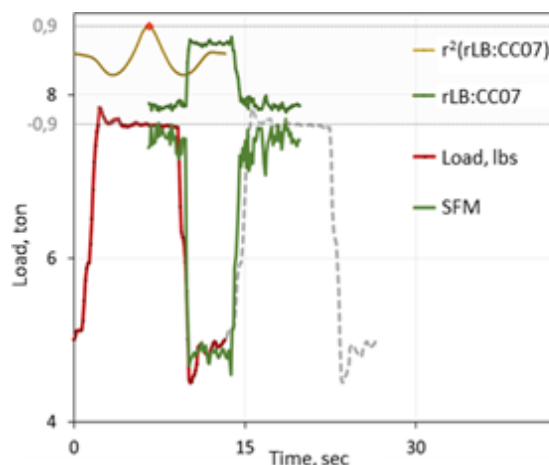


Figure 68: Example of correlation

Every DC is correlated with more than 20 sound files recorded the same day, each presented by 266 sound features. At the end, there are more than 300,000 r^2 calculations. A special tool that provides automated computation is created in order to facilitate this work. The tool moves the sound feature line along the DC plot (load versus time) and searches the point where the r^2 value is the highest (see in Figure 68). In many cases, the point of the highest r^2 does not occur at the beginning of the upstroke, but few data points after. This phenomenon can be explained by the delay at the downhole caused by the wave motion of the rods.

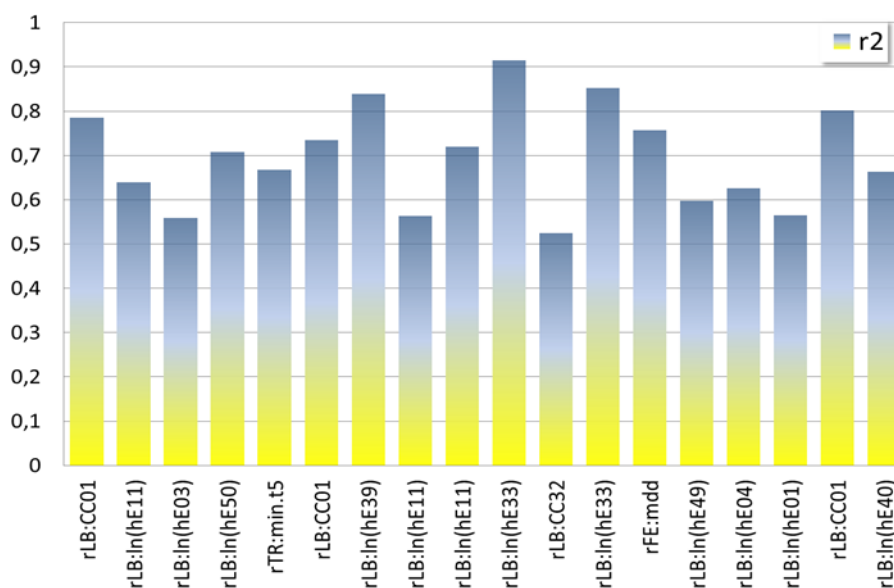


Figure 69: The features with the highest r^2 over a day

An example how the determination coefficient changes over the day is shown in Figure 69 for well V-041 during 28 December 2011. The highest r^2 values of the corresponding feature names are plotted. The best correlative features for this well are linear band based (e.g. $rLB:ln(hE39)$, $rLB:ln(hE33)$).

Other types of graphic illustrations are used to plot the results; for example, a radar plot depicts the load and sound feature in a circular mode, which can be useful to present their change as a function of the crank motion (Figure 70). The upstroke starts at the 12 o'clock position.

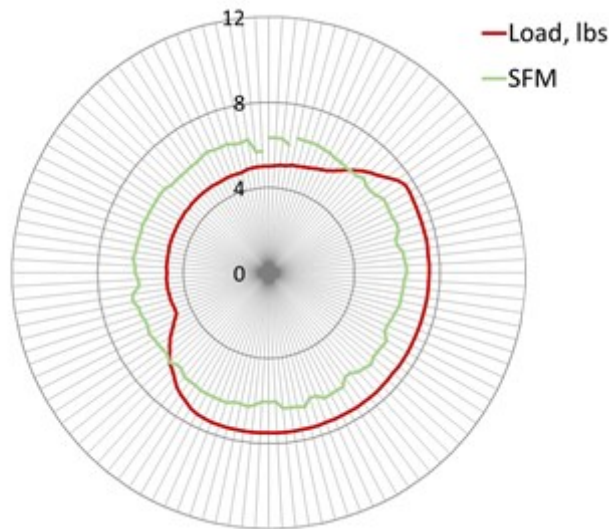


Figure 70: Radar plot of the sound feature rLB:CC44 and the polished rod load

The green line is the sound feature and the red line is the load, both starting from the upstroke. There are 120 data points for each line. The radius of the plot represents both, DC load and the feature values. As shown in the figure, two data sets have a good correlation. Here, the feature “rLB:CC44” of the sound file “s_BH-003__HDJD____20120802_092948.WAV” is correlated with the DC taken on 8th August 2012.

All DCs are correlated with the corresponding sound files. The overall result of the correlation of the first type proves that sound and DC are interconnected. Each well has its own set of features with a strong correlation. Table 13 comprises information about the most and least effective correlating features and gives the average overall determination coefficient for each well.

Table 13: Correlation results

Well	Best feature		Worst feature		Average r^2 value
	r^2 value	Name	r^2 value	Name	
BH-003	0,9304	rLB:CC45	0,1225	rLB:CC58	0,41043
BH-009	0,7598	rLB:ln(hE55)	0,0009	rTR:av	0,3234
V-041	0,9145	rLB:ln(hE33)	0,0018	rTR:av	0,5079

For the well BH-003, the cepstral coefficients of different linear bands show the strongest correlations. Nevertheless, this type of sound features is the most and least efficient at the same time. It means that the sound in the well BH-003 has frequencies of some bands which are strongly influenced by load alternation (bands 30 – 36); and at the same time frequencies of other orders are not related to the rods’ load (bands 1 to 20, 42 to 52). The least correlated with the DC sound feature rTR:av is the same for both wells BH-009 and V-041; these wells have also the same type of

the most correlated sound feature, log of Hanning tapered linear band energies. The reason why well BH-003 has different the most correlated features might be the polylined tubing.

As mentioned before, the polyline cover is different to the steel damping coefficient, which might result in damping one range of frequencies more than others, thus influencing the composition of the resultant sound. Well BH-009 has the lowest determination coefficient as it has the least number of the sound files to allow for efficient correlation. The percentage of the total amount of the determination coefficients with values higher than 0.7 and 0.5 for each well is shown in Table 14.

Table 14: Determination coefficient percentage per well

Well	$r^2 > 0,7$	$r^2 > 0,5$
BH-003	26,0 %	34,7 %
BH-009	4,6 %	13,8 %
V-041	12,3 %	42,8 %

Figure 71 shows an example of the correlation process. This figure contains all types of plots discussed before and provides full information on the correlation results.

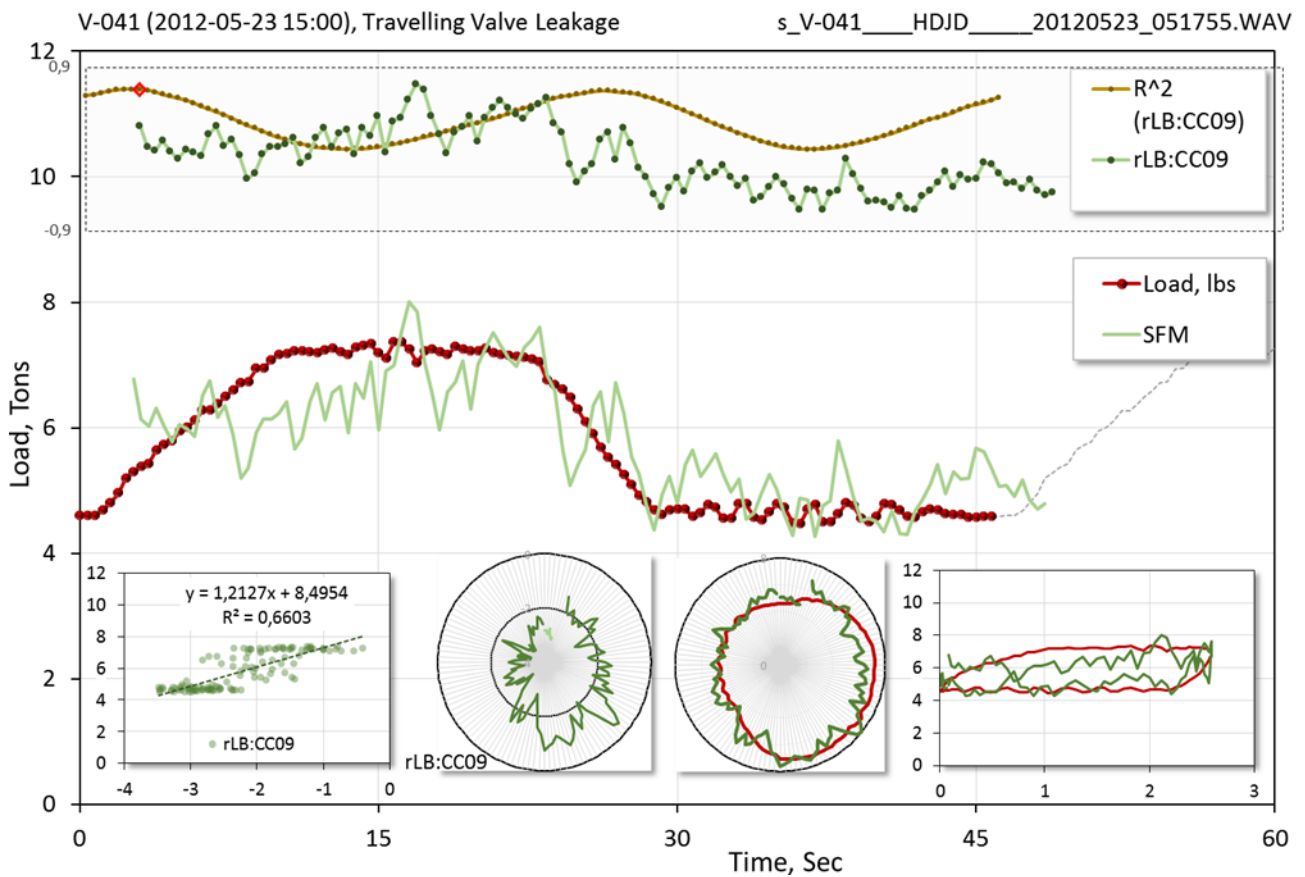


Figure 71: Final correlation plots

5.2 Second Type of Correlation

The second type of correlation searches and examines relationship between DC features and sound features. The obtained sound to DC features relationship then is utilized to model DC features. DC features available for the duration of the research period are continuous representations of the changes in the pump system and assist in system behavior analysis and monitoring. A DC is characterized with six features described in Chapter 3.5, Dynamometer Card Features. Three of them are calculated for the downstroke (E_{dn} , F_{dn} and P_{dn}), and three others for the upstroke (E_{up} , F_{up} and P_{up}). Each sound feature (see Chapter 4.3, Sound Features) is described with 120 data points. The correlation of both DC features and sound features requires them to be of equal length. In order to fulfill this requirement, the sound features need to be decreased to two values: one number for the sound feature in the upstroke and another for the downstroke. There are several ways to reduce data to one value, yet keep it logical and representative.

The most common statistical tools that are used to describe distribution are average and standard deviation. They form the basis of the statistics and indicate texture of the group of data, data spread and data density. Standard deviation (SD) and average (AV) are used here to reduce the sets of sound features. Each sound feature set is broken into 2 subsets: 60 data points for the upstroke and 60 for the downstroke, and SD and AV for each of the subsets are computed. To sum up, each sound file is presented with 1064 features: 2 (upstroke and downstroke) \times 266 (number of features) \times 2 (SD and AV).

There are not so many DCs available compared to the enormous amount of sound files. The concept to correlate a DC to only one sound file does not give statistically acceptable results. To guarantee correct computations, the margin of sound files is applied. This margin includes sound files recorded two days before and two days after the day when the DC was taken. For the correlation, all 266 sound features of each recording are associated with each DC feature.

To resolve the lack of the DCs, the neural networks model the absent data by using sound features. The NN application is explained in Figure 72. First, it is necessary to train NN to design a model for DC features calculation. For this purpose sound files with corresponding DCs are used to provide known input and output. NN takes the sound features as input and the DC features as output. Through doing this, the NN is being trained to find relationships between them and releases in this way a model that illustrates this relationship (Figure 72, a). There are three different types of models according to the input information:

- 1) averaged sound features (av);
- 2) standard deviation sound features (sd);
- 3) averaged and standard deviation sound features together (avsd).

Individual models are created for each DC feature, upstroke and downstroke. The notation of the NN models for the DC features computation is straightforward. It includes the name of the feature desired and the way in which the sound features are decreased (AV or SD, or both). For example, $P_{up\ avsd}$ means that to obtain the upstroke power, both the average and standard deviation of sound features are used together. $E_{dn\ sd}$ means that sound features reduced with standard deviation are applied to compute the downstroke energy. In total, 108 models are designed. To acquire the

missing DC features, NN applies these models (Figure 72, b). Computed sound features are fed into NN as input along with the corresponding model. The output of this procedure is a set of calculated DC features. Each model yields in one DC feature.

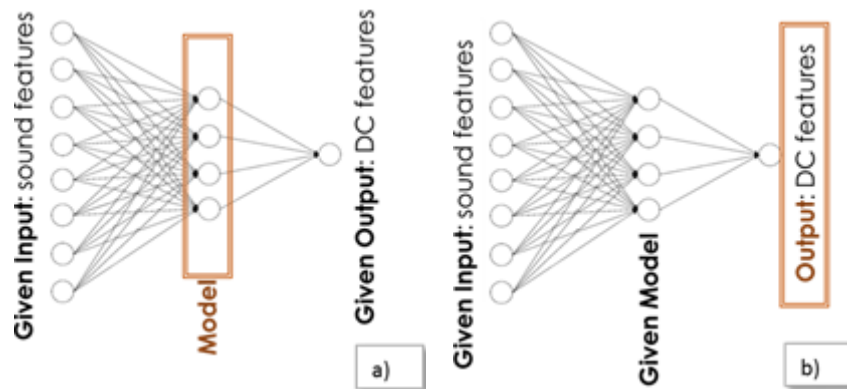


Figure 72: NN application for DC features modelling

DC features modelling with the sound features ensures that all sound files are “equipped” with the corresponding DC features. Figure 73 to Figure 82 show plots of modelled DC features and production events versus time. This approach is helpful when searching for system behavior patterns and dependences.

Figure 73 shows the behavior of the average force of both the downstroke (F_{dn}) and upstroke (F_{up}) for the duration of the research period in well BH-003. Together with the DC feature type, it also includes information about the computational model (avsd). The left ordinate axis represents values of the average force in tons; the right ordinate axis represents SPM; registered production dates are plotted in abscissa with available DCs. Figure 73 points at the clear relationship between DC features and pumped-off (POF) state. The F_{dn} of the well in the POF state has higher values comparing to the state when the well is not POF. Moreover, before the well is in POF, the values of F_{dn} start increasing in magnitude (from October 2012). This trend can be an indicator that the state of the well changes as the F_{dn} is gradually increases, having its max value during POF state days.

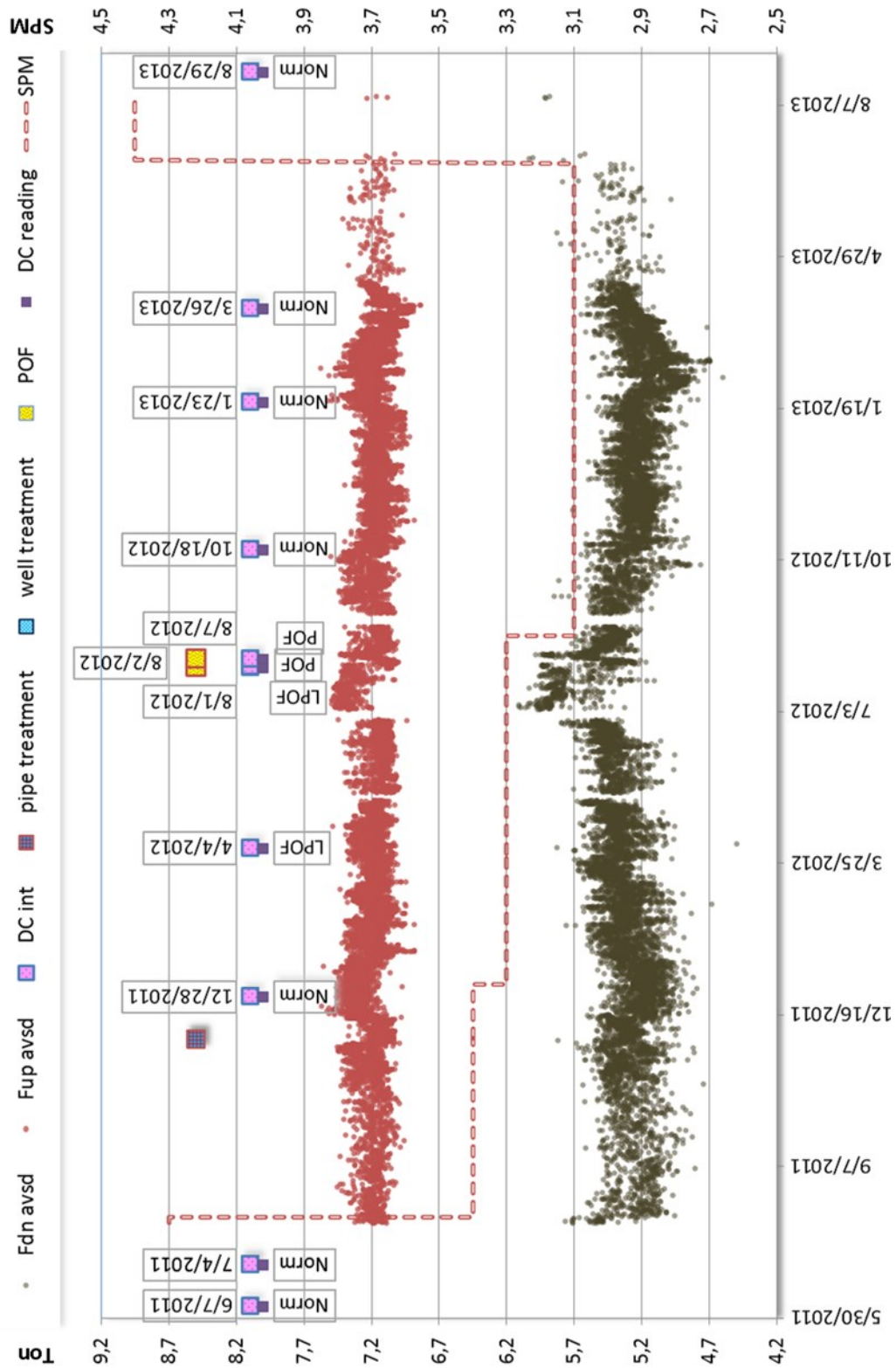


Figure 73: BH-003 Production events. $F_{dn\ avsd}$ and $F_{up\ avsd}$

The pipe treatment (PT), which is shown on 30 November 2011, has an effect on F_{up} behavior. As Figure 73 shows, F_{up} decreases significantly after the PT, but values of the F_{dn} do not change. Other DC features are also connected with the PT. Immediately after the pipe treatment, the P_{up} and E_{up}

drop significantly (Figure 74 and Figure 75), which means that pipe treatment results in reduced power and energy necessary for the upstroke. This phenomenon can be explained with the fact that conducted PT decreases backpressure in the pipelines and the system needs less energy, power and force. To summarize, *carrying out PT in the SRP system leads to a decrease in upstroke energy, power and average force without changing downstroke DC features.*

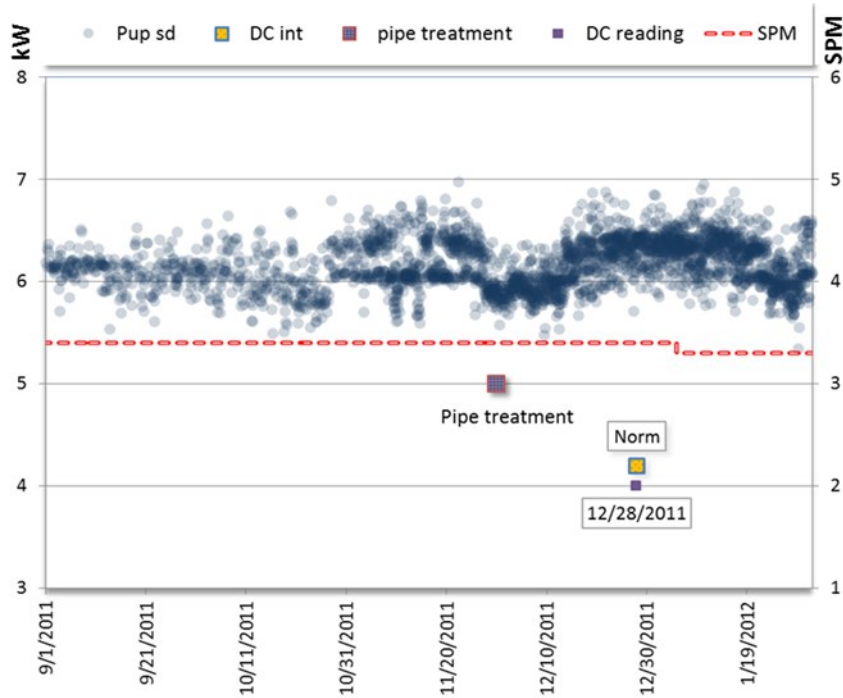


Figure 74: BH-003. Enlarged pipe treatment event $P_{up\ sd}$

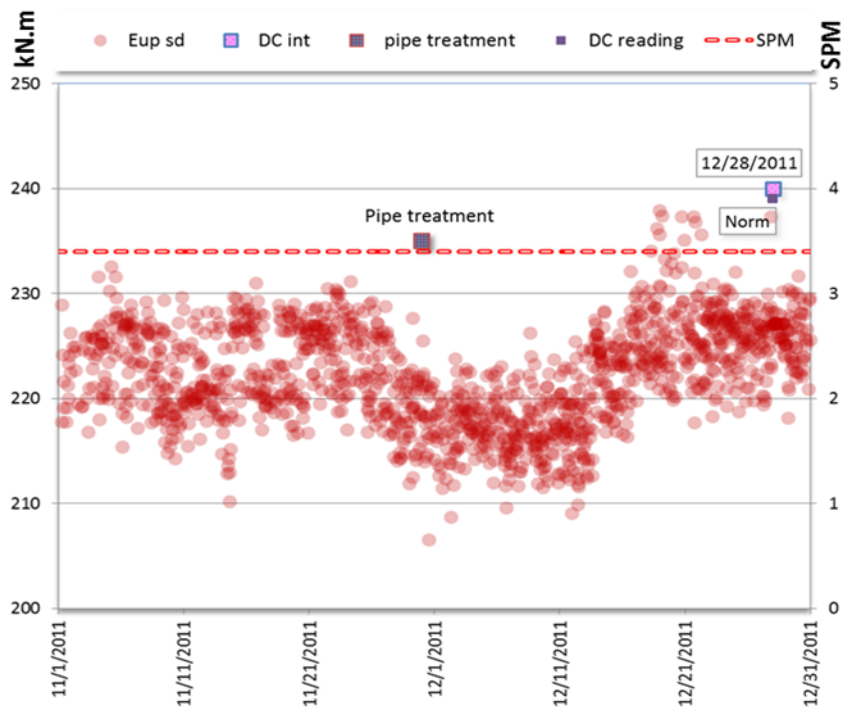


Figure 75: BH-003. Enlarged pipe treatment event $E_{up\ sd}$

Figure 76 presents the results for the well BH-009. The feature plotted here is the downstroke energy. Due to lack of the sound data the graph cannot be properly examined.

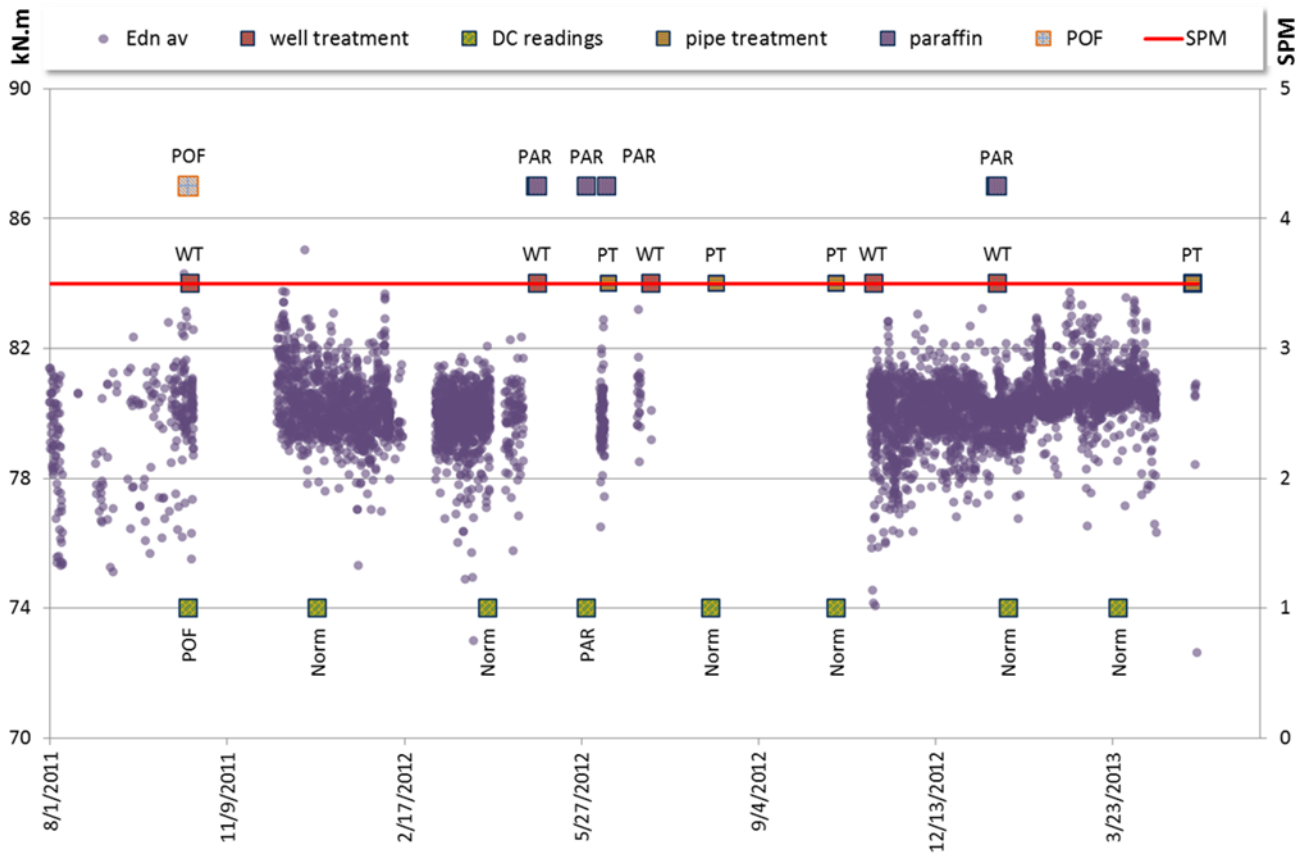


Figure 76: BH-009 Production events $E_{dn\ av}$

Well V-041 presents an event filled production history, which provides good opportunities for investigation. Figure 77 contains the production events and the modelled upstroke and downstroke energy from the averaged sound features data. The ordinate axis on the left is for the energy scaling, while the right ordinate axis corresponds to the SPM. Like in the previous figures, abscissa states the dates. The graph indicates many relationships: the stroke energy reflects changes in the production states. Downstroke and upstroke energy magnitude is different when the well is POF, both with paraffin and when SPM alternates. The following diagrams show these states in more detail.

One of the examples is the paraffin precipitation in the tubing, which is a problem common in Austrian wells. To combat this, there are several methods which can be used (discussed in Chapter 2.7.4, Paraffin Precipitation). The consequences of paraffin appearance can be very severe. It can block the rods from moving and stop the pumping. Figure 77 shows that both E_{up} and E_{dn} have great magnitude variations when the well is with paraffin. DC energy varies from very low values to very high. High magnitudes are explained with the increased friction forces that rods have to overcome when moving up, whereas extra friction force reduces weight when moving down. Smaller magnitudes are derived from partially blocked rods. They cannot travel the length of the entire stroke and do just a small part of it, thus carrying lighter loads. To sum it up, *upstroke energy*

can be used as an indicator of the paraffin building process as it increases before the paraffin situation occurs (Figure 78). Upstroke and downstroke power are also good indicators of paraffin precipitation (Figure 80).

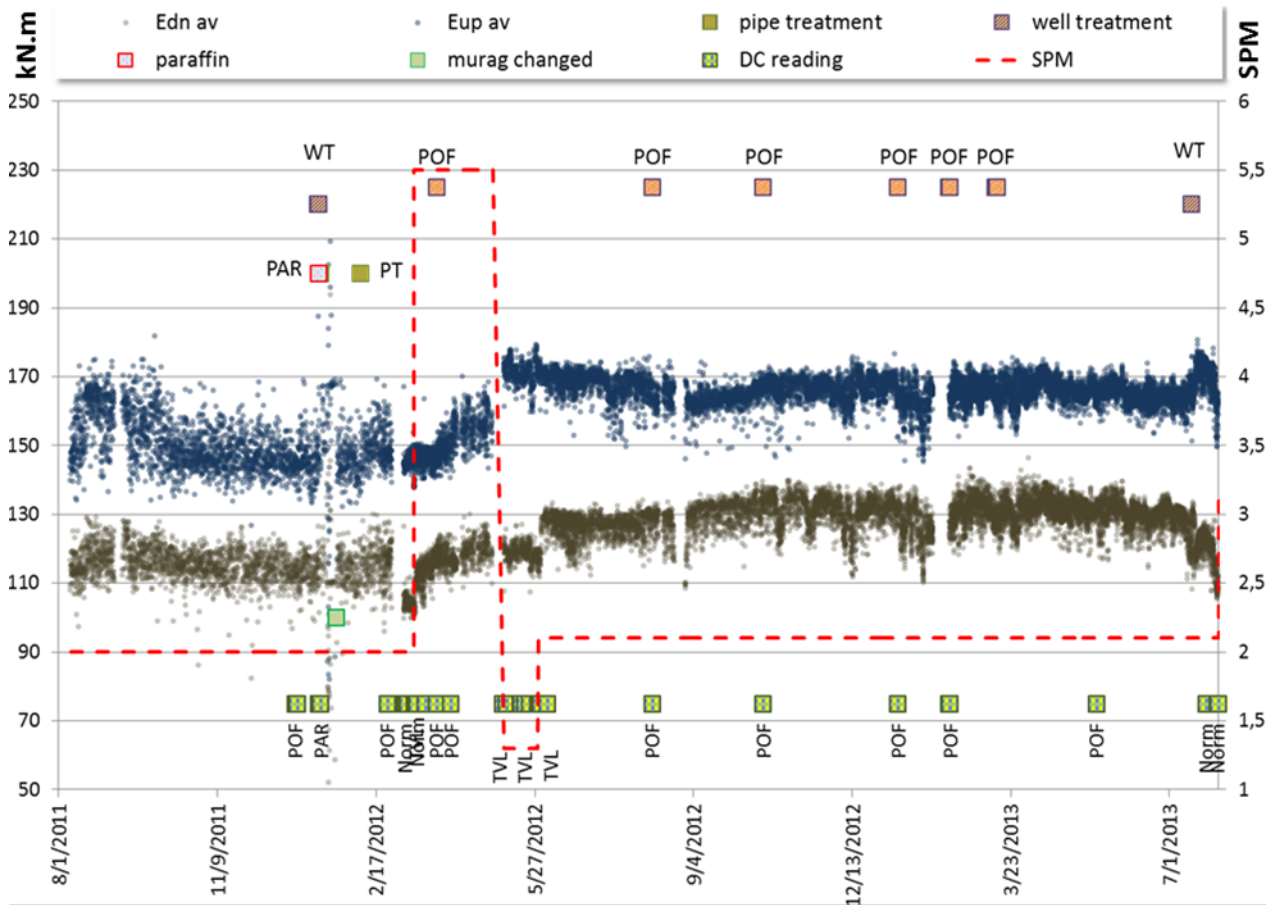


Figure 77: V-041 Production events $E_{dn\ av}$ and $E_{up\ av}$

Figure 80 shows that magnitude of the stroke power is mostly stable for the duration of the research time, but reacts on the POF state. When the SPM of the pump is increased from 2 to 5.5, the pump works faster, more fluid is removed, and it leads to the pumped off state of the well.

Figure 79 shows change of the modelled upstroke power before and during the POF state. DCs taken in the beginning after the SPM changed indicate normal pumping conditions and the Pup stays flat. The increase in upstroke power magnitude is synchronous to the DCs with POF. Upstroke power is the best indicator of well V-041 entering the POF state. Thus, *constant monitoring of the P_{up} can be used for the POF prediction.*

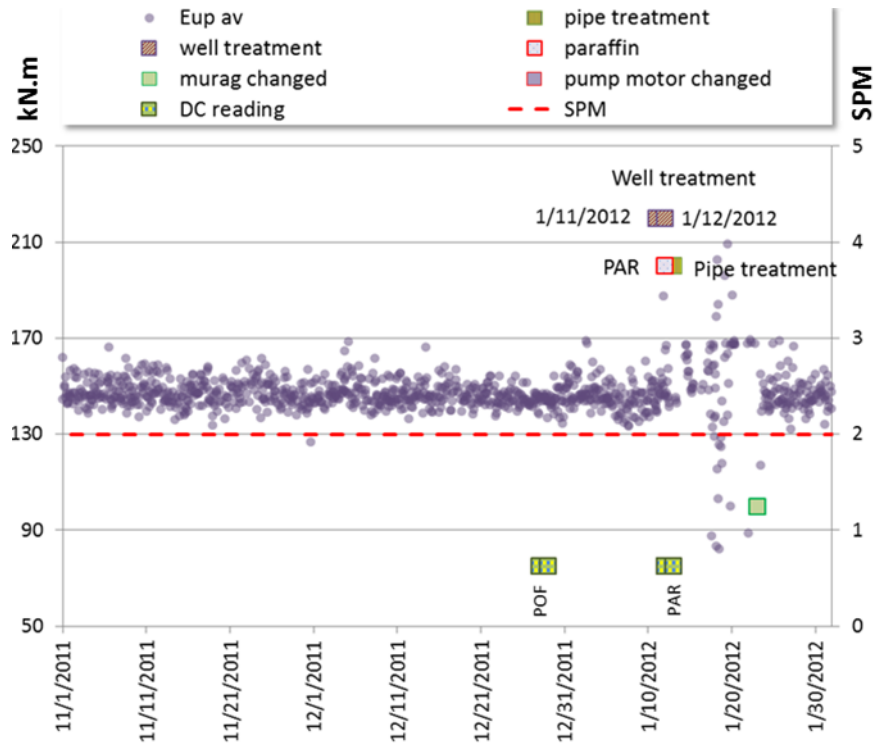


Figure 78: V-041 Paraffin case $E_{up\ av}$

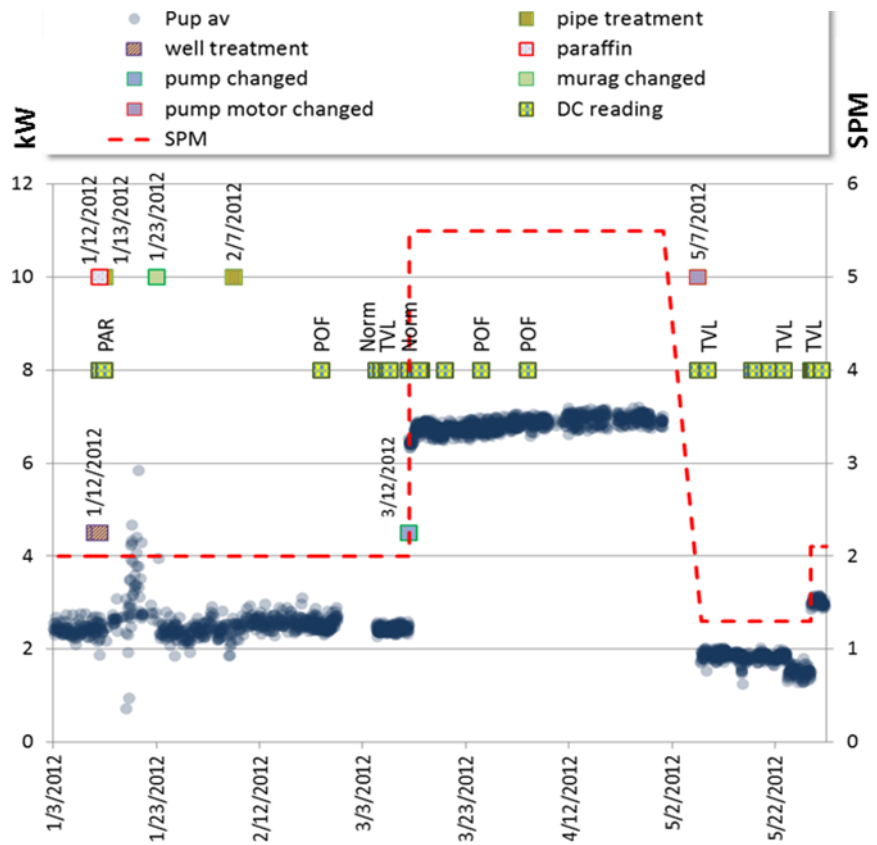


Figure 79: V-041 POF state $P_{up\ av}$

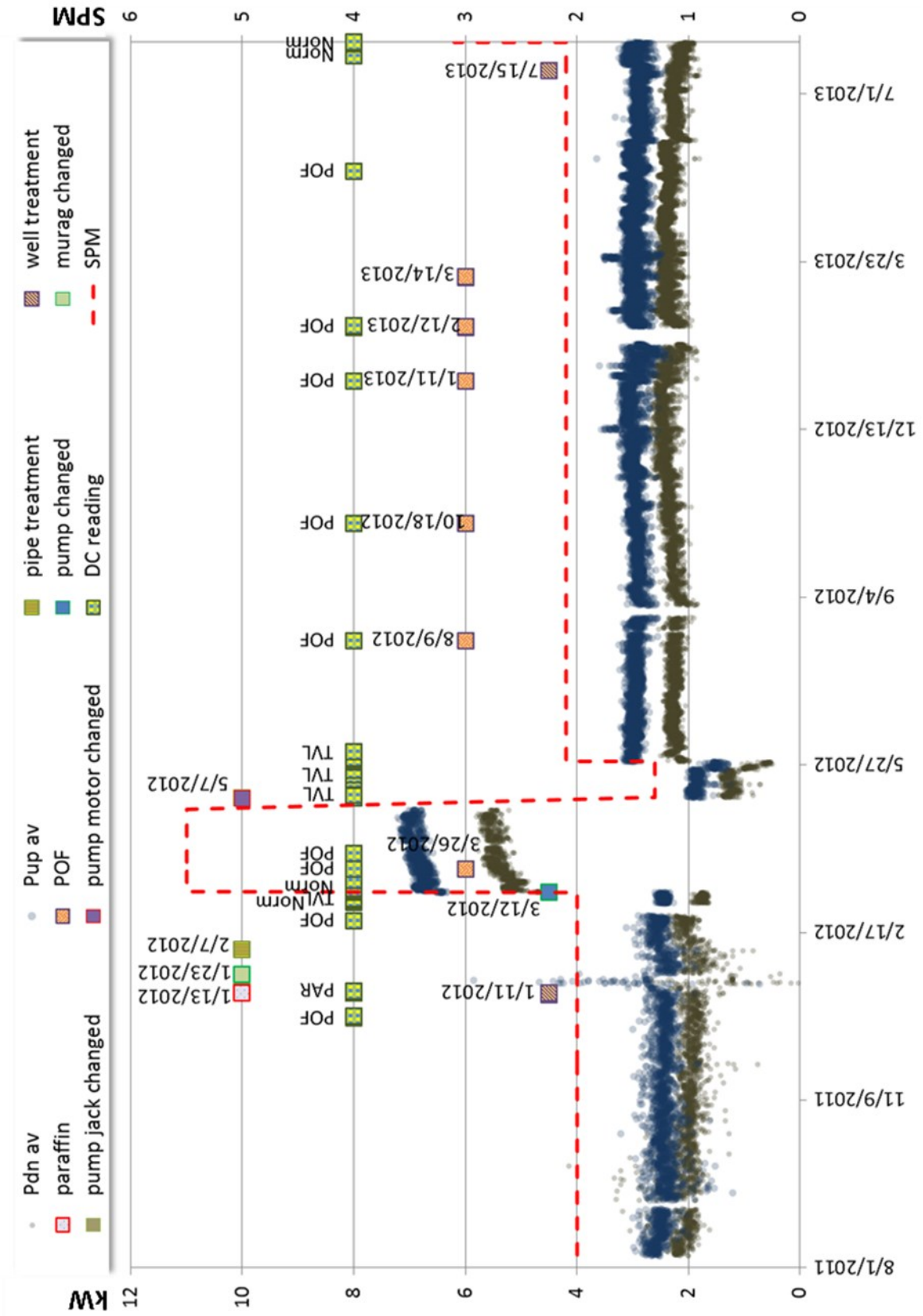


Figure 80: V-041 Production events $P_{up\ av}$ and $P_{dn\ av}$

The well treatment (WT) conducted on 15 July 2013, can be seen by the change of modelled average force (Figure 81). This example is particularly interesting, due to upstroke average force and downstroke average force changing their behavior oppositely after WT. This WT is a scheduled event to combat paraffin build up. Its effectiveness can be estimated with the help of F_{up} and F_{dn} . *The after effects of the WT are increased upstroke average force and decreased downstroke average force.* Calculating how much more energy would then be needed to operate the well can provide an answer as to whether the WT is necessary. The ascending trend of modelled F_{up} suggests that WT could be a trigger for another paraffin event.

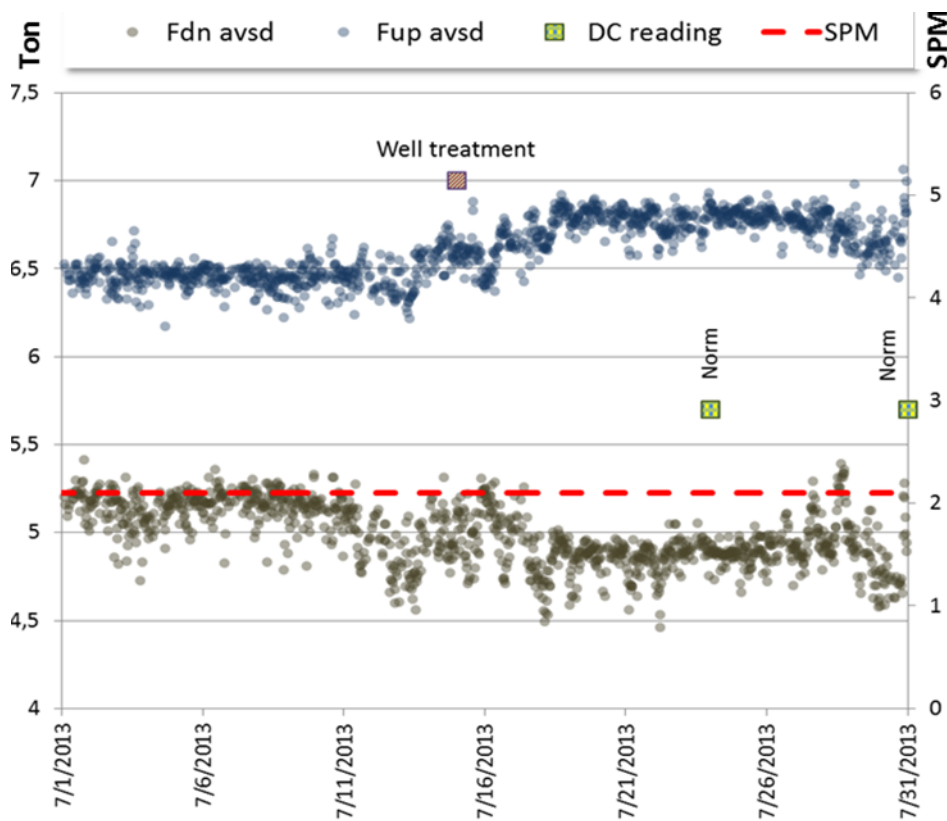


Figure 81: V-041 well treatment $F_{dn\ avsd}$

Figure 82 shows an overview of the modelled F_{up} and F_{dn} behavior for the duration of the research. The *downstroke average force is very dependent on the SPM*. It has higher values with higher SPM and lower with a slower pumping speed (compare SPM=1.1, 2 and 5.5).

Table 15 sums up the findings of the relationships between sound modelled DC features and SRP states. It presents evaluation of the DC features from the aspect of how well they reflect changes in the pump states. The green color of the cell indicates the best result and marked with “++”. The inferior result’ mark is “-“and colored with blue. Due to the lack of available sound data, well BH-009 cannot be properly examined; therefore the table does not include this well.

As can be seen, for well BH-003, the most efficient modelled DC feature that can be used for SRP states recognition is stroke energy. The easiest state to recognize is the pipe treatment. For well V-041 many DC features can be used as states indicators. $E_{up\ avsd}$ is a feature that can identify all available SRP states. Average stroke forces ($F_{up\ av}$ and $F_{dn\ av}$) are also efficient flags. Many sound

modelled DC features are good indicators of POF and PAR states. The pipe treatment, however, is identified by some features only. In the end, the SRP operating states can be described by different modelled DC features and combinations of them, and mostly by changing their behavior prior to and/or after the state.

Table 15: Estimation of the DC features as SRP states indicators

		BH-003				V-041			
		POF	WT	PT	PAR	POF	WT	PT	PAR
av	Eup	+-	na	++	na	++	++	-	++
	Edn	++	na	++	na	++	++	+-	++
	Fup	+	na	++	na	++	++	++	+-
	Fdn	+	na	+-	na	++	++	+-	+-
	Pup	+	na	+	na	++	-	+-	++
	Pdn	+-	na	++	na	++	-	+-	++
sd	Eup	++	na	++	na	+-	+-	-	+-
	Edn	++	na	++	na	++	+-	-	+-
	Fup	+	na	++	na	++	++	-	++
	Fdn	+	na	-	na	++	++	+-	++
	Pup	+	na	+	na	+-	+	+	++
	Pdn	+-	na	++	na	+-	+	-	++
avsd	Eup	++	na	++	na	++	++	++	++
	Edn	++	na	++	na	+-	+-	+-	++
	Fup	++	na	++	na	++	-	++	++
	Fdn	+	na	+-	na	++	+-	++	++
	Pup	+-	na	++	na	++	+-	+	++
	Pdn	+	na	+-	na	++	+	+	++

The result of this part of the research leads to the conclusion that sound modelled DC features can be used as robust indicators for SRP states monitoring; the application of acoustics for the DC features modelling is positive and reliable. In future, this approach can be expanded to modelling the polished rod load by using the sound. Correct implementation of the sound to model DC features can be a solution to obtain missing production data and provide continuous monitoring. Recognition of DC by sound behavior trends can be put into good use by the production engineers in terms of SRP system control and prediction.

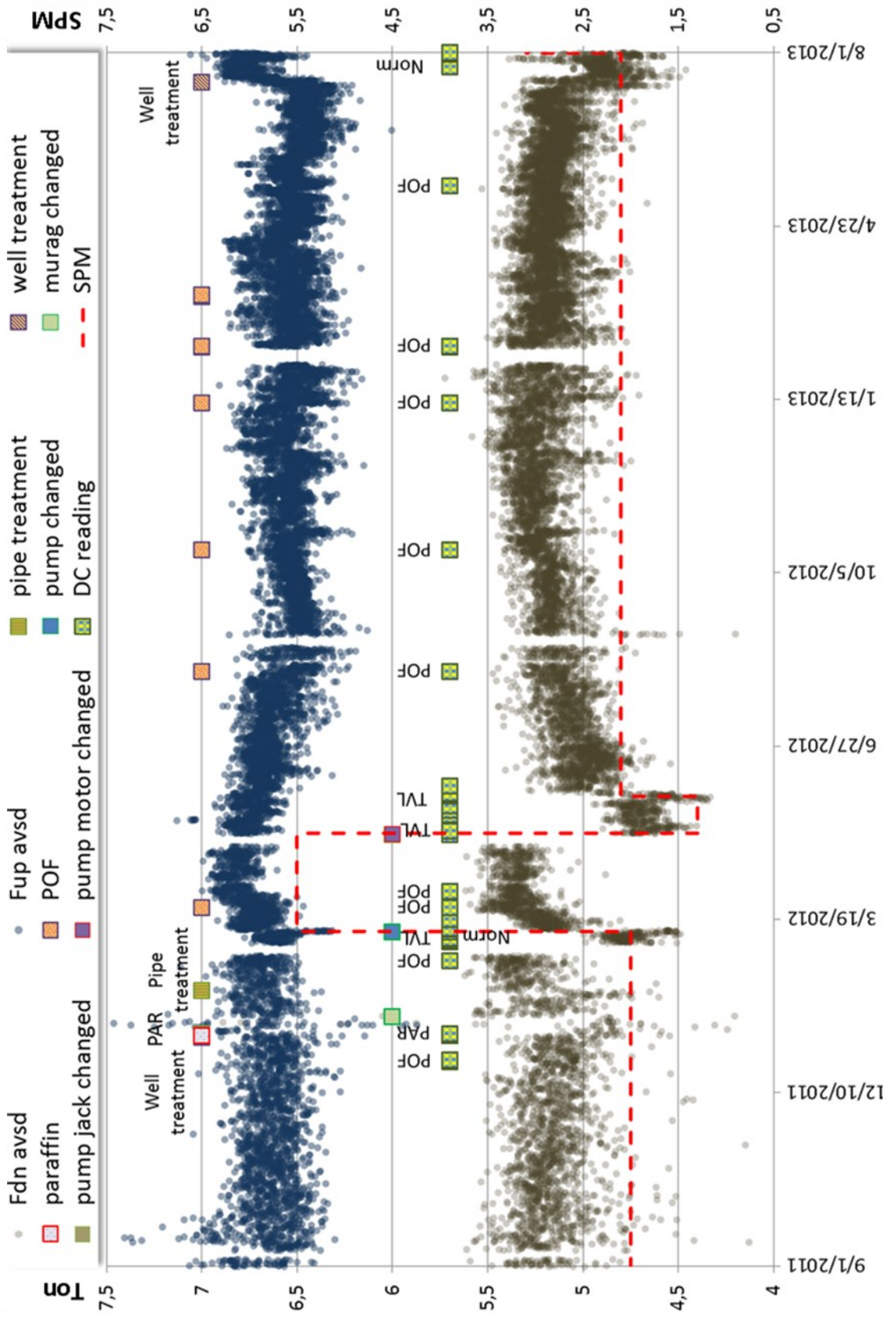


Figure 82: V-041 Production events $F_{up\ avsd}$ and $F_{dn\ avsd}$

6 Recommendations

This chapter summarizes key recommendations for future research and development. These recommendations are the outcome of the discussions, assumptions and considerations taken during the research. The goal of the chapter is to outline current and past challenges in the project and to propose possibilities for further development in the field of acoustic and statistical analysis of SRP states. The experienced gathered throughout the research confirms that there are issues that need to be addressed. This summary introduces a selection of concerns that should be targeted for further studies and development.

On the following pages are promising prospects for further development recommendations. Each section explores current challenges, ideas on content and ways to approach the issues. Recommendations are structured around the following key topics that arise from the research findings:

1. correctly selected sound sensor;
2. underground sensor installation;
3. separated installation of the sound sensor;
4. additional research on the influence of the sound transferring medium;
5. well manager installation;
6. collect a larger selection of different operating states;
7. installation of the local sensors;
8. use of the pump sound to model DC;
9. design of the automated SRP state recognition tool;
10. application of new features and feature calculation techniques;
11. other methods to obtain data dependency.

The list of recommendations is formed based on the experience collected during this research. The author believes that the research has great potential, and these recommendations can help simplify further work in this area.

1. Correctly selected sound sensor

The first research results have shown that the frequencies of greatest interest belong to the range 0 to 3 kHz. It means that a sound sensor can have a smaller sampling frequency and provide good results. There are many sensors on the market that can perform this task and be more suitable for the structure-borne sound registration. Temperature fluctuations in the researched wells might be one of the governing factors in the sensor selection. The media in the casing has a direct influence

on the quality of sound collected, due to the changes in the damping and transmitting features of the system caused by GOR and gas composition. From the range of microphones available nowadays, prepolarized condensers are recommended. They show good results in tough and humid environments, possess the best sensitivity and are widely available on the market, which means moderate costs. External polarized condensers are also applicable, but more expensive. Undoubtedly, a correctly selected sound sensor can improve the quality of the recorded data and facilitate sound analysis.

2. Underground sensor installation

Exterior installation of the Murag box can result in the unit catching surface noise during recording. Experiments have shown that the Murag box registers disturbances from the surface, which are particularly considerable if the noise is caused by the wellhead, casing and the valve where Murag is installed. This can happen in situations when the field personnel work with any piece of the aforementioned equipment, or when they walk on the metal net that touches the wellhead and the casing valve. Underground installation of the sound registering device can be considered as a method to reduce the possibility of catching unwanted noise. In addition, isolation might be considered to eliminate this problem.

3. Separated sound sensor installation

As seen from the practice, the adjacent installation of the Gond-40 and Gond-20 hinders the sound collecting process and worsens data quality. The Gond-40 is automatically shut down when the Gond-20 performs DFL measurements. The result of this are many damaged sound files that cannot be used for data analysis. Separated installation of the sound collecting system can ensure a greater amount of quality data.

4. Additional research on the influence of the sound transferring medium

The media through which the sound is being transferred is an important factor that influences the quality of the acquired sound. In most cases, the casing fluid has foam forming on the gas – liquid border due to gas evaporation. Foams have high damping coefficients that vary according to the foam thickness, bubbles size and chemical composition. Moreover, the casing media, due to changing in humidity and composition, also generates different damping coefficients. The presence of foam, different gas mixtures and how they impact the formed sound need to be researched further.

5. A well manager installation

The ideal conditions for the sound and DCs correlation requires to have individual DC for each sound file. To ensure the best match they need to be sampled simultaneously. A well manager, WM (e.g. S.A.M. available from Lufkin Inc.) can be used for this purpose. A well manager can provide downhole and surface dynamometer cards and monitor the motor power for every stroke. The WM can be suitably adjusted to record a DC at the time when the sound recording is triggered. Apparent advantages of this system are the digitized output of the DC and the opportunity to collect as many DCs as desired. This process can be automated, monitored and controlled remotely. Moreover, such a method of data collection will guarantee minimization of the induced errors and assist in maximization of the correlation coefficients.

6. Collect greater variety of operating states

The research uses two styles of databases, which intersect and supplement each other. The first type involves production data (DCs included) that describe different states of the pump and the well. The second type of database comprises of the sound files. Over time, these libraries extend and receive examples, which are used to learn sound-to-pump relationships and dependencies, both of which will be used for the SRP states prediction in the long term. To build a good quality database, more different states with a detailed description are needed. For this purpose, it is recommended to register each change to the system carefully and precisely.

7. Installation of the local sensors

This research does not aim to understand how each component of the SRP system contributes to the sound formation. Nevertheless, this information can reveal the relationship between sound and system parts and assist in data analysis. For further research, it is recommended to identify as many noise sources that induce sound alternation as possible. Special sensors can be installed along the rods, on the pump and its parts, polished rod, couplings connections, etc., to collect local sounds and vibrations. Data acquired this way can represent each part of the SRP system acoustically, display frequencies emitted by different components and show how all the components of the system interact.

8. Use of the pump sound to model DC

Positive results of the DC and sound features correlation allow using the sound to model the DC features. In further applications the usage of the sound features can be extended to the possibility to construct an entire DC. The distinct advantage of this approach is the opportunity to acquire DC remotely and online. This challenge can be also widened to modelling the downhole dynamometer card.

9. Design of the automated SRP state recognition tool

The application of the acoustics for the SRP states description, leads to the conclusion that sound can be applied to model DC features. DC features plotted over time might be used as indicators of the system behavior and recognize failures and accidents. As shown in the research, every production state is characterized by different values of the DC features, which change together with the production status. A tool that can determine the operating condition using only sound might have a great application in the industry. This tool will be fully automated, with a database of the different SRP operating states, remote and might have more monitoring and analyzing options. The findings of this research strongly support this concept. They support the idea from the first positive results, indicate the direction to follow, and might be a base for the further research.

10. Application of new features and calculation techniques

Sound features are an essential part in the SRP acoustic analysis. Correctly selected, they can improve and ensure positive research results. The features used in the research have a good balance between their representativity and completeness of the extraction methods. Based on the experience collected in the research, several features and methods of their calculation can be extended and some discarded. For example, cepstral coefficients and the logs of the Hanning tapered data of some bands show the best results in DC correlation. This leads to the idea to use

the linear bands approach for the future investigation. However, more features can be implemented using alternative methods: wavelets transform could be considered to identify time varying models; the Hidden Markov model can be utilized to identify the data states; other sound feature extracting methods might be applied also.

11. Other types to obtain data dependency

In this research, correlation and cross-correlation are the methods used to measure time-dependent similarities between DC and sound data in the lag-applied manner. For that matter, there are other methods which are not limited to correlations only, but check any type of dependency the data sets might have. Big Data, Data Mining and other methods are approaches that might be investigated also.

7 References

- [1] Oppenheim, A.V., R.W. Schafer. *Discrete - Time Signal Processing*. Engelwood Cliffs, New Jersey 07632: Prentice - Hall, Inc., 1989.
- [2] Bracewell, R.N. "The Fourier Transform." *Scientific American* Jun. 1989: 86-95.
- [3] Chui, C.K. *An Introduction to Wavelets*. San Diego, CA, USA: Academic Press, 1992.
- [4] Canadian Oilwell Systems Company. "Basic Artificial Lift." *COSCO*. Canadian Oilwell Systems Company Ltd, 22 Jan 2011. Web. 22 Jan. 2011.
- [5] Hendricks, C.T., R.D. Stevens. "Sucker Rod Failure Analysis." *Alberta Oil Tool*. A Dover Company, 30 Oct. 2001. Web. 26 Nov. 2011.
- [6] Kendrick, J.F., P.D. Cornelius. "The Sucker-rod Pump as a Problem in Elasticity." *Transactions of the AIME* (Dec. 1937): 15-31.
- [7] Corpoven, M.V.O. "Real Time Expert System (R.T.E.S.) for Rod Pumping Optimization." Paper SPE-30185-MS presented at the Petroleum Computer Conference, Houston, Texas, 11-14 Jun. 1995.
- [8] cVision User's Manual. "Optimal Network Size." *NGS*. Neuro Genetic Solutions GmbH, 5 Aug. 2009. Web. 24 Jan. 2014.
- [9] Erickson, D.D., V.G. Niesen, T.S. Brown. "Thermodynamic Measurement and Prediction of Paraffin Precipitation in Crude Oil." Paper SPE-26604-MS presented at the 68-th Annual Technical Conference and Exhibition of the SPE, Houston, Texas, 3-6 Oct. 1993.
- [10] Kernerman Webster's College Dictionary. K Dictionaries Ltd by Random House, 2010.
- [11] Dubnov, S. "Generalization of Spectral Flatness Measure for Non-Gaussian Linear Processes." *Signal Processing Letters, IEEE* 11, Iss. 8 (Aug. 2004): 698-701.
- [12] Sam, G., M. Kaestenbauer, C. Burgstaller, E. Chevelcha. "Fully Automated Fluid Level Measurement Tool." Paper SPE-145434-MS presented at the SPE Asia Pacific Oil and Gas Conference and Exhibition, Jakarta, Indonesia, 20-22 Sep. 2011.
- [13] Moisés, G.V.L., S.F.A. Andrade, A.C.B. Garcia. "Sucker-Rod Pumping Failures Diagnostic System." Paper SPE-134975-MS presented at the SPE Annual Technical Conference and Exhibition, Florence, Italy, 19-22 Sep. 2010.
- [14] Ghatak, A. *Optics*. 3rd ed. New Deli: Tata McGraw-Hill Education, 2005. ISBN: 9780070585836.
- [15] Gibbs, S.G. "Predicting the Behavior of Sucker-Rod Pumping Systems." *Journal of Petroleum Technology* (Jan. 1963): 769-778.
- [16] Gray, H.E. "Kinematics of Oil-well Pumping Units." *American Petroleum Institute* (Mar. 1963): 156-165.
- [17] Rischmüller, H., H. Meier. *Oil Production with Subsurface Sucker Rod Pumps*. Ternitz, Austria: Schoeller-Bleckmann GmbH., 1989.
- [18] Heinzel, G., A. Rüdiger, R. Schilling. "Spectrum and spectral density estimation by the Discrete Fourier transform (DFT), including a comprehensive list of window functions and some new flat-top windows." *Max-Planck-Institut für Gravitationsphysik (Albert-Einstein-Institut)*, Teilinstitut Hannover, 2002.
- [19] Instruments National. "Decimation (Digital Filter Design Toolkit)." *LabVIEW 2011 Digital Filter Design Toolkit Help*. National Instruments, Jun. 2011. Web. 12 Jun. 2013.
- [20] Breebaart J., M.F. McKinney. "Features for Audio Classification." *Proceedings SOIA2002, Philips Symposium on Intelligent Algorithms*, Eindhoven, 2002.
- [21] Lea, J.F., P.D. Pattillo, W.R. Studenmund. "Interpretation of Calculated Forces on Sucker Rods." *SPE Production & Facilities* Feb. 1995: 41-45.

- [22] Lea, J.F., H.W. Winkler, R.E. Snyder. "What's new in artificial lift. Part 1 - Fourteen new systems for beam, progressing-cavity, plunger-lift pumping and gas lift." *WorldOil Magazine* 224 No.4 Apr. 2003: 59-75.
- [23] Filliben, J.J., et al. *Engineering Statistics Handbook*. IST/SEMATECH: U.S. Commerce Department's Technology Administration, 2003.
- [24] Johansson, M. "The Hilbert Transform." MA thesis Växjö University, Applied Mathematics. Web. 29 May 2012.
- [25] Marple, L.Jr. *Digital Spectral Analysis with Applications*. Engelwood Cliffs, NJ: Prentice-Hall, Inc., 1987.
- [26] Kay, S.M. *Modern spectral estimation*. Pearson Education India, 1988.
- [27] Knapp, R.M. "A Dynamic Investigation of Sucker-Rod Pumping." MA thesis University of Kansas, Kansas, 1963. *KU ScholarWorks | The University of Kansas Theses and Dissertations Collection*.
- [28] Kropp, W. "Physical Phenomena." *Ljudlandskap*. Chalmers University of Technology, 7 Dec. 2007. Web. 10 May 2013.
- [29] Cremer, L., M. Heckl, B.A.T. Petersson. *Structure-Borne Sound. Structural Vibrations and Sound Radiation at Audio Frequencies*. 3rd ed. Heidelberg, Germany: Springer-Verlag Berlin Heidelberg, 2005.
- [30] Lyons, R.G. *Understanding Digital Signal Processing*. 3rd ed. Michigan, USA: Prentice Hall, 2010.
- [31] Barreto Filho, M.A., M. Tygel, A.F. Rocha, C.K. Morooka. "Automatic Downhole Card Generation And Classification." Paper SPE-36605-MS presented at the SPE Annual Technical Conference and Exhibition, Denver, Colorado, 6-9 Oct. 1996.
- [32] Nias, C.L., J.M. Mendel. "Signal Processing with Higher-Order Spectra." *IEEE Signal Processing Magazine* Jul. 1993: 10-37.
- [33] Taner, M.T., F. Koehler, R.E. Sheriff. "Complex Seismic Trace Analysis." *Geophysics* 44, No. 6 (Jun. 1979): 1041-1063.
- [34] Mahoney, M.W. "Pitfalls in Performance-Data Tracking of Sucker-Rod Pumped wells." Paper SPE-101845-MS presented at the SPE Annual Technical Conference and Exhibition, San Antonio, Texas, USA, 24-27 Sep. 2006.
- [35] Matlab R2013a Help Documentation. Web. 20 Dec.2012.
- [36] McKinney, M.F., J. Breebaart. "Features for Audio and Music Classification." *Proceedings of the 4-th International Symposium on Music Information Retrieval* (2003): 151-158.
- [37] Davis, S., P. Mermelstein. "Comparison of Parametric Representations for Monosyllabic Word Recognition in Continuously Spoken Sentences." *IEEE Transactions on Acoustics, Speech, and Signal Processing* 28, No. 4 (1980): 357-366.
- [38] Huang, X., A. Acero, H. Hon. *Spoken Language Processing: A Guide to Theory, Algorithm, and System Development*. Upper Saddle River, NJ, USA: Prentice Hall, 2001.
- [39] Milivojević, Z. *Digital Filter Design*. Belgrade, Serbia: mikroElektronika, 2009.
- [40] Naidu, P.S. *Modern Spectrum Analysis of Time Series*. Boca Raton, Florida: CRC Press, 1996.
- [41] Nind, T.E.W. *Principles of Oil Well Production*. New York: McGraw-Hill Companies, 1981. ISBN-10: 0070465754, ISBN-13: 9780070465756.
- [42] Nuttall, A. H. "Some Windows with Very Good Sidelobe Behavior." *IEEE Transactions on Acoustics, Speech, and Signal Processing* 29 (1) (Feb. 1981): 84-91.
- [43] Smith, J.O. *Mathematics of the Discrete Fourier Transform(DFT) with Audio Applications*. 2nd ed. W3K Publishing: <http://books.w3k.org/>, 2007. ISBN 978-0-9745607-4-8.
- [44] O'Shaughnessy, D. *Speech Communications: Human and Machine*. Reading, Massachusetts: Addison-Wesley Publishing Company, 1987. ISBN 978-0-201-16520-3.
- [45] Kiranbala, P., S. Hemant, D.P. Bharambe. "Performance Based Designing of Wax Crystal Growth Inhibitors." *Energy & Fuels* 22 (6) (2008): 3930-3938.
- [46] Paliwal, K.K. "Spectral Subband Centroid Features For Speech Recognition." *Proceedings of the 1998 IEEE International 2*, (1998): 617-620. ISBN: 0-7803-4428-6.
- [47] Paschal, J. "Eliminating Pumping Problems." *Darttsystems*. The Dartt® Valve Co, 18 Nov. 2010. Web. 12 Jan. 2012.
- [48] Peterson, R. "Increase Pumping Efficiency by Controlling." *UNICOUS*. Oil and Gas Automation Solutions, Feb.2003. Web. 14 Jan. 2014.
- [49] McCulloch, W.S., W.H. Pitts. "A Logical Calculus of the Ideas Immanent in Nervous Activity." *Bulletin of Mathematical Biophysics* 5 (1943): 115-133.

- [50] Winkler R., W.Pannert, M. Merkel, A.Öchsner. "Structure Borne Soud in Metallic Hollow Sphere Structures." *Materialwissenschaft und Werkstofftechnik* 42 No.5. 2011: 365-369.
- [51] Raichel, D.R. *The Science and Applications of Acoustics*. 2nd ed. Fort Collins, USA: Springer Science+Business Media Inc, 2006. ISBN-10: 0-387-26062-5.
- [52] Yu, R.C., et al. "Quality control of semi-continuous mobility size-fractionated particle number concentration data." *Atmospheric Environment* 38, Iss. 20 (Jun. 2004): 3341-3348.
- [53] Stevens, R., S. Malone. "Protecting your investment in sucker rods. Part 3: Well Optimization." *Well Servicing* Nov. -Dec. 2005: 54-57.
- [54] Smith, S.W. *The Scientist and Engineer's Guide to Digital Signal Processing*. San Diego, California, USA: California Technical Publishing, 2011.
- [55] StatTrek. "The mean and median: Measures of Central Tendency." *Stat Trek*. StarTrek.com. Web, 1 Apr. 2013.
- [56] Stevenson, J.D. "Structural damping values as a function of dynamic response stress and deformation levels." *Nuclear Engineering and Design* 60, Iss. 2 (Sep. 1982.): 211-237.
- [57] Subramanian, H. "Audio Signal Classification." *M.Tech. Credit Seminar Report* IIT Bombay, Nov.2004.
- [58] Svinos, J.G. "Exact Kinematic Analysis of Pumping Units." Paper SPE-12201-MS presented at the 58th Annual Technical Conference and Exhibition, San Francisco, CA, USA, 5-8 Oct. 1983.
- [59] Takacs, G. *Sucker-Rod Pumping Manual*. Tulsa, Oklahoma, USA: PennWell Corporation, 2003. ISBN-10: 0878148922, ISBN-13: 978-0878148929.
- [60] Tsai, S.-J.S. "Power Transformer Partial Discharge (PD) Acoustic Signal Detection using Fiber Sensors and Wavelet Analysis, Modeling, and Simulation." *Digital Library and Archives etds*. Virginia Polytechnic Institute and State Univeristy, 6 Dec. 2002. Master Thesis, Web. 17 Dec. 2013.
- [61] Cooley, J.W., J.W. Tukey. "An Algorithm for the Machine Calculation of Complex Fourier Series." *Mathematics Computation* 19 (1965): 297-301.
- [62] Lecture Notes. "Statistics with Matlab." *Uni-Postdam*. University of Potsdam. Web. 05 Apr. 2013.
- [63] Press, W.H., S.A. Teukolsky, W.T. Vetterling, B.P. Flannery. *Numerical Recipes*. 3rd ed. New York, NY 10013-2473, USA: Cambridge University Press, 2007.
- [64] Zbigniew, L., T. Lobos, J. Szymanda, P. Ruczewski. "Application Of Higher-Order Spectra For Signal Processing In Electrical Power Engineering." *Technical University of Wroslaw*, 1998. Web. 20 Mar. 2013.
- [65] Gilbert, W.E. *An Oil-Well Pump Dynagraph*. Shell Oil Company: Production Practice, 1936: 94 - 115.
- [66] Bangert, P.D. *Optimization for Industrial Problems*. USA: Springer Verlag, 2012.
- [67] Therrien, C.W. *Discrete Random Signals and Statistical Signal Processing*. Englewood Cliffs, New Jersey: Prentice-Hall, 1992: 614-655.
- [68] Gibbs, S.C. "Computing Gearbox Torque and Motor Loading for Beam Pumping Units with Consideration of Inertia Effects." *Journal of Petroleum Technology* Sep. 1975: 1153-1159.
- [69] "API Specification for Pumping Units." API STD 11E, 12th ed, Jan. 1982.
- [70] Timoshenko, S., J.N. Goodier. *Theory of Elasticity*. 2nd ed. USA: McGraw-Hill Book Company, 1951.
- [71] Tan, C., et al. "Predicting the Dynamometer Card of a Rod Pump." *Algorithmica Technologies GmbH* 2008. Web. 15 May 2014.
- [72] "2008/2009 General Lufkin Catalog." *Lufkin Oilfield Products Group*, Lufkin Industries, Inc. USA, 2010.
- [73] Boashash, B. "Estimating and Interpreting The Instantaneous Frequency of a Signal-Part 1: Fundamentals." *Proceedings of the IEEE* 80, No.4 (Apr. 1992): 520-538.
- [74] Gibbs, S.G, A.B. Neely. "Computer Diagnosis of Downhole Condition in Sucker Rod Pumping Wells." *Journal of Petroleum Technology* (Jan. 1966). Mitchell, R.F. "Buckling Behavior of Well Tubing: The Packer Effect." *Society of Petroleum Engineers Journal* 22, Iss. 5 (1982): 616-624.
- [75] Chevelcha, E., C.J. Langbauer, H. Hofstaetter. "Listening Sucker Rod Pump: Stroke's Signature." Paper SPE-165035-MS presented at the SPE Artificial Lift Conference-Americas, Cartagena, Columbia, 21-22 May 2013.
- [76] Barnes, A.E. "The calculation of instantaneous frequency and instantaneous bandwidth." *Geophysics* 57, No. 11 (Nov. 1992): 1520-1524.

[77] Peeters, G. "A large set of audio features for sound description (similarity and classification) in the CUIDADO project." Report V1.0, 04 Apr. 2004.

[78] Haase, S. "Spectral and Statistical Methods for Vibration Analysis in Steel Rolling." PhD thesis Montanuniversitaet Leoben, Austria, 2002. *VDI Verlag Gmb,,: Düsseldorf, 2002.*

[79] Haal, P., S.C. Morton. "On the estimation of the entropy." *Ann. Inst. Statist. Math.* 45, No. 1 (1993): 69-88.

[80] Bishop, C.M. *Neural Networks for Pattern Recognition.* Oxford: Clarendon Press, 1995.

[81] Fruhwirth, R.K, S.P. Steinlechner. "A systematic approach to the optimal design of feed forward neural networks applied to log-synthesis." Expanded Abstracts at the EAGE 66th Conference and Exhibition, Paris, France, 2004.

Appendix A General Completion Information

Global Items	BH-003		BH-009		V-041	
Stroke Length, m	3.15		1.88		2.59	
Tubing Diameter, in	1.75		1.50		1.25	
Tubing Type (Steel, Polylined)	PL		ST		ST	
Well Cemented at, m	2224		2260.0		2335.0	
Gas Anchor	yes		yes		yes	
Centralizer	no		no		yes	
Centralizer Position, m	n.a.		n.a.		2173.3	
Liner	yes		yes		no	
Top Liner Depth, m	1902.5		940.0		n.a.	
Perforation Depth (MD), m	from	to	from	to	from	to
	2083.2	2085.0	2074.2	2075.2	2193.5	2196.5
	2087.0	2088.6	2078.8	2079.8	2199.0	2202.0
	2093.2	2094.0	2082.0	2083.0	2211.5	2213.0
	2095.1	2100.8	2084.0	2086.0	2214.5	2218.5
	2102.1	2103.7				
	2110.4	2111.8				
Comments						
			2h Pump OFF		2194m MD=2080m TVD	
			1h Pump ON		2212m MD=2097m TVD	

Appendix C Well BH - 009 History

Strokes per Minute		
Date/Time	SPM	Comment
1/1/2010 0:00	3.5	
1/1/2012 0:00	3.5	
Pump Depth (MD)		
Date/Time	PDMD, m	Comment
1/1/2010 0:00	1907.00	
Pump Type		
Date/Time	PTP	Comment
1/1/2010 0:00	PT2	2 3/8" x 1 1/2" x 20ft RHBC IV
Pump Motor Type		
Date/Time	PMT	Comment
1/1/2010 0:00	Motor1	SBS D 1074
Pump Jack Type		
Date/Time	PJT	Comment
Leaking Valve (According to DC)		
Date/Time	LV	Comment
1/1/2010 0:00	n	No leaking valve
Pumped Off		
Date/Time	PO	Comment
10/18/2011 0:00	y	Time n/a

Well Treatment		
Date/Time	WT	Comment
10/19/2011 0:00	CT	Condensate treatment
5/2/2012 0:00	HW	HW Csg after rods stuck
7/5/2012 0:00	CT	CT Csg
11/8/2012 0:00	HW	HW Csg
1/17/2013 0:00	HW	HW Csg after rods stuck
5/7/2013 0:00	HW	HW Csg
6/27/2013 0:00	HW	HW Csg
Pipe Treatment		
Date/Time	PT	Comment
6/11/2012 0:00	HW	Hot water treatment
8/11/2012 0:00	HW	Hot water treatment
10/18/2012 0:00	HW	Hot water treatment
5/7/2013 0:00	HW	Hot water treatment
Murag Microphone Type		
Date/Time	MMT	Comment
1/1/2010 0:00	MM1	GOND40
Paraffin		
Date/Time	PAR	Comment
5/1/2012 0:00	y	Paraffin failure
5/2/2012 0:00	y	Paraffin failure
5/30/2012 0:00	y	No sound files
6/10/2012 0:00	y	No sound files
1/16/2013 0:00	y	Rods stuck
1/17/2013 0:00	y	Rods stuck
Pump Changed		
Date/Time	PC	Comment
		No change

Production Pars						
Date/Time	Oil, m3/d	Gas, Nm3/d	DFL, m	Pcsg, bar	Ptbg, bar	Comment
13/08/2010 00:00:00	2.2	340	1400	10	9	
14/10/2010 00:00:00	2.7	460	1700	11.5	10	
6/3/2011 0:00	2.7	460	1700	11.5	10	
5/1/2012 0:00	2.3	460	1700	10.5	9.5	
17/08/2012 00:00:00	2	430	1700	10.5	9.5	
6/2/2013 0:00	1.9	220	1700	10.7	10.1	
6/6/2013 0:00	1.9	224	1700	10	9.5	
Pump On/Off (Example)						
Date/Time	POO					Comment
1/7/2011 15:51	OFF					invalid v. Treiber
1/7/2011 15:51	OFF					OK
1/7/2011 15:52	OFF					invalid v. Treiber
1/7/2011 15:52	OFF					Generalabfr
5/7/2011 0:35	OFF					invalid v. Treiber
5/7/2011 0:35	OFF					OK
5/7/2011 0:35	OFF					invalid v. Treiber
5/7/2011 0:36	OFF					Generalabfr
8/7/2011 8:04	ON					OK
8/7/2011 8:04	OFF					OK
8/7/2011 11:43	ON					OK
9/7/2011 4:45	ON					Generalabfr
11/7/2011 11:21	OFF					OK
11/7/2011 14:06	ON					OK
13/07/2011 02:45:37	OFF					OK
13/07/2011 05:45:38	ON					OK
13/07/2011 06:25:37	OFF					OK
13/07/2011 09:25:40	ON					OK
13/07/2011 10:40:27	OFF					OK
13/07/2011 13:40:22	ON					OK
13/07/2011 15:05:29	OFF					OK
13/07/2011 18:05:44	ON					OK

Appendix E Dynamometer Cards Full Table

#	File Name	Date	Time	SPM from DC	Comment	Notation	Digitized
1	BH003-26.04.2010	26.04.2010		5,4	Normal	Norm	y
2	BH003-17.11.2010	17.11.2010		4,2	Normal	Norm	y
3	BH003-13.01.2011	13.01.2011		NA	Normal	Norm	y
4	BH003-19.01.2011	19.01.2011		4	Normal	Norm	y
5	BH003-07.06.2011	07.06.2011		4	Normal	Norm	y
6	BH003-04.07.2011	04.07.2011		3,5	Normal	Norm	y
7	BH003-04.07.2011-1	04.07.2011		4	Normal	Norm	y
8	BH003-28.12.2011	28.12.2011		3,4	Normal	Norm	y
9	BH003-04.04.2012	04.04.2012		3,4	light POF	LPOF	y
10	BH003-01.08.2012	01.08.2012		3,5	light POF	LPOF	y
11	BH003-02.08.2012	02.08.2012		4,5	Pumped-off Well	POF	y
12	BH003-07.08.2012	07.08.2012		3,4	Pumped-off Well	POF	y
13	BH003-18.10.2012	18.10.2012		3	Normal	Norm	y
14	BH003-23.01.2013	23.01.2013		3,2	Normal	Norm	y
15	BH003-26.03.2013	23.03.2013		3,4	Normal	Norm	y
16	BH003-29.08.2013	29.08.2013		4,6	Normal	Norm	y
17	BH009-24.06.2010	24.06.2010		4,8	NA	NA	y
18	BH009-25.06.2010	25.06.2010		4,8	Normal	Norm	y
19	BH009-27.06.2010	27.06.2010		NA	Normal	Norm	y
20	BH009-28.06.2010	28.06.2010		NA	Normal	Norm	y
21	BH009-08.07.2010	08.07.2010		4,8	beginning of pumping	Norm	y
22	BH009-08.07.2010-1	08.07.2010		4,8	end of pumping	Norm	y
23	BH009-12.07.2010	12.07.2010		3,5	POF	POF	y
24	BH009-10.08.2010	10.08.2010		3,5	Normal	Norm	y
25	BH009-08.06.2011	08.06.2011		3,5	Normal	Norm	y
26	BH009-18.10.2011	18.10.2011		3,5	POF, long pumping	POF	y
27	BH009-18.10.2011-1	18.10.2011		3,5	POF, after staying time	POF	n
28	BH009-30.12.2011	30.12.2011		3,5	Normal	Norm	y
29	BH009-04.04.2012	04.04.2012		3,5	Normal	Norm	y
30	BH009-30.05.2012	30.05.2012		3,5	Paraffin, rods stuck	PAR	n
31	BH009-08.08.2012	08.08.2012		3,5	Normal	Norm	y
32	BH009-18.10.2012	18.10.2012		3,5	Normal	Norm	y
33	BH009-23.01.2013	23.01.2013		3,5	Normal	Norm	y
34	BH009-26.03.2013	26.03.2013		3,5	Normal	Norm	y
35	BH009-29.08.2013	29.08.2013		3,5	Normal	Norm	y
36	V041-30.09.2010	30.09.2010		2	POF	POF	y
37	V041-28.10.2010	28.10.2010		2	TV leaks	TVL	y
38	V041-16.11.2010	16.11.2010		2	Normal	Norm	y

39	V041-18.11.2010	18.11.2010		2	Knocking down valve	KnoV	y
40	V041-24.11.2010	24.11.2010		2	TV leaks	TVL	y
41	V041-26.11.2010	26.11.2010		2	TV leaks	TVL	y
42	V041-30.11.2010	30.11.2010		2	Normal	Norm	y
43	V041-02.03.2011	02.03.2011		2	POF	POF	y
44	V041-08.06.2011	08.06.2011		2	POF, end of pumping	POF	y
45	V041-28.12.2011	28.12.2011		2	Normal	Norm	y
46	V041-29.12.2011	29.12.2011		2	POF, end of pumping	POF	y
47	V041-12.01.2012	12.01.2012		2	Paraffin	PAR	n
48	V041-12.01.2012-1	12.01.2012		2	Paraffin, 1 day after CT	PAR	y
49	V041-12.01.2012-2	12.01.2012		2	Paraffin, after HW	PAR	y
50	V041-12.01.2012-3	12.01.2012		2	Paraffin, after HW	PAR	n
51	V041-13.01.2012	13.01.2012		2	TV leaks	TVL	y
52	V041-24.02.2012	24.02.2012		2	POF, before well treatment	POF	y
53	V041-05.03.2012-18.30	05.03.2012	0:18:30	2	Normal	Norm	y
54	V041-06.03.2012-16.00	06.03.2012	0:16:00	2	TV leaks	TVL	y
55	V041-07.03.2012-16.00	07.03.2012	0:16:00	2	TV leaks	TVL	y
56	V041-08.03.2012	08.03.2012	0:06:40	2	TV leaks	TVL	y
57	V041-12.03.2012	12.03.2012		2	TV leaks	TVL	n
58	V041-12.03.2012-1	12.03.2012		2	before motor changed	Norm	y
59	V041-12.03.2012-12.00	12.03.2012		5,5	New motor, Normal	Norm	y
60	V041-13.03.2012-08.00	13.03.2012	0:08:00	5,5	POF	POF	y
61	V041-14.03.2012	14.03.2012		5,5	POF	POF	n
62	V041-14.03.2012-07.00	14.03.2012	0:07:00	5,5	POF	POF	y
63	V041-26.03.2012	26.03.2012		5,5	POF	POF	y
64	V041-26.03.2012-1	26.03.2012		5,5	POF	POF	n
65	V041-04.04.2012	04.04.2012		5,5	POF	POF	y
66	V041-07.05.2012	07.05.2012		1,3	TV leaks	TVL	y
67	V041-09.05.2012	09.05.2012		1,3	TV leaks	TVL	y
68	V041-17.05.2012-15.00	17.05.2012	0:15:00	1,3	TV leaks	TVL	y
69	V041-18.05.2012-07.00	18.05.2012	0:07:00	1,3	TV leaks	TVL	y
70	V041-20.05.2012-21.00	20.05.2012	0:21:00	1,3	TV leaks	TVL	y
71	V041-23.05.2012-15.00.	23.05.2012	0:15:00	1,3	TV leaks	TVL	y
72	V041-29.05.2012	29.05.2012		1,3	TV leaks	TVL	y

73	V041-29.05.2012-09.00	29.05.2012	0:09:00	1,3	TV leaks	TVL	y
74	V041-29.05.2012-18.00	29.05.2012	0:18:00	2,1	TV leaks	TVL	y
75	V041-31.05.2012	31.05.2012		2,1	light POF	LPOF	y
76	V041-04.06.2012	04.06.2012		2,1	POF	POF	y
77	V041-09.08.2012	09.08.2012		2,1	POF	POF	y
78	V041-18.10.2012	18.10.2012		2,1	POF	POF	y
79	V041-11.01.2013	11.01.2013		2,1	POF	POF	y
80	V041-12.02.2013-14.52	12.02.2013	0:14:52	2,1	POF	POF	y
81	V041-12.02.2013-15.24	12.02.2013	0:15:24	2,1	Knocking down valve	KnoV	y
82	V041-12.02.2013-16.00	12.02.2013	0:16:00	2,1	Normal	Norm	y
83	V041-16.05.2013	16.05.2013		2,1	POF	POF	y
84	V041-24.07.2013	24.07.2013		2,1	Normal	Norm	y
85	V041-31.07.2013	31.07.2013		2,1	tight stuffing box	box	n
86	V041-01.08.2013	01.08.2013		2,1	Normal	Norm	n
87	V041-29.08.2013	29.08.2013		3,1	Normal	Norm	y

Appendix F Final List of the Sound Features

#	Head	Comment
1	rTR:av	mean value of data-rTR
2	rTR:sd	standard deviation of data-rTR
3	rTR:sk	skewness of data-rTR
4	rTR:ku	kurtosis of data-rTR
5	rTR:rms	root mean square of data-rTR
6	rTR:rng	range of data-rTR
7	rTR:min	min value of data-rTR
8	rTR:med	median of data-rTR
9	rTR:max	max value of data-rTR
10	rTR:mod	mode of data-rTR
11	rTR:mad	mean abs deviation of data-rTR
12	rTR:mdd	median abs deviation of data-rTR
13	rTR:av.t5	mean value of Trim5(data-rTR)
14	rTR:sd.t5	standard deviation of Trim5(data-rTR)
15	rTR:sk.t5	skewness of Trim5(data-rTR)
16	rTR:ku.t5	kurtosis of Trim5(data-rTR)
17	rTR:rms.t5	root mean square of Trim5(data-rTR)
18	rTR:rng.t5	range of Trim5(data-rTR)
19	rTR:min.t5	min value of Trim5(data-rTR)
20	rTR:med.t5	median of Trim5(data-rTR)
21	rTR:max.t5	max value of Trim5(data-rTR)
22	rTR:mod.t5	mode of Trim5(data-rTR)
23	rTR:mad.t5	mean abs deviation of Trim5(data-rTR)
24	rTR:mdd.t5	median abs deviation of Trim5(data-rTR)
25	rTE:av	mean value of data-rTE
26	rTE:sd	standard deviation of data-rTE
27	rTE:sk	skewness of data-rTE
28	rTE:ku	kurtosis of data-rTE
29	rTE:rms	root mean square of data-rTE
30	rTE:rng	range of data-rTE
31	rTE:min	min value of data-rTE
32	rTE:med	median of data-rTE

33	rTE:max	max value of data-rTE
34	rTE:mod	mode of data-rTE
35	rTE:mad	mean abs deviation of data-rTE
36	rTE:mdd	median abs deviation of data-rTE
37	rFE:av	mean value of data-rFE
38	rFE:sd	standard deviation of data-rFE
39	rFE:sk	skewness of data-rFE
40	rFE:ku	kurtosis of data-rFE
41	rFE:rms	root mean square of data-rFE
42	rFE:rng	range of data-rFE
43	rFE:min	min value of data-rFE
44	rFE:med	median of data-rFE
45	rFE:max	max value of data-rFE
46	rFE:mod	mode of data-rFE
47	rFE:mad	mean abs deviation of data-rFE
48	rFE:mdd	median abs deviation of data-rFE
49	rTE:av.l	mean value of Ln(data-rTE)
50	rTE:sd.l	standard deviation of Ln(data-rTE)
51	rTE:sk.l	skewness of Ln(data-rTE)
52	rTE:ku.l	kurtosis of Ln(data-rTE)
53	rTE:rms.l	root mean square of Ln(data-rTE)
54	rTE:rng.l	range of Ln(data-rTE)
55	rTE:min.l	min value of Ln(data-rTE)
56	rTE:med.l	median of Ln(data-rTE)
57	rTE:max.l	max value of Ln(data-rTE)
58	rTE:mod.l	mode of Ln(data-rTE)
59	rTE:mad.l	mean abs deviation of Ln(data-rTE)
60	rTE:mdd.l	median abs deviation of Ln(data-rTE)
61	rFE:av.l	mean value of Ln(data-rFE)
62	rFE:sd.l	standard deviation of Ln(data-rFE)
63	rFE:sk.l	skewness of Ln(data-rFE)
64	rFE:ku.l	kurtosis of Ln(data-rFE)
65	rFE:rms.l	root mean square of Ln(data-rFE)
66	rFE:rng.l	range of Ln(data-rFE)
67	rFE:min.l	min value of Ln(data-rFE)

68	rFE:med.l	median of Ln(data-rFE)
69	rFE:max.l	max value of Ln(data-rFE)
70	rFE:mod.l	mode of Ln(data-rFE)
71	rFE:mad.l	mean abs deviation of Ln(data-rFE)
72	rFE:mdd.l	median abs deviation of Ln(data-rFE)
73	rTE:C	temporal centroid of data-rTE
74	rTE:C0	temporal centroid (normalized) of data-rTE
75	rTE:W	temporal spread of data-rTE
76	rTE:W0	temporal spread (normalized) of data-rTE
77	rTE:S	temporal skewness of data-rTE
78	rTE:K	temporal kurtosis of data-rTE
79	rTE:E	temporal entropy of data-rTE
80	rTE:F	temporal flatness of data-rTE
81	rFE:C	spectral centroid of data-rFE
82	rFE:C0	spectral centroid (normalized) of data-rFE
83	rFE:W	spectral spread of data-rFE
84	rFE:W0	spectral spread (normalized) of data-rFE
85	rFE:S	spectral skewness of data-rFE
86	rFE:K	spectral kurtosis of data-rFE
87	rFE:E	spectral entropy of data-rFE
88	rFE:F	spectral flatness of data-rFE
89	rXE:CC	(temporal centroid of data-rTE) x (spectral centroid of data-rFE)
90	rXE:CC0	(temporal centroid (normalized) of data-rTE) x (spectral centroid (normalized) of data-rFE)
91	rXE:SS	(temporal spread of data-rTE) x (spectral spread of data-rFE)
92	rXE:SS0	(temporal spread (normalized) of data-rTE) x (spectral spread (normalized) of data-rFE)
93	rTE:C.l	temporal centroid of Ln(data-rTE)
94	rTE:C0.l	temporal centroid (normalized) of Ln(data-rTE)
95	rTE:W.l	temporal spread of Ln(data-rTE)
96	rTE:W0.l	temporal spread (normalized) of Ln(data-rTE)
97	rTE:S.l	temporal skewness of Ln(data-rTE)
98	rTE:K.l	temporal kurtosis of Ln(data-rTE)
99	rFE:C.l	spectral centroid of Ln(data-rFE)
100	rFE:C0.l	spectral centroid (normalized) of Ln(data-rFE)
101	rFE:W.l	spectral spread of Ln(data-rFE)

102	rFE:W0.l	spectral spread (normalized) of Ln(data-rFE)
103	rFE:S.l	spectral skewness of Ln(data-rFE)
104	rFE:K.l	spectral kurtosis of Ln(data-rFE)
105	rXE:CC.l	(temporal centroid of Ln(data-rTE)) x (spectral centroid of Ln(data-rFE))
106	rXE:CC0.l	(temporal centroid (normalized) of Ln(data-rTE)) x (spectral centroid (normalized) of Ln(data-rFE))
107	rXE:SS.l	(temporal spread of Ln(data-rTE)) x (spectral spread of Ln(data-rFE))
108	rXE:SS0.l	(temporal spread (normalized) of Ln(data-rTE)) x (spectral spread (normalized) of Ln(data-rFE))
109	rTR:ln(sd)	log of (standard deviation of data-rTR)
110	rTR:ln(rms)	log of (root mean square of data-rTR)
111	rTR:ln(rng)	log of (range of data-rTR)
112	rTR:ln(mad)	log of (mean abs deviation of data-rTR)
113	rTR:ln(mdd)	log of (median abs deviation of data-rTR)
114	rTR:ln(sd.t5)	log of (standard deviation of Trim5(data-rTR))
115	rTR:ln(rms.t5)	log of (root mean square of Trim5(data-rTR))
116	rTR:ln(rng.t5)	log of (range of Trim5(data-rTR))
117	rTR:ln(mad.t5)	log of (mean abs deviation of Trim5(data-rTR))
118	rTR:ln(mdd.t5)	log of (median abs deviation of Trim5(data-rTR))
119	rTE:ln(av)	log of (mean value of data-rTE)
120	rTE:ln(sd)	log of (standard deviation of data-rTE)
121	rTE:ln(rms)	log of (root mean square of data-rTE)
122	rTE:ln(rng)	log of (range of data-rTE)
123	rTE:ln(min)	log of (min value of data-rTE)
124	rTE:ln(med)	log of (median of data-rTE)
125	rTE:ln(max)	log of (max value of data-rTE)
126	rTE:ln(mod)	log of (mode of data-rTE)
127	rTE:ln(mad)	log of (mean abs deviation of data-rTE)
128	rTE:ln(mdd)	log of (median abs deviation of data-rTE)
129	rFE:ln(av)	log of (mean value of data-rFE)
130	rFE:ln(sd)	log of (standard deviation of data-rFE)
131	rFE:ln(rms)	log of (root mean square of data-rFE)
132	rFE:ln(rng)	log of (range of data-rFE)
133	rFE:ln(min)	log of (min value of data-rFE)
134	rFE:ln(med)	log of (median of data-rFE)
135	rFE:ln(max)	log of (max value of data-rFE)

136	rFE:ln(mod)	log of (mode of data-rFE)
137	rFE:ln(mad)	log of (mean abs deviation of data-rFE)
138	rFE:ln(mdd)	log of (median abs deviation of data-rFE)
139	rTE:ln(sd.l)	log of (standard deviation of Ln(data-rTE))
140	rTE:ln(rms.l)	log of (root mean square of Ln(data-rTE))
141	rTE:ln(rng.l)	log of (range of Ln(data-rTE))
142	rTE:ln(mad.l)	log of (mean abs deviation of Ln(data-rTE))
143	rTE:ln(mdd.l)	log of (median abs deviation of Ln(data-rTE))
144	rFE:ln(sd.l)	log of (standard deviation of Ln(data-rFE))
145	rFE:ln(rms.l)	log of (root mean square of Ln(data-rFE))
146	rFE:ln(rng.l)	log of (range of Ln(data-rFE))
147	rFE:ln(mad.l)	log of (mean abs deviation of Ln(data-rFE))
148	rFE:ln(mdd.l)	log of (median abs deviation of Ln(data-rFE))
149	rLB:ln(hE01)	log of (Hanning Tapered Linear Band Energy 0-100 Hz)
150	rLB:ln(hE02)	log of (Hanning Tapered Linear Band Energy 50-150 Hz)
151	rLB:ln(hE03)	log of (Hanning Tapered Linear Band Energy 100-200 Hz)
152	rLB:ln(hE04)	log of (Hanning Tapered Linear Band Energy 150-250 Hz)
153	rLB:ln(hE05)	log of (Hanning Tapered Linear Band Energy 200-300 Hz)
154	rLB:ln(hE06)	log of (Hanning Tapered Linear Band Energy 250-350 Hz)
155	rLB:ln(hE07)	log of (Hanning Tapered Linear Band Energy 300-400 Hz)
156	rLB:ln(hE08)	log of (Hanning Tapered Linear Band Energy 350-450 Hz)
157	rLB:ln(hE09)	log of (Hanning Tapered Linear Band Energy 400-500 Hz)
158	rLB:ln(hE10)	log of (Hanning Tapered Linear Band Energy 450-550 Hz)
159	rLB:ln(hE11)	log of (Hanning Tapered Linear Band Energy 500-600 Hz)
160	rLB:ln(hE12)	log of (Hanning Tapered Linear Band Energy 550-650 Hz)
161	rLB:ln(hE13)	log of (Hanning Tapered Linear Band Energy 600-700 Hz)
162	rLB:ln(hE14)	log of (Hanning Tapered Linear Band Energy 650-750 Hz)
163	rLB:ln(hE15)	log of (Hanning Tapered Linear Band Energy 700-800 Hz)
164	rLB:ln(hE16)	log of (Hanning Tapered Linear Band Energy 750-850 Hz)
165	rLB:ln(hE17)	log of (Hanning Tapered Linear Band Energy 800-900 Hz)
166	rLB:ln(hE18)	log of (Hanning Tapered Linear Band Energy 850-950 Hz)
167	rLB:ln(hE19)	log of (Hanning Tapered Linear Band Energy 900-1000 Hz)
168	rLB:ln(hE20)	log of (Hanning Tapered Linear Band Energy 950-1050 Hz)
169	rLB:ln(hE21)	log of (Hanning Tapered Linear Band Energy 1000-1100 Hz)
170	rLB:ln(hE22)	log of (Hanning Tapered Linear Band Energy 1050-1150 Hz)

171	rLB:ln(hE23)	log of (Hanning Tapered Linear Band Energy 1100-1200 Hz)
172	rLB:ln(hE24)	log of (Hanning Tapered Linear Band Energy 1150-1250 Hz)
173	rLB:ln(hE25)	log of (Hanning Tapered Linear Band Energy 1200-1300 Hz)
174	rLB:ln(hE26)	log of (Hanning Tapered Linear Band Energy 1250-1350 Hz)
175	rLB:ln(hE27)	log of (Hanning Tapered Linear Band Energy 1300-1400 Hz)
176	rLB:ln(hE28)	log of (Hanning Tapered Linear Band Energy 1350-1450 Hz)
177	rLB:ln(hE29)	log of (Hanning Tapered Linear Band Energy 1400-1500 Hz)
178	rLB:ln(hE30)	log of (Hanning Tapered Linear Band Energy 1450-1550 Hz)
179	rLB:ln(hE31)	log of (Hanning Tapered Linear Band Energy 1500-1600 Hz)
180	rLB:ln(hE32)	log of (Hanning Tapered Linear Band Energy 1550-1650 Hz)
181	rLB:ln(hE33)	log of (Hanning Tapered Linear Band Energy 1600-1700 Hz)
182	rLB:ln(hE34)	log of (Hanning Tapered Linear Band Energy 1650-1750 Hz)
183	rLB:ln(hE35)	log of (Hanning Tapered Linear Band Energy 1700-1800 Hz)
184	rLB:ln(hE36)	log of (Hanning Tapered Linear Band Energy 1750-1850 Hz)
185	rLB:ln(hE37)	log of (Hanning Tapered Linear Band Energy 1800-1900 Hz)
186	rLB:ln(hE38)	log of (Hanning Tapered Linear Band Energy 1850-1950 Hz)
187	rLB:ln(hE39)	log of (Hanning Tapered Linear Band Energy 1900-2000 Hz)
188	rLB:ln(hE40)	log of (Hanning Tapered Linear Band Energy 1950-2050 Hz)
189	rLB:ln(hE41)	log of (Hanning Tapered Linear Band Energy 2000-2100 Hz)
190	rLB:ln(hE42)	log of (Hanning Tapered Linear Band Energy 2050-2150 Hz)
191	rLB:ln(hE43)	log of (Hanning Tapered Linear Band Energy 2100-2200 Hz)
192	rLB:ln(hE44)	log of (Hanning Tapered Linear Band Energy 2150-2250 Hz)
193	rLB:ln(hE45)	log of (Hanning Tapered Linear Band Energy 2200-2300 Hz)
194	rLB:ln(hE46)	log of (Hanning Tapered Linear Band Energy 2250-2350 Hz)
195	rLB:ln(hE47)	log of (Hanning Tapered Linear Band Energy 2300-2400 Hz)
196	rLB:ln(hE48)	log of (Hanning Tapered Linear Band Energy 2350-2450 Hz)
197	rLB:ln(hE49)	log of (Hanning Tapered Linear Band Energy 2400-2500 Hz)
198	rLB:ln(hE50)	log of (Hanning Tapered Linear Band Energy 2450-2550 Hz)
199	rLB:ln(hE51)	log of (Hanning Tapered Linear Band Energy 2500-2600 Hz)
200	rLB:ln(hE52)	log of (Hanning Tapered Linear Band Energy 2550-2650 Hz)
201	rLB:ln(hE53)	log of (Hanning Tapered Linear Band Energy 2600-2700 Hz)
202	rLB:ln(hE54)	log of (Hanning Tapered Linear Band Energy 2650-2750 Hz)
203	rLB:ln(hE55)	log of (Hanning Tapered Linear Band Energy 2700-2800 Hz)
204	rLB:ln(hE56)	log of (Hanning Tapered Linear Band Energy 2750-2850 Hz)
205	rLB:ln(hE57)	log of (Hanning Tapered Linear Band Energy 2800-2900 Hz)

206	rLB:ln(hE58)	log of (Hanning Tapered Linear Band Energy 2850-2950 Hz)
207	rLB:ln(hE59)	log of (Hanning Tapered Linear Band Energy 2900-3000 Hz)
208	rLB:CC01	Cepstral Coefficient No.-1 of rLB
209	rLB:CC02	Cepstral Coefficient No.-2 of rLB
210	rLB:CC03	Cepstral Coefficient No.-3 of rLB
211	rLB:CC04	Cepstral Coefficient No.-4 of rLB
212	rLB:CC05	Cepstral Coefficient No.-5 of rLB
213	rLB:CC06	Cepstral Coefficient No.-6 of rLB
214	rLB:CC07	Cepstral Coefficient No.-7 of rLB
215	rLB:CC08	Cepstral Coefficient No.-8 of rLB
216	rLB:CC09	Cepstral Coefficient No.-9 of rLB
217	rLB:CC10	Cepstral Coefficient No.-10 of rLB
218	rLB:CC11	Cepstral Coefficient No.-11 of rLB
219	rLB:CC12	Cepstral Coefficient No.-12 of rLB
220	rLB:CC13	Cepstral Coefficient No.-13 of rLB
221	rLB:CC14	Cepstral Coefficient No.-14 of rLB
222	rLB:CC15	Cepstral Coefficient No.-15 of rLB
223	rLB:CC16	Cepstral Coefficient No.-16 of rLB
224	rLB:CC17	Cepstral Coefficient No.-17 of rLB
225	rLB:CC18	Cepstral Coefficient No.-18 of rLB
226	rLB:CC19	Cepstral Coefficient No.-19 of rLB
227	rLB:CC20	Cepstral Coefficient No.-20 of rLB
228	rLB:CC21	Cepstral Coefficient No.-21 of rLB
229	rLB:CC22	Cepstral Coefficient No.-22 of rLB
230	rLB:CC23	Cepstral Coefficient No.-23 of rLB
231	rLB:CC24	Cepstral Coefficient No.-24 of rLB
232	rLB:CC25	Cepstral Coefficient No.-25 of rLB
233	rLB:CC26	Cepstral Coefficient No.-26 of rLB
234	rLB:CC27	Cepstral Coefficient No.-27 of rLB
235	rLB:CC28	Cepstral Coefficient No.-28 of rLB
236	rLB:CC29	Cepstral Coefficient No.-29 of rLB
237	rLB:CC30	Cepstral Coefficient No.-30 of rLB
238	rLB:CC31	Cepstral Coefficient No.-31 of rLB
239	rLB:CC32	Cepstral Coefficient No.-32 of rLB
240	rLB:CC33	Cepstral Coefficient No.-33 of rLB

241	rLB:CC34	Cepstral Coefficient No.-34 of rLB
242	rLB:CC35	Cepstral Coefficient No.-35 of rLB
243	rLB:CC36	Cepstral Coefficient No.-36 of rLB
244	rLB:CC37	Cepstral Coefficient No.-37 of rLB
245	rLB:CC38	Cepstral Coefficient No.-38 of rLB
246	rLB:CC39	Cepstral Coefficient No.-39 of rLB
247	rLB:CC40	Cepstral Coefficient No.-40 of rLB
248	rLB:CC41	Cepstral Coefficient No.-41 of rLB
249	rLB:CC42	Cepstral Coefficient No.-42 of rLB
250	rLB:CC43	Cepstral Coefficient No.-43 of rLB
251	rLB:CC44	Cepstral Coefficient No.-44 of rLB
252	rLB:CC45	Cepstral Coefficient No.-45 of rLB
253	rLB:CC46	Cepstral Coefficient No.-46 of rLB
254	rLB:CC47	Cepstral Coefficient No.-47 of rLB
255	rLB:CC48	Cepstral Coefficient No.-48 of rLB
256	rLB:CC49	Cepstral Coefficient No.-49 of rLB
257	rLB:CC50	Cepstral Coefficient No.-50 of rLB
258	rLB:CC51	Cepstral Coefficient No.-51 of rLB
259	rLB:CC52	Cepstral Coefficient No.-52 of rLB
260	rLB:CC53	Cepstral Coefficient No.-53 of rLB
261	rLB:CC54	Cepstral Coefficient No.-54 of rLB
262	rLB:CC55	Cepstral Coefficient No.-55 of rLB
263	rLB:CC56	Cepstral Coefficient No.-56 of rLB
264	rLB:CC57	Cepstral Coefficient No.-57 of rLB
265	rLB:CC58	Cepstral Coefficient No.-58 of rLB
266	rLB:CC59	Cepstral Coefficient No.-59 of rLB